nks

Nordisk kerne-sikkerheds-forskning | Nordisk kärn-säkerhets-forskning | Pohjoismainen ydin-turvallisuus-tutkimus | Nordic nuclear safety research

RAK-2

NKS/RAK-2(97)TR-A4

ISBN 87-7893-020-0

ON CORE DEBRIS BEHAVIOUR IN THE PRESSURE VESSEL LOWER HEAD OF NORDIC BOILING WATER REACTORS

I. Lindholm[1]
K. Hedberg[2]
K. Thomsen[3]
K. Ikonen[1]

[1]VTT Energy
Espoo, Finland
[2]Vattenfall Energisystem AB
Stockholm, Sweden
[3]Risø National Laboratory
Roskilde, Denmark

October 1997

Informationsservice, Risø, 1998

NKS/RAK-2(97)TR-A4
ISBN 87-7893-020-0

Rapporten er udgivet af:
NKS-sekretariatet
Bygning 100
Postboks 49
DK-4000 Roskilde

Tlf. +45 4677 4045
Fax +45 4677 4046
E-mail annette.lemmens@risoe.dk
http://www.risoe.dk/nks

ON CORE DEBRIS BEHAVIOUR IN THE PRESSURE VESSEL LOWER HEAD OF NORDIC BOILING WATER REACTORS

ABSTRACT

In-vessel melt progression in Nordic BWRs has been studied as part of the RAK-2 project within the Nordic Nuclear Safety Programme 1994-1997. A part of the study was the evaluation of the late phase melt progression phenomena and the thermal behaviour of core debris, the pressure vessel wall and the lower head penetrations during a severe accident. The investigations presented here focus on BWR cases.

The MELCOR/Bottom Head Package was applied to investigate the core debris bed behaviour and thermal response of structures in the case of the Olkiluoto 1 and 2 reactor vessel lower head. Both low and high pressure scenarios were analysed with sensitivity studies addressing the effects of debris bed porosity, debris particle size and reflooding of the dry debris bed. Lower head failure mechanisms and timing were examined by allowing instrument tube failure (normal case) or by deactivating the penetration failure model with an input option. Due to modelling assumptions in MELCOR, all presented calculations examine thermal behaviour of a rubble bed in the lower head. Calculated results are evaluated against experimental data.

Studies using Forsmark 3 input data were carried out with the MAAP4 code. Studied cases covered also low and high pressure sequences, and a number of sensitivity calculations varying a few key parameters were performed. Only creep rupture of the reactor pressure vessel (RPV) was considered in the MAAP4 analyses. The reason for discarding penetration failures was that the current MAAP4 model for ejection of penetration tubes is not deemed to be applicable to ABB reactor specific penetrations.

The current MAAP4 model with entrainment and fragmentation of the debris jet from the core to the lower plenum results in creep rupture close to the bottom of the RPV. For the reflooding cases both at high and low system pressure, the postulated critical heat flux gap boiling model proves to be very efficient in saving the RPV from creep rupture even if reflooding is started late in the sequence. This is because of the assumption that heat can be removed effectively from both crust and the RPV wall more or less immediately after the start of reflooding. The results indicate that the MAAP4 lower plenum model with several layers (particulate debris, metal layer and oxidic debris) requires a finer nodalization at the bottom of the vessel, where MAAP4 predicts the creep rupture is most likely to take place.

TABLE OF CONTENTS

ACKNOWLEDGEMENTS

This work was partially sponsored by the Swedish Nuclear Power Inspectorate (SKI), the Finnish Ministry of Trade and Industry (KTM) and Forsmarks Kraftgrupp (FKA), which is gratefully acknowledged.

The authors are indebted to Dr. Wiktor Frid from SKI and Mr. Heikki Sjövall from Teollisuuden Voima Oy (TVO) for valuable technical support during the work and for reviewing this report. The valuable user support of Drs. Stephen Hodge and Randy Sanders from Oak Ridge National Laboratory to set up the plant input for the BH package in MELCOR is gratefully acknowledged.

EXECUTIVE SUMMARY

The former two stages of the in-vessel melt progression studies within the RAK-2.1 project addressed the phenomena related to reflooding and coolability of core material in the original core boundary and the possibility of a partially damaged core to reach recriticality during reflooding. In cases, where core damage progression cannot be terminated by reflooding in the early phase, the core melt will eventually relocate into the lower head water pool. This study evaluates the thermal behaviour of core debris, and its thermal and structural effects on the pressure vessel wall and the lower head penetrations during a severe accident. The investigations presented here focus on BWR configuration.

The objective of this study is to investigate how and when core melt discharges into the pressure vessel lower head, what is the temperature and the chemical composition of the melt and in what form (melt pool / rubble bed) does the corium reside in the lower head. Furthermore we seek to assess what is the likely failure mechanism of the lower head. In addition to these issues, this study addresses the possibility of cooling the debris by water injection in the lower head to prevent the vessel failure.

The code comparison is aimed at trying to get a deeper understanding of the phenomena in the lower head and to evaluate and compare different models with respect to corium coolability in the lower head. The possibility of debris quenching in the lower head could delay the vessel failure and change the course of the accident. It also means that in-vessel retention might be feasible. The codes studies include both sensitivity analysis of the influence of different input parameters and comparison of the results from different codes.

The plant case studies on late phase melt progression were carried out using two integrated risk-analysis codes - MAAP4 and MELCOR- and a special thermal and structural analysis code PASULA. Calculations were performed with Forsmark 3 and Olkiluoto 1&2 input data.

The analyses focused on performing comparative studies of the MAAP4 and MELCOR codes for lower head failure with creep rupture and MELCOR and PASULA model comparisons on lower head failure due to penetration failure. In the Forsmark studies with MAAP4, only creep rupture was investigated, because the penetration weld model in MAAP4 is not directly applicable to ABB reactor type penetrations. In fact, the current MAAP4 model would produce non-conservative results for penetration failure cases. For the Olkiluoto analyses with MELCOR, both creep rupture and penetration failure were examined. In case of penetration failure the MELCOR results were "checked" by calculation of the structural integrity of the penetration with the detailed PASULA model taking the thermal load affecting the penetration from the MELCOR calculation. Thus one could assess the confidence in the MELCOR predictions.

Two base accident scenarios were investigated: station blackout with successful depressurization of the RCS (low pressure case) and station blackout with failure to depressurize the RCS (high pressure cases). A few reflooding cases were also calculated to study the coolability of the debris bed in the lower head. Several sensitivity runs were performed with both MAAP4 and MELCOR codes, varying key parameters like debris particle size, debris porosity, debris fragmentation and a number of more code specific modelling parameters.

Certain input parameter values, like particle size, were set by taking values from experimental data (e.g. FARO tests). The results were assessed in the light of experimental observations from applicable simulant or prototypic material tests.

The Bottom Head Package (BH) specially developed to address BWR lower head features was activated in the MELCOR code and applied to investigate the core debris behaviour and the thermal response of structures in the Olkiluoto 1&2 reactor vessel lower head both at low and high reactor coolant system pressures. Lower head failure mechanisms and timing were examined by allowing instrument tube failure (normal case) or by deactivating penetration failure model, which rendered the creep rupture and the wall ablation the feasible lower head failure modes. Due to modelling assumptions in MELCOR all presented studies examine the thermal behaviour of a rubble bed in the lower head.

In the low pressure cases MELCOR predicted that the falling debris was partially quenched in the lower head during the initial fall-down from the core region. The lower head water pool boiled off in 21-40 minutes. If the lower head penetration model was active, lower head failed by instrument tube melting in multiple radial locations above 60 cm (second axial layer) from the bottom of the vessel. According to MELCOR this occurred 13-57 minutes after lower head dryout in the low pressure cases and between 55 minutes and 1 h 17 minutes in the high pressure cases. According to PASULA calculations for Olkiluoto low pressure case, the lower head failure would occur most likely due to instrument tube weld failure at the periphery of the lower head hemisphere about 1 h after lower head dryout. The instrument tubes in the centre of the lower head would fail due melting in about 5000 s at an elevation of about 1 m from the bottom wall. However, it is unlikely, that the debris pouring into the flow channel would not freeze and block the channel before discharging out of the vessel. According to PASULA calculations the control rod nozzles would also loose strength at about 4000 s after lower head dryout near the periphery of the lower head, but since the control rod guide tubes are supported by a common tieplate, this failure is deemed not to lead into debris discharge out of the vessel.

If the instrument tube failure was precluded in the MELCOR calculation, the lower head failed due to creep rupture 5.5 hours from lower head dryout in a wall node close to the connection of the hemispherical and cylindrical parts of the RPV wall. The reflooding of the dry debris bed did not prevent the lower head failure under low system pressure. On the contrary, the failure occurred earlier due to excess heat release from Zirconium oxidation. The Zirconium oxidation fraction in the non-reflooding case was 16 % and in reflooding cases 47...75 % corresponding to release of 420-925 kg of hydrogen.

In the respective MAAP4 calculations for Forsmark 3 low pressure cases the boiloff of the lower head water pool took 51 min ... 1 h 41 min, depending of the particle size and the particulate debris fraction. The RPV failure by creep rupture occurred substantially earlier in the MAAP4 calculations, 1 h 14 min ... 1 h 56 min from the lower head dryout, than in the MELCOR results. MAAP4 also calculated that the creep rupture takes place at the bottom node of the vessel wall, which also differs from the MELCOR prediction. The reason for the differences lies in the different compositions and structure of debris layers in the bottom head, which are largely defined by hard-wired modelling assumptions in the two codes: in MAAP4 the metal layer resides on top of debris bed, whereas in MELCOR the bottom layer has the highest metals content and the mixing of the layers is limited due to high fraction of solids. The hottest part of the debris is the oxide layer generating decay heat.

MAAP4 also predicted the effects of reflooding of a dry debris bed differently from MELCOR. MAAP4 model assumes that no oxidation takes place in the debris bed in the lower plenum. Another, even more powerful means of achieving coolability in MAAP4 is the assumed formation of a gap between the lower head wall and the debris bed lower crust adjacent to the wall. The water

is assumed to be able to penetrate into the small gap and remove heat effectively enough to prevent the vessel failure. A lot of research is being done to verify the effectiveness of the gap cooling. In a sensitivity case, where gap cooling was precluded through the input, the RPV failed, despite reflooding, about 2 h after the lower head dryout.

In the high pressure cases MELCOR predicted that the debris was initially totally quenched in the lower head water pool. The boiloff of the pool took 21-47 minutes. If the instrument tubes were modelled in the lower head, the RPV failed due to instrument tube melting at the elevation of debris layer 2, with the failure time varying from 55 minutes to 1 h 17 minutes from the lower head dryout. If the penetration failure was precluded the lower head failed due to creep rupture at 3.3 hours from the lower head dryout. Reflooding of the dry lower head debris bed prevented the (creep rupture) failure of the lower head only, if reflooding was started immediately (1 min) after lower head dryout. In all other cases reflooding speeded up the failure of lower head by enhanced oxidation. A total of 330-627 kg of hydrogen was released during lower head reflooding.

In the MAAP4 predictions for high pressure sequences the boiloff of the lower head water pool took a longer time, 35 min ... 1.4 h, than in the MELCOR calculations. The time from lower head dryout to the lower head creep rupture varied from 48 min to 1 h 11 minutes. It is noticeable that MAAP4 and MELCOR predictions for creep rupture timing agreed better in high pressure cases. Also the predicted failure locations agreed better in high pressure cases.

The results of reflooding cases showed the same trends as with low pressure cases. MAAP4 predicted better cooling than MELCOR. According to MAAP4 results the creep rupture can be avoided if the reflooding is started at 20 minutes prior to calculated creep rupture time. If the water injection begins later than 10 minutes before creep rupture, the RPV failure cannot be avoided.

1 INTRODUCTION

This report summarises the results from the studies on late phase melt progression performed at VTT Energy, Vattenfall Energisystem AB and Risø National Laboratory for Nordic BWRs within the Nordic RAK-2 project in 1996-1997. The work on melt-structure-water interactions carried out at the Royal Institute of Technology for the RAK-2 project has been reported separately [1].

The former two stages of the in-vessel melt progression studies within the RAK-2.1 project addressed the phenomena related to reflooding and coolability of core material within the original core boundary and the possibility of a partially damaged core to reach recriticality during reflooding. In cases, where core damage progression cannot be terminated by reflooding in the early phase, the core melt will eventually relocate into the lower-head water pool.

When considering the severe accident phenomenology in the lower head, the first important matter is to know, how the core debris relocates into the lower head water pool, whether it pours out as a coherent jet or drains in smaller quantities from different locations around the core support plate. This will affect the initial quenching process in the water pool, particularly fragmentation versus quenched porous cake/melt pool formation. Another important parameter is the chemical composition of the core debris.

When the water pool in the lower head is boiled off, the dry debris bed will start to heatup and form a melt pool. The distribution and layering of different materials - metals and oxides generating heat - in the debris bed may affect the melting of material. During the heat up of the debris bed, the upward heat transfer by radiation may heat up the steel structures in the lower plenum to melting temperatures and cause additional material relocations into the lower head debris bed. This will affect the temperature and composition of the corium pool.

Finally, the thermal and structural behaviour of the control rod guide tubes and even thinner instrumentation guide tubes need to be assessed. Even if an early lower head penetration failure seemed inevitable, the melt flow out through the tube or opening in the lower head needs to be evaluated. In case the flow paths through the lower head penetrations will be blocked by crust formation, the lower head failure may occur due to creeping or vessel wall thermal attack and ablation and cause a massive pour of core debris out of the pressure vessel. The creeping of the vessel lower head is strongly affected by the pressure difference between the inside of the vessel and the containment.

The performed study seeks to give some insight into all of the above mentioned phenomena.

2 OBJECTIVES

The objective of this study is to investigate how and when core melt relocates into the pressure vessel lower head, what is the temperature and the chemical composition of the melt and in what form (melt pool / rubble bed) does the corium reside in the lower head. Furthermore, this study seeks to assess what is the likely failure mechanism of the lower head. In addition to these objectives, this report will address the possibility to cool the debris in the lower head to prevent lower head failure and the respective consequences of water injection.

The code comparison is aimed at trying to get a deeper understanding of the phenomena in the lower head and to evaluate and compare different models with respect to corium coolability in the lower head. The potential debris quenching in the lower head could delay the vessel failure and change the course of the accident. It also means that in-vessel retention might be feasible. The code studies include both sensitivity analysis of the effect of different input parameters and comparison of the results obtained with different codes.

The use of the PASULA code aims at getting more detailed predictions of structural integrity of ABB reactor specific instrument tubes - also in granular debris bed. This study will complement the earlier studies on thermal and structural response of instrument tubes embedded in a hot melt pool.

The literature study aimed at gathering information on different experiments related to late phase melt progression, especially to fragmentation and coolability of debris for the purpose of defining plausible values to different computer code input data and for evaluation of the uncertainties connected with the calculated results. Also the literature study on other published computational analyses of lower head thermal and structural response under severe accident conditions helped in evaluation of the calculated plant specific results produced within this effort.

3 BACKGROUND

The TMI-2 accident in 1979 aroused great interest in severe accident research. The TMI-2 Accident Evaluation Program (1984-88) revealed serious damage to the reactor core with meltdown and relocation of nearly 20 tons of molten material into the lower head of the Reactor Pressure Vessel (RPV). It was concluded that the vessel would not have survived this challenge without the existence of some cooling process that had prevented overheating and failure of the vessel. This motivated further investigations in the joint international TMI-2 Vessel Investigation Project (1988-93) as well as extensive experimental programmes and code development. An important objective was to investigate the relocation process and especially the quest for mechanisms that can lead to the formation of potentially coolable configurations of debris in the lower head. The TMI-2 investigations and some of these experiments have been selected for the following review and as a basis for the evaluations in Chapter 8.

3.1 TMI-2 Accident Investigations

The TMI-2 PWR accident [3,4,7] started as a LOCA through a stuck-open pressure relief valve, and the situation came out of control due to human error. After inadvertent tripping of the HPI pumps the RPV water level dropped due to net loss of coolant. During uncovery of the core the fuel heated up by decay heat and energy released from cladding oxidation. After 2.9 hours from scram, when the water level attained its minimum of ½-1 m above the core bottom, an unsuccessful attempt was made to re-establish primary coolant circulation. At that time, metals candling down the fuel and the control rods froze near the water surface and formed blockages, which were developing into a crucible-like crust, shaped by the escaping steam at the periphery (Fig. 1). It is assumed that the central part of the core collapsed into a rubble bed at the introduction of the cooler water from the bottom of the primary loop. The debris continued to heat up under vigorous oxidation. The peak temperature was close to the fuel melting point (~3100 K) at about 3.33 hours, when finally the core was reflooded by high pressure injection. The upper debris bed was quenched, but it was too late to cool down the melting debris in the crucible region.

At 3.73 hours into the accident the crucible contained a pool of about 62 tons of almost fully oxidized, molten corium. The peripheral crust reached the outer edge of the core, where suddenly the corium, superheated by 200-300 K, broke through a hole melted in the baffle plates in the east side of the reactor. During the next two minutes, about 29 tons of corium was released into the bypass region, where it drained down through holes in the core former plates and further down via the lower core support assembly to the lower head, leaving about 10 tons of frozen material along the relocation path. There was no significant fragmentation during the relocation through lower plenum water. The pressure, which was about 10 MPa, increased by ~1.8 MPa in the same period.

The temperature of the remaining 19 tons of corium at the arrival on the lower head is unknown. Due to precipitation of low-melting-point materials in the grain boundaries, corium retains some fluidity, like wet sand, down to temperatures near the melting point of steel. It is likely that the first material arrived in a relatively cool state, while the temperature increased as the plates along the relocation path heated up. There was no significant ablation on the lower core support assembly.

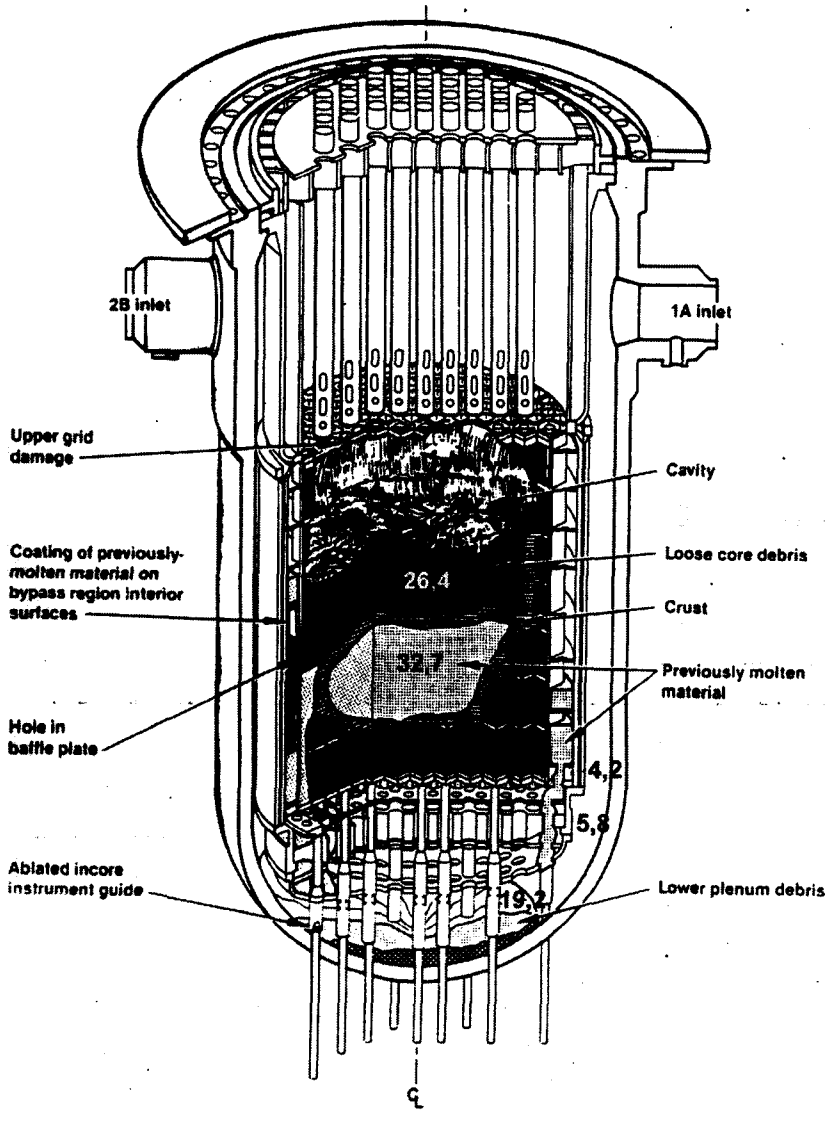

Figure 1. *The TMI-2 core end-state configuration (Source: Ref [3], with addition of masses in tons). Note: The drawing is not revised according to the VIP findings (nozzle and guide tube damage; no debris layering).*

According to the proposed relocation scenario, based upon evidence from extensive corium, vessel wall, and nozzle sample examinations [3], the corium dropped down through the holes around the periphery of the lower core support assembly. The first, relatively cool material formed a protective layer covering a large part of the lower head and many nozzles. This cool, insulating layer formed mounds at the periphery, which guided the subsequent hotter material toward an unprotected area near the centre. This area became a hot spot, where the nozzles were melted off almost flush with the bottom. On its way, the hot material also melted off the ends of many instrument guide tubes and the unprotected tops of nozzles, which were not fully embedded in the protective layer.

From metallurgical investigations of lower head steel samples, it was found that the peak hot spot temperature had been about 1100 °C for about half an hour. Due to water ingress into a postulated gap between the debris and the lower head, the steel subsequently cooled down rapidly as indicated by hardness measurements. The quenching caused hot tearing creating numerous cracks in the stainless steel cladding. Internal debris temperatures remained high for several days.

The margin to failure with respect to tube rupture and weld failure was large (bottom weld location). No clearly discernible creep deformation occurred to the lower head. However, the thermal load was not sufficiently known to evaluate the vessel margin to failure. Instead, the thermal-mechanical response analysis provided insight as to global and localised failure modes and to the effect of slow and rapid cooling mechanisms associated with water penetration into channels and gaps in the debris.

The critical review [4] revealed that the final VIP report [3] was biased, overemphasizing the importance of the hard debris layer found beneath the loose debris on the lower head. The loose debris, apparently created by thermal cracking, was not given much attention, although it constituted about half the lower head debris mass and obviously caused the melting of many instrument guide tubes.

Although the rapid cooling of the lower head was ascribed to water penetration through gaps and fractures, the gap formation and fracturing mechanisms were not considered adequately explained. This problem is further discussed in [4], where it is proposed (as an alternative to the MAAP model) that the gap formation was caused by thermal contraction of the cooling debris crust. When the crust starts detaching from the vessel at the periphery, water ingress causes further cooling and maybe cracking, and thus the gap propagates towards the hot spot.

3.2 Late Phase Melt Progression Experiments

The MP experiments [5,6] carried out at Sandia National Laboratories (SNL) were designed to investigate the melt progression in rubblized oxidic fuel material and the interaction between the melt and crust in a geometry corresponding to the lower core region of TMI-2. In the accident, the metallic crust must necessarily have been separated from the molten pool by a frozen ceramic layer due to the difference in melting points. The experiments are of direct relevance to bottom crust failure, which was long (and erroneously) assumed to be the origin of the TMI-2 relocation path (via the core plate), but they also have some bearing on the side crust melt-out, which is not easily understood in the light of current models [7].

The test sections of the two experiments, MP-1 and MP-2, consisted of a 16.5 cm high UO_2-ZrO_2 rubble bed resting on a pre-formed 3.5 cm thick, mainly metallic crust surrounding the upper ends of 32 short fuel rod stubs, whose base was a massive stainless steel heat sink at the bottom of the test crucible. The tests were carried out in an inert atmosphere with stepwise nuclear heating in the ACRR reactor over a period of hours.

The MP-1 test progressed to partial melting and settling of the debris bed. A molten pool was formed, while no material was melted in the crust and stub regions. The MP-2 test progressed further so that the ceramic fuel melt failed the crust and began to enter the intact fuel rod region together with metallic melt.

The Ex-reactor (XR) experiments [8, 9] were conducted at SNL to investigate metallic core melt relocation under BWR 'dry core' conditions. As illustrated in Fig. 2, the BWR melt progression is expected to follow the TMI-like 'wet core' path in the event of ADS failure, resulting in high pressure and high water level, whereas successful depressurization leads to below-core water level and steam starvation. In the latter 'dry core' case, the melt progression may follow the 'continuous drainage path'. The reduced cooling together with the bottom skewed BWR axial power

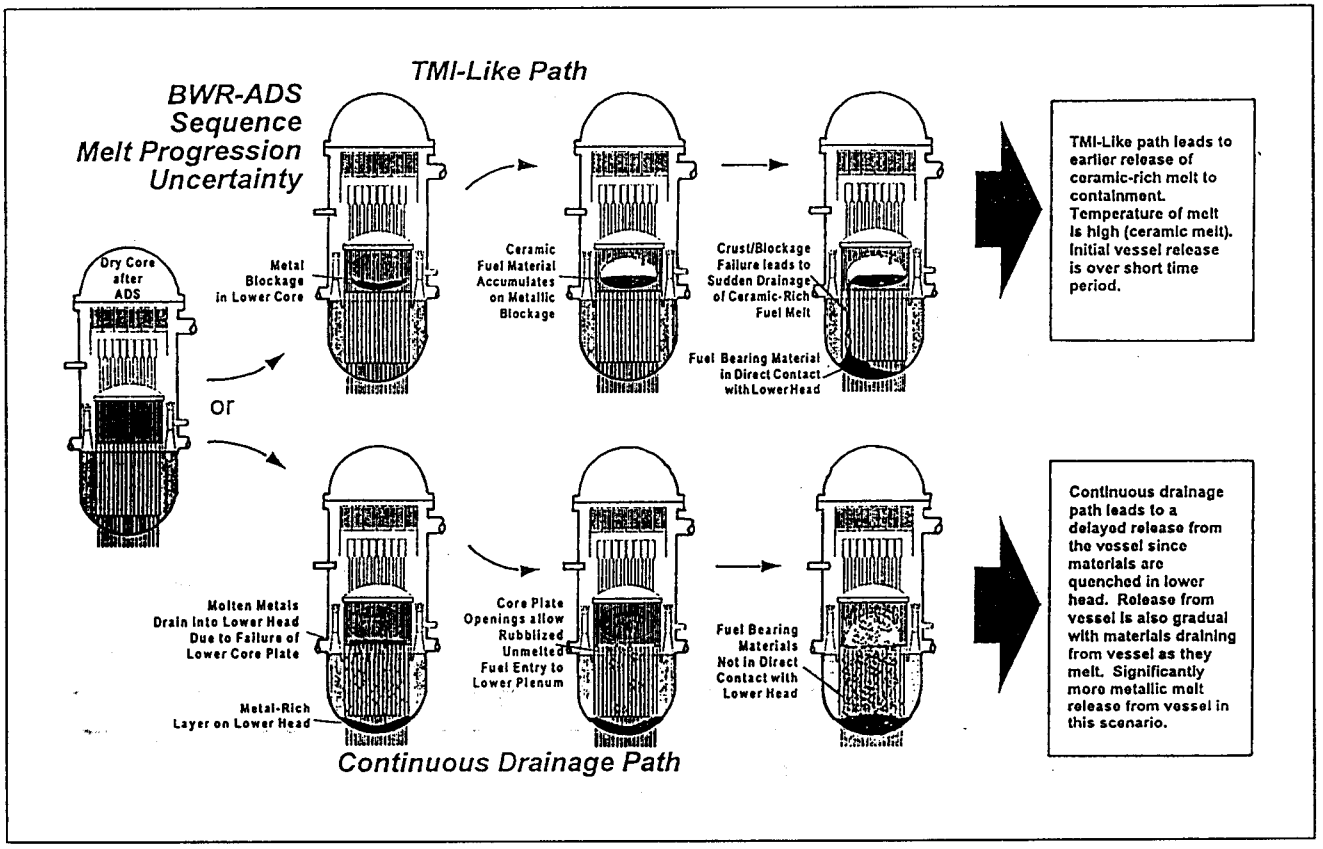

Figure 2. *Illustration of the melt progression branchpoint uncertainty for 'dry core' and 'wet core' scenarios* [*9*].

distribution can potentially lead to early core plate failure induced by the draining metallic melt, and subsequently to relocation of rubblized, unmelted fuel onto the metallic debris layer in the lower head. The purpose of the XR experiments is to determine dry core conditions under which the metallic melt will drain out of the core or freeze to form blockages in the lower portion of the core.

After two simplified tests, the XR2-1 experiment considered here was carried out. The test section was a replica of the complex BWR (GE) core plate region including 0.5 m of 64 fuel rods, fuel boxes with nosepieces, gaps between boxes, B_4C-filled control blades, and the downward extension through the fuel support piece into the control rod guide tube with velocity limiter. A typical axial temperature gradient (1600-700 K) was imposed prior to the test, which was performed in an inert atmosphere. Molten control blade alloy and Zircaloy (~2600 K) was then slowly dribbled by radiative heating of hanging wire ends onto the top of the test section to simulate the draining of molten material from the upper regions of the core.

The melt behaviour was characterised on the basis of recordings from thermocouples and a real-time x-ray imaging system. They showed that metallic melt formed three temporary blockages above the core plate in the course of the test (~30 minutes). The blockages led to pool accumulation followed by sudden drainage through multiple pathways to the lower plenum and into the guide tube via the control blade access slot. The fuel canister/bypass geometry degraded early in the core melt progression, when the channel walls were destroyed by the highly aggressive eutectic reaction of the control blade alloy. The subsequently draining Zircaloy melt caused significant degradation of the

fuel rod configuration. The test progressed to collapse of the fuel rods into particulate debris form. Roughly half of the metallic melt (but no fuel) was found in the lower plenum and on the velocity limiter after the test. Frozen melt was also found in the inlet nozzle and the nosepiece. No control blade or channel box remnants were visible, whereas the core plate was intact at the end of the test.

A notable difference of the Swedish and Finnish reactors from the GE design is the absence of a solid core plate. This implies reduced stability as each individual control rod guide tube with its fuel support piece may yield separately under the thermal and mechanical load from the fuel. Furthermore, the 'melt outlets' flush with the bottom provide easier drainage access.

3.3 Molten Jet Fragmentation and Quenching Experiments

The understanding of the break-up of a molten stream poured in water usually departs from consideration of isothermal liquid jet break-up in air or water [10, 11, 12]. Continuous large-diameter jet fragmentation occurs by erosion from the sides. An important mechanism is the formation of droplets at the interface by the growth of short-wave capillary instabilities (Kelvin-Helmholtz). Thus the approximate shape of the jet becomes an inverted cone. In the first approximation, the fragmented mass rate per unit area is proportional to the velocity, whence the lenght-to-diameter ratio L/D becomes independent of the velocity (within some We-range). Furthermore, L/D becomes larger in gas than in water.

Molten jet fragmentation in water is further complicated due to simultaneous boiling. The rapidly rising steam typically forms a thin film at the lower end, expanding into a wider, two-phase, low-velocity zone at the upper end, at least when the water is near saturation. The erosion (both on the jet and the water side) is most efficient in the thin-film region, where the relative velocities are large. During dispersion and settling in the water the droplets/fragments release part of their heat by film boiling.

One experimental concern is the limited mass of melt available. Other break-up mechanisms (e.g. Taylor instability or stripping at the leading edge) are active during the initial penetration of the jet in water. The falling jet may not even attain the quasi-steady state, and if it does, the duration may be so short that the results are not fully representative of larger releases under accident conditions. It may be noted that since the molten jet fragmentation and quenching are so intimately coupled, the initial transient (including the level swell) is longer than in the isothermal case. Furthermore, the cover gas usually applied in the experiments, is initially entrained into the water, until it is swept away by steam.

The Corium-Coolant Mixing (CCM) tests [11] were carried out at Argonne National Laboratory. The tests were performed using corium (60% UO_2, 16% ZrO_2, 24% SSt) heated to ~ 3080 K in a thermite reaction. The melt drained through an orifice into a vessel with varying mass and depth of water close to atmospheric pressure. The controlled variables in the six tests included the corium mass (~ 4 - 12 kg), the released stream diameter (25.4, 50.8 mm), and water subcooling (0 - 45 °C). The depth was ~ 1.1 m except for CCM-2 with four streams (diameter 20.2 mm, depth 0.63 m).

Jet break-up lengths determined indirectly from the velocity change to particle settling velocities, indicated by the time sequence of centre-line thermocouple responses, ranged from ~ 10 to 19 diameters (probably without achieving a quasi-steady state). In the single-jet cases, the corium fall stage quench fractions ranged from 55 to 72 % with subcooled water and from 33 to 45 % with

saturated water. The metal (SSt) oxidation ranged from ~ 2 to 35 % (low for subcooled water). The initial jet velocity and water-to-corium mass ratio had no detectable effects. The post-test examination showed beds of loosely sintered particles with mass-median particle sizes ranging from ~ 1 to 5 mm and e.g. bed porosities of 53 and 65 % for CCM-1 and CCM-3 (excluding internal particle porosities). The four-jet case led to significantly reduced quench fraction due to high voiding between the jets (pitch 26.4 mm) and lower depth. In this case the particles were sintered together in large chunks with a bed porosity of 39%.

The FARO experiments underway at JRC Ispra comprised, by May 1996, six successful corium melt jet quenching tests, approximately one per year [12,13,14,15,16,17,18,19,20]. The corium (generally 80 % UO_2, 20 % ZrO_2) was electrically heated to temperatures in the range 2820-3070 K. In all the tests, the melt was released through a 100 mm diameter orifice into nearly saturated water generally at a pressure of about 5 MPa. The parameters varied were the melt mass (18-157 kg), its composition (addition of 4.1 % metallic Zr in one test), the free fall height in gas (1.09-1.99 m), the water depth (0.87-2.05 m), the gas volume (0.46-1.65 m^3), the water mass (120-675 kg), and the initial pressure (2 MPa in the last test).

The first two 'scoping tests', L-06 and L-08 [13,14,15], were performed with relatively small melt masses (18 - 44 kg) and in a smaller diameter vessel than the rest. The first test with a larger melt mass (nominally 150 kg) was L-11 [16,17,18] in which the effect of metallic Zr addition was investigated. This was the only test in which the melt was fully fragmented. The break-up length was ~14 diameters. The 2.15-s fall stage pressure rise of 5.1 MPa and level swell ~ 2.1 m were considerably higher than in the next test L-14, or any other test. This was ascribed to the effects of rapid oxidation contributing 0.272 kg of H_2, 20% energy increase and enhanced steam production due to increased break-up [18]. However, this conclusion was obscured by the finding of similar amounts of hydrogen production in L-19 and L-20 using pure oxidic melt (oxidation of UO_2 to U_3O_8 ?) but without so violent response [20].

In all other tests than L-11, the loose debris fraction was 50 -85 %. Generally, the fall stage quench fractions ranged from 22 to 64 % of the melt energy. Very high heat transfer rates (8 - 10.5 MW/m^2) from the debris bed to the water during the first ten seconds was attributed to fluidization before settling [15]. It was uncertain to what extent the 'cake' of unfragmented debris found on the bottom plate contained reagglomerated/embedded particles. The mass-median particle sizes ranged from 3.5 to 4.8 mm. The bottom plate was intact after the tests. The peak surface temperature rises ranged from 17 to 330 K and the downward heat fluxes ranged up to 0.8 MW/m^2.

The KROTOS FCI Tests [16,17,19,20] were carried out in parallel with the FARO tests to study the phenomena of molten fuel-coolant interactions related to steam explosions. In a series of tests, about 3 kg of prototypic molten corium was released in saturated or subcooled water, but neither spontaneous nor triggered explosions were achieved. Another series was performed with molten alumina to explore conditions under which energetic interactions do occur.

It is worthwhile noting, that even if the possibility of steam explosions with corium cannot be excluded, it is practically impossible to conceive of steam explosions under accident conditions of such a magnitude that they can endanger the reactor vessel. A sufficiently large explosion would require premixing within a few milliseconds of unrealistically large masses of molten corium in water. The detailed arguments are given in the account of the Swedish steam explosion committee [30]. Steam explosions are not considered any further in this report.

The Degraded Core Coolability (DCC) experiments [21,22], comprising three in-pile tests at SNL in the mid eighties investigated the coolability of hot particulate debris beds in water over the full (PWR) pressure range up to 17 MPa. The corium simulant was fully oxidized UO_2 with 10% enrichment and with a small amount of Gd_2O_3 (for neutronic stabilization purposes). The 50 cm deep by 10 cm diameter debris bed was placed in a double walled, insulated crucible for nuclear heating in the ACRR reactor to investigate the dryout and quench behaviour.

In DCC-1 the debris bed had a broad particle size distribution ranging from 0.075 mm to 12 mm, with a mean diameter of 0.75 mm. The debris bed porosity was 34.5 %. The dryout heat fluxes ranging from 41 kW/m^2 (0.012 W/g) at 100 °C (atmospheric pressure) to 69 kW/m^2 (0.021 W/g) at 340 °C were lower than predicted at high pressures. After dryout at increased power, the power was reduced to zero. The quench front was uniform, but quenching of the debris took hours. In DCC-2 the particles were larger and the size distribution narrower, ranging from 1 to 8 mm. The debris bed porosity was 41 %. The quenching of debris occurred in 10 min, but the quench front was not uniform having a liquid finger reaching the bottom of the debris bed in the middle, while the upward steam flow occurred at the outer boundary of the particle bed. It was also noted in [21] that temperatures high enough to start the oxidation could be reached in particle beds with nonuniform size distribution. The last test DCC-3, examined the effect of particle stratification on coolability [22]. Large particles (4.67 mm) constituted the 40 cm deep bottom layer on top of which was placed a 10 cm deep layer of smaller particles (1.18 mm). The test results suggested that stratification reduces the coolability and can inhibit quenching of the debris at elevated temperatures. Measured dryout powers ranged from 0.04 to 0.10 W/g. However, water inlet flow at the base of the debris bed enhanced the cooling effects significantly.

4.0 WORK TOOLS

This study applied the two integrated risk analysis codes - MAAP4 and MELCOR - currently used in Sweden and in Finland for plant calculations and a special thermal and structural analysis code PASULA for specific lower head penetration analyses.

4.1 MELCOR/BH Model

Olkiluoto 1 and 2 calculations were performed with the MELCOR 1.8.3 code. In particular, the more detailed Lower Plenum Debris Bed model (i.e. BH package) developed by Oak Ridge National Laboratory was activated for examination of thermal effects of a dry debris bed on the lower head.

The early phase of core heatup, melting and material relocations into the lower head are modelled with the original COR package in MELCOR. The Olkiluoto core model has five radial rings and 14 axial nodes. The ten topmost axial levels represent the active core region, axial node 4 models the core support plate and the three bottom axial nodes house the lower plenum. The MELCOR model predicts that material relocations in the core begin with eutectic formation between B_4C and stainless steel at the temperature of 1453 K. Molten control rod material flows down onto the core support plate. Fuel disintegration starts, when metallic Zircaloy reaches its melting point at 2098 K. Cladding relocates downwards and the code model predicts that fuel pellets and ZrO_2 collapse to form particulate debris. Particulate debris is supported from below by intact components or channel blockages formed by refrozen metals. The core support plate is assumed to fail separately in each radial location when the steel structure reaches a user input temperature - in this study being 1500 K. Radial melt relocation is modelled parametrically by setting a user specified time delay for radial movement of material to the adjacent node. This time delay can be defined separately for oxides and metals. In the Olkiluoto calculations the time delays were 360 s and 60 s respectively.

The quench of the debris falling through the lower head water pool is evaluated with a parametric model in MELCOR. The falling debris is assumed to be fully fragmented (conceived as molten jet break-up products or un-molten rubble). The user activates the falling debris quench model by defining the heat transfer coefficient between debris particles and surrounding water, debris particle diameter (only one-size particles are allowed in the MELCOR model) and fall velocity of the particles in the input. The MELCOR model assumes formation of a rubble bed in the lower head but takes into account the possible remelting of particulate debris. The oxidation during core heatup and slumping into the lower head is calculated applying a parabolic kinetic rate law using the Urbanic-Heidrich correlation. The oxidation fractions in the core region remain relatively low since the material relocations begin already at ~ 2200 K.

When the lower head water pool has boiled off, the BH model is initiated. The BH package calculates the heatup of the lower plenum debris bed, the thermal response of the reactor vessel bottom head and penetrations and the release of core and structural materials to the drywell after failure of the lower head [23]. Originally the BH model was developed separately from MELCOR and it was only later that the two codes were integrated. This is probably the reason why there is a slight discontinuity point in the calculation at the start of the BH model (e.g. the existing lower head debris bed nodalization is reorganised at the start of the BH model).

At the initialisation of the BH model the debris bed is reorganised into three axial debris layers and 5 radial rings with the outer ring representing the side crust according to Figure 3.

The vertical lines in the lower head node scheme are drawn so that the initial volumes of the three nodes in the layer 1 are equal and also the volumes of nodes (2,3) and (2,4) are equal. The nodes (2,5) and (3,5) are defined by the crust thickness given in the input. The node heights vary with time, accounting for the material movements in the debris bed.

The vessel bottom head wall is divided into 18 radial nodes with each node having three layers as shown in Figure 3.

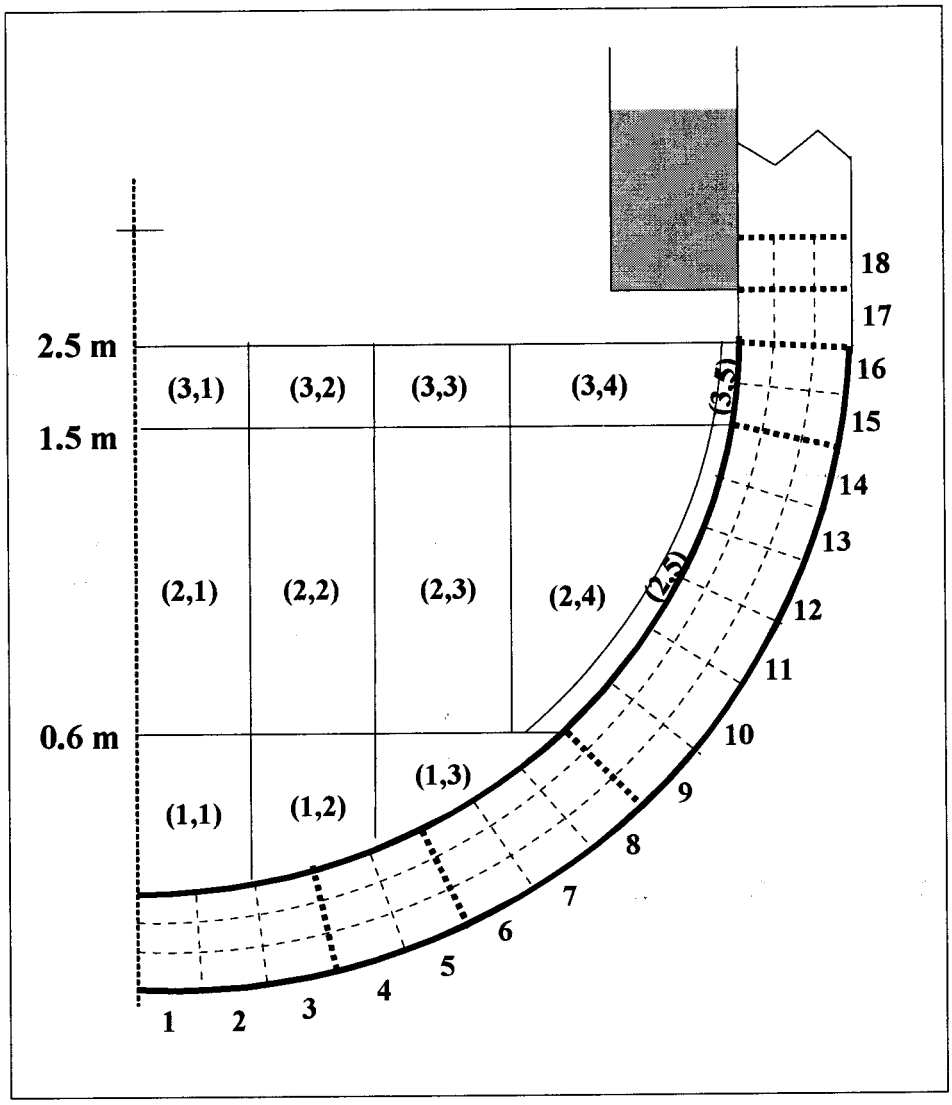

Figure 3. *Olkiluoto 1 & 2 lower head debris bed and reactor vessel wall nodalization in BH model. Nodes (2,5) and (3,5) represent crust.*

The BH package calculates composition dependent material properties like porosity, specific heat and thermal conductivity of debris in each node. Heat transfer between debris nodes is determined by using the effective thermal conductivity of porous media. Radiation and convection heat transfer to vessel atmosphere and the radiation from debris to lower head structures is calculated as well as radiation exchange between different lower head structures. The melting of baffle plate (shroud support structure) is assumed to occur when the baffle plate temperature exceeds a user specified input value (in these studies 1500 K). After failure of the baffle plate, the shroud heat structures are assumed to slump into the lower head debris bed (19 200 kg of steel in the Olkiluoto case).

Zirconium oxidation in steam is calculated with the Cathcart correlation below 1853 K and with the Baker-Just correlation for temperatures above 1853 K.

The melting, relocation, freezing and remelting of material are represented in the lower head model. The melting of materials as pure species and as components of eutectic mixtures are modelled. The formation of four different eutectic mixtures (Table 1) were assumed in these studies.

Table 1. *Eutectic mixture compositions in lower head debris bed calculations in MELCOR.*

EUTECTIC MIXTURE	MOLE FRACTIONS	MELTING TEMPERATURE [K]
Zr-SS*	0.1- 0.65977- 0.17237- 0.06768	1523.
Fe-Cr-Ni	0.73308- 0.129152- 0.0754	1700.
Zr-SS*-UO_2	0.36712- 0.60532- 0.02756	1873.
ZrO_2-UO_2	0.868- 0.132	2573.

* SS = stainless steel

The BH model recognizes four failure modes of the lower head: melting of instrument guide tubes, failure of penetration welds, failure of vessel wall due to creep rupture and the ablation failure of the vessel wall. The penetration welds in the BH model are assumed to be located near the inner surface of the vessel wall. In Olkiluoto (and also in Forsmark 3) the instrument tube welds are located higher, joining the instrument tube to a stub tube at an elevation of ~ 20 cm above the inner surface of the lower head wall.

The failure of an instrument tube within the debris bed occurs, if the temperature of the middle debris layer exceeds the melting point of stainless steel, and enough molten material has flown into the bottom layer so that the porosity of the first layer is at most 10 % . Molten material must be available in the middle layer to flow into the guide tubes. Instrument guide tube failure can also occur in any of the bottom layer nodes, if the local temperature exceeds the stainless steel melting temperature.

The ablation of the hole created by melt flow is determined with the user defined parameters: heat transfer coefficient between melt flow and the wall (1000 W/m^2 K in these studies) and wall material ablation temperature (1755.4 K in these calculations).

The control rod penetration failure was not considered in the current MELCOR calculations. PASULA code analyses address also the control rod nozzle integrity.

The creep rupture failure of the vessel head is determined in the following manner:

1. The wall tensile stresses are determined by the debris mass in the lower head and the pressure difference between the reactor vessel and the drywell:

$$S_{tensile} = \frac{9.8 \cdot M_{debris} + \pi \cdot R^2 \cdot \Delta p}{A \cdot 10^6} \qquad (1)$$

where

S = wall tensile stress [MPa]
M_{debris} = mass of bottom head debris plus mass of vessel wall and pendant assemblies in this wall node [kg].
R = inner radius of the vessel [m]
Δp = differential pressure between RPV and drywell [Pa]
A = cross-sectional area of vessel wall based upon local wall thickness including effect of any local wall melting [m^2]

2. The local Larson-Miller parameter *ALMP* is determined from the wall tensile stress with a correlation based on carbon steel rupture tests performed in Idaho National Laboratory (1991):

$$\begin{cases} 31.11 - 0.9880 \cdot (S_{tensile} - 2.0) & S_{tensile} < 5.0 \\ 28.06 - 0.3221 \cdot (S_{tensile} - 5.5) & 5.0 \le S_{tensile} < 20.0 \\ 22.83 - 0.0955 \cdot (S_{tensile} - 30.0) & S_{tensile} \ge 20.0 \end{cases} \quad (2)$$

3. According to the manual [32] the remaining time t_i to creep rupture is calculated at the end of each time step to each wall node i from the formula (3):

$$t_i = e^{BWF - AWF \cdot T_i} \quad [s] \quad (3)$$

where T_i = current average wall node temperature [K]
$AWF = 1.0 / (2.6316 \bullet ALMP)$
$BWF = 51.9378$
$ALMP$ = calculated Larson-Miller parameter

The model of the lower head reflooding in the BH package is activated by an input control function defining the mass rate of water addition on top of the debris and the temperature of the water. The heat transfer, evaporation and penetration of water into the porous debris bed is calculated with Lipinski's method for determining the dryout heat flux. The oxidation of debris is determined according to Cathcart and Baker-Just correlations.

4.2 MAAP4 Model

4.2.1 Relocation and Entrainment of Melt to the Lower Plenum

Relocation of melt from the core to the lower plenum is assumed to take place in the form of a corium (or debris) molten jet from the core plate. The particulate debris is formed through entrainment of the molten debris jet, when it pours from the core plate into the water pool in the

lower plenum. The entrainment in the water pool is modelled as erosion of a cylindrical jet using a simple jet fragmentation model.

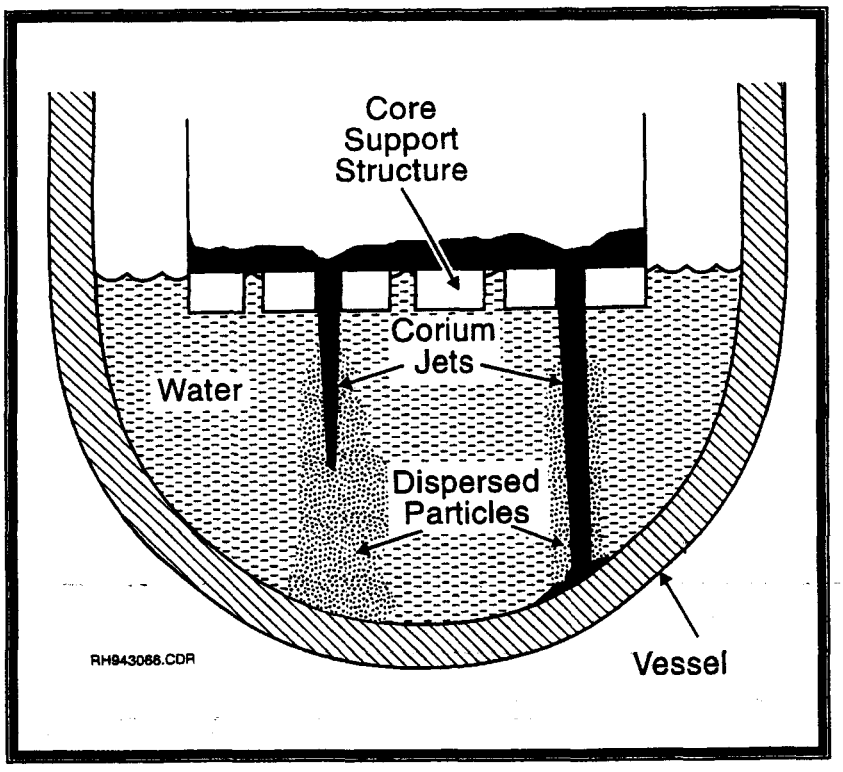

Figure 4. *MAAP4 models of relocation of melt from core to lower plenum.*

The parameter controlling the entrainment (a simple multiplier in the entrained massflow formula) can be altered in MAAP and is used for sensitivity calculations.

The particle size is given by a correlation. In the default MAAP input, the particle size ranges between 1.8 and 3.6 mm. For the current F3 input and calculations presented here, the particle size was 3.6 mm. The particle size can be adjusted with a multiplicative sensitivity coefficient.

Oxidation of debris particles is considered only during the entrainment and the falling. Debris oxidation is calculated with a correlation based on the Baker and Just model, giving the fraction of particle mass reacted as a function of the mean particle size. No oxidation is considered in the debris bed in the lower plenum.

4.2.2 Nodalization of Lower Plenum

The Reactor Pressure Vessel wall and the adjacent debris lower crust are nodalized into 5 nodes of equal height in axial direction, assuming the lower head to be a hemisphere (Fig. 5).

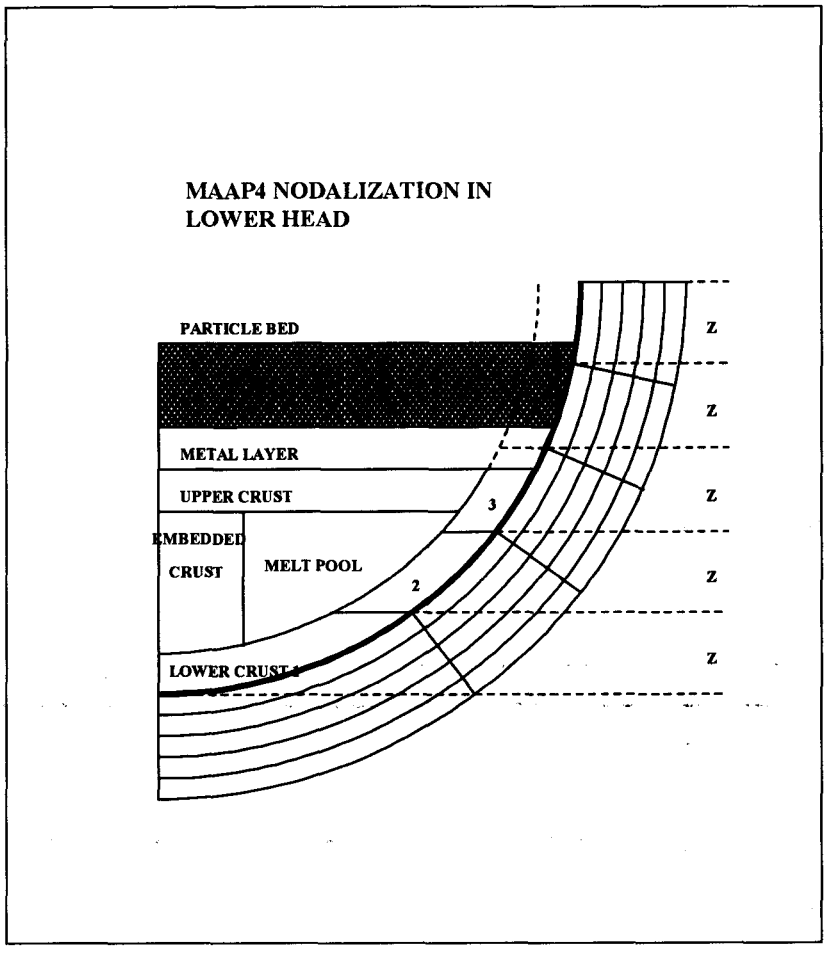

Figure 5. *MAAP4 nodalization of the lower plenum and organization of debris bed.*

The oxidic debris includes the lower, upper, and embedded crusts and the melt pool. The crusts and the pool share the same thermophysical properties. The metal layer consists of all non-oxidized metal. The material in the particle bed can remelt and then enter the oxidic debris or metal layer. The heat sinks in the lower plenum, on which the embedded crust is formed, can also melt and then enter the oxidic debris or metal layer. The embedded crust is formed on the heat sinks (Control Rod Drive Guide tubes etc.) in the lower plenum.

The MAAP4 is based on the assumption that a gap is created between the lower crust and the RPV lower head wall, if water is present when the lower crust forms. The adopted model calculates the cooling of both the crust and the vessel wall by water with Critical Heat Flux boiling in the gap. The gap is assumed to be initiated when the debris first contacts the wall and forms a crust surface. The contact with the crust causes creeping of the RPV wall due to internal overpressure initiating gap growth, while the crust surface remains structurally stiff.

The porosity of the particle bed is given a user-specified fixed value (=0.4) in the plant specific parameter file. This porosity remains constant throughout the calculation.

4.2.3 Vessel Failure Modes

There are five possible modes of vessel failure in MAAP4, which are described below.

Melttrough of penetration

The molten core debris relocated to the lower plenum is assumed to ablate through the penetrations and enter the flow channel of the penetration. The model estimates, how far the melt will travel inside the penetration. This drained length depends on how much superheat the melt has and on the geometry of the penetration. If the melt flows beyond the outer surface of the vessel wall, the vessel is assumed to have failed.

Ejection of penetration

This failure mode occurs if the welds that connect the penetrations with the RPV are weakened by the heat from the debris. The penetration is ejected from the lower head due to pressure difference between the RCS and the containment.

Creep rupture of RPV wall

The creep rupture time is calculated for each layer in the lower head given the stress profile and the temperature. For each timestep, the length of the timestep is divided with the creep rupture time and a creep rupture time fraction is obtained. The creep rupture time fraction is accumulated (this sum is named the damage fraction) until it reaches unity at which point the RPV is assumed to fail in the considered node.

Debris jet impingement on RPV wall

This failure mode is only considered during the first melt relocation from the core to the lower plenum. For later marerial relocations any previously relocated melt would protect the lower head wall from further impingement.

Molten metal layer attacking RPV wall

An evaluation of whether the heat from the metal layer is enough to weaken the RPV wall to rupture is performed with the help of a linear temperature profile in the RPV wall. The interface between the metal layer and the vessel wall is assumed to be at the material melting temperature. The same convection circulation in the metal layer that transports the decay heat from the debris bed upwards drives the sideward heat transfer to the RPV wall interface.

In the penetration ejection model, the temperature of the weld between the penetration and the RPV lower head is assumed to be equal to that of the innermost node of the RPV lower head wall. However, the critical weld in the ABB reactor penetrations is located at a higher elevation (Fig.6). In the ABB reactor case the temperature of the weld would be higher than that of the lower head wall, implying that the current MAAP4 penetration model would give non-conservative results. Therefore, the calculations in this study were performed considering only the creep rupture mode, which is relevant only in cases without penetration ejection or with blockage formatin of frozen material in the penetrations.

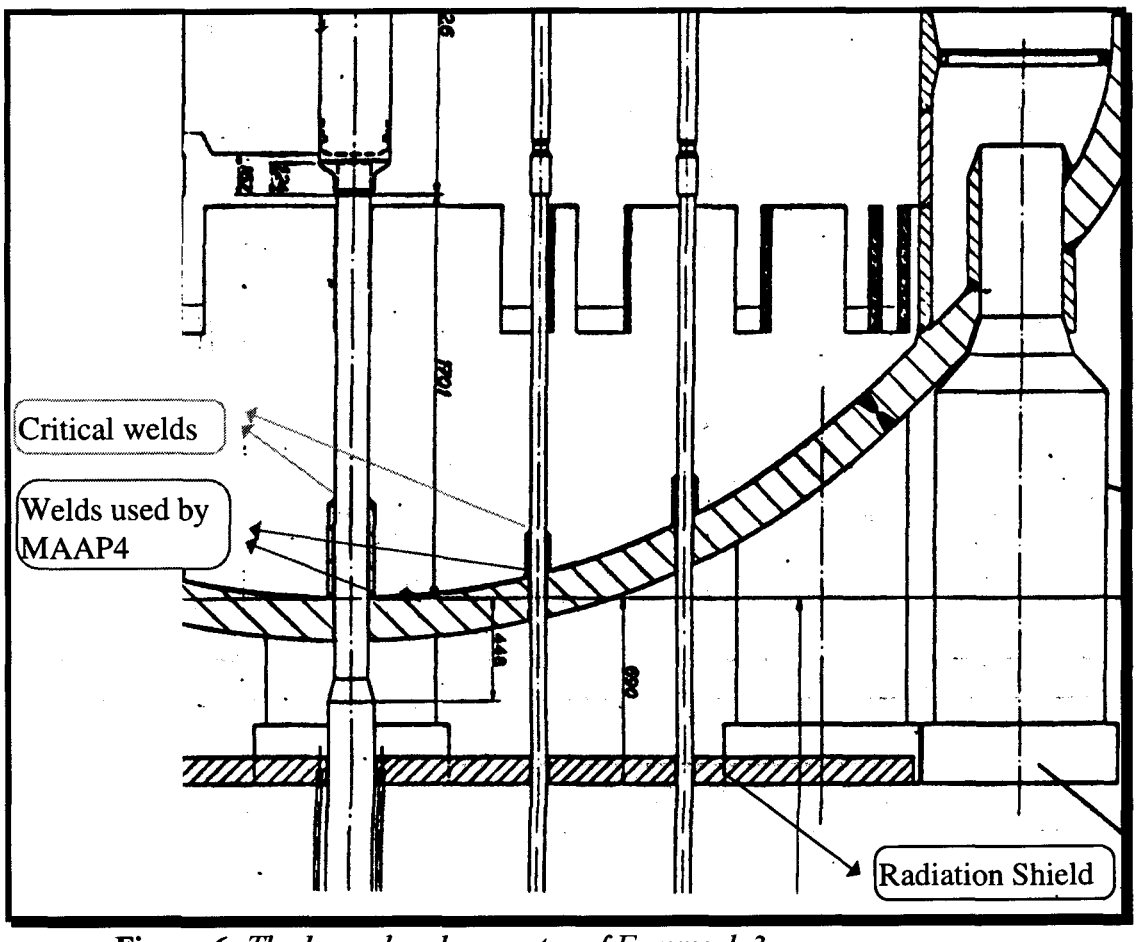

Figure 6. *The lower head geometry of Forsmark 3.*

Studies of the RPV failure with a modified penetration model taking the weld temperature at a higher elevation inside the lower head has been performed by Waaranperä [24]. The modified penetration ejection model is planned to be adopted as default in the Nordic MAAP4 BWR code version for the ABB reactors.

4.3 PASULA Model

PASULA is a common name for the group of heat conduction and structural analysis programs developed at VTT Energy. Heat conduction and convection analysis codes for two- and three dimensional cases are based on the finite difference and control volume method. The codes are non-linear and take into account the phase changes and latent heat. A new model for calculation of the effective heat conductivity in a porous or granular material was developed for the PASULA. The PASULA model was applied to investigate the thermal response of the penetrations structures in more detail. The boundary conditions, i.e. the bulk debris temperature as a function of time, the changing debris composition and consequently the temperature and composition dependent thermal conductivities and specific heat capacities were taken from MELCOR calculations. The time dependent debris porosity was also taken from the MELCOR calculations. By preserving the accident history of the MELCOR calculation through time-dependent boundary conditions, the PASULA code results are readily comparable with the MELCOR results. The major advantage gained with PASULA is that very detailed material and structural characteristics of the different penetrations could be taken into account as well as the new effective heat transfer coefficient developed for granular debris could be applied.

The bottom area of the ABB Atom BWR reactor pressure vessel contains 121 control rod nozzles and 50 nozzles for neutron monitors and other instrumentation. The details of the nozzles are presented in the Figs. 7 and 8.

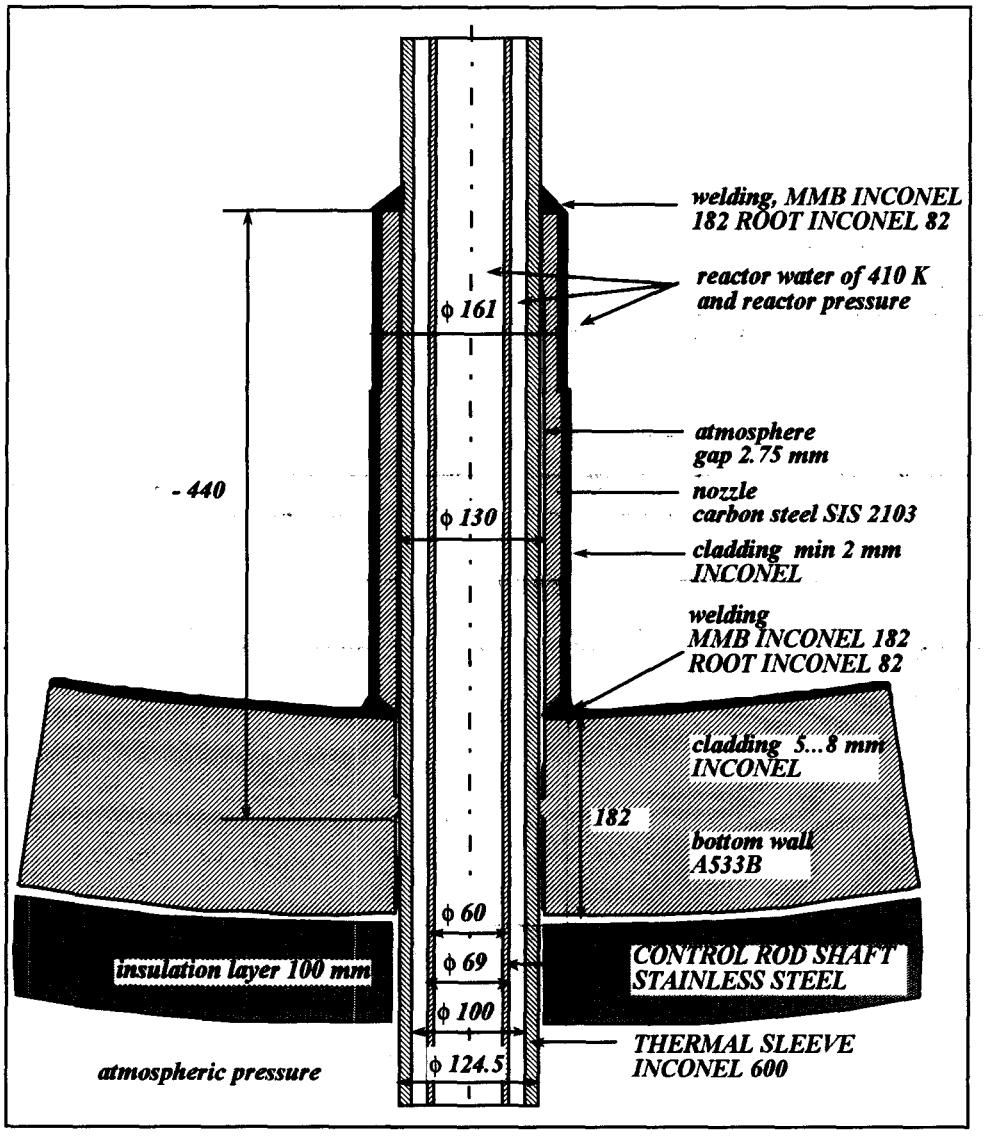

Figure 7. *ABB reactor type of control rod nozzle area.*

The thermal sleeve tubes of the control rods are bolted at their lower ends to a common radiation protection plate, which is not supported by other structures. The weight of the control rod system is resting on the welds.

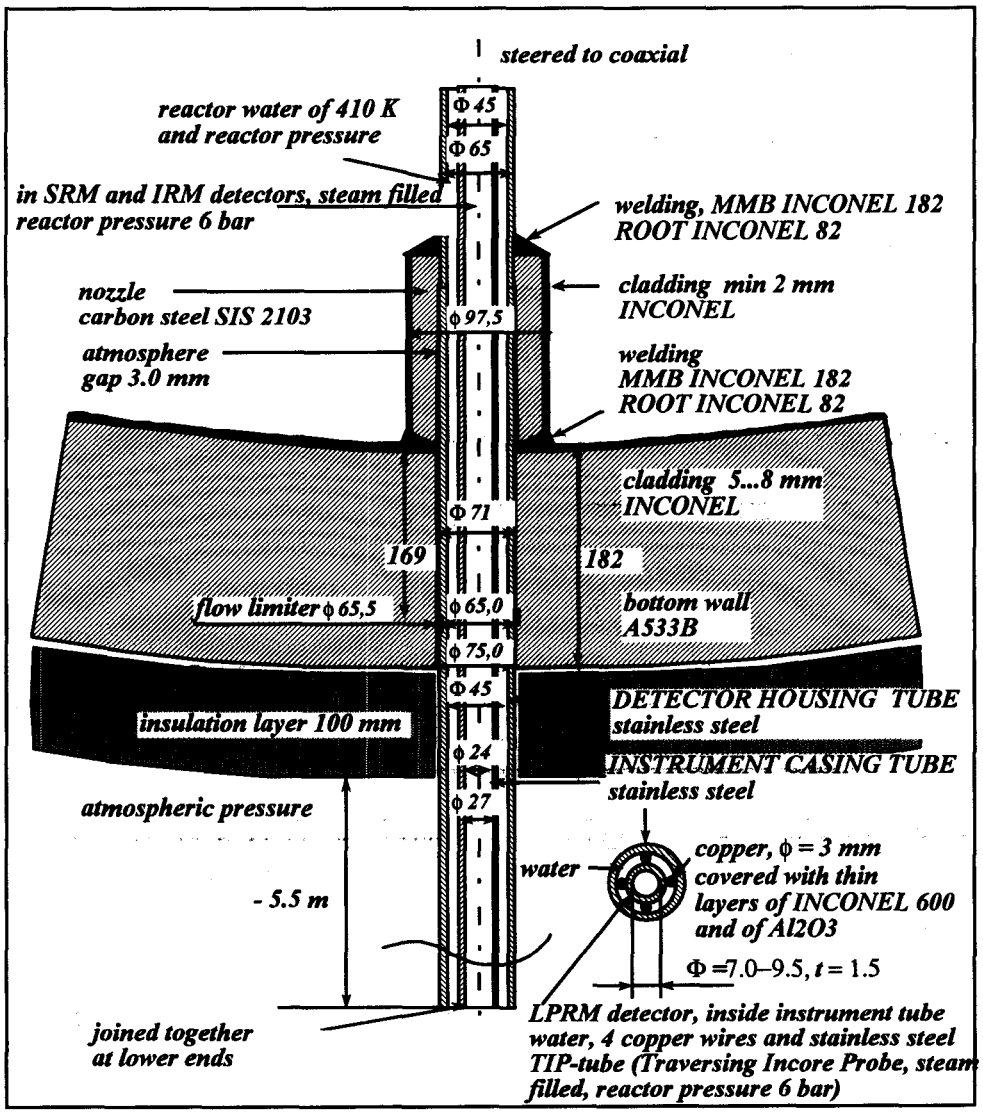

Figure 8. *ABB reactor type of instrument nozzle area.*

The instrumentation nozzles in SRM (Source Range Monitor) and IRM (Intermediate Range Monitor) detector housing tubes (total number of 8) are filled with steam at the reactor system pressure. LPRM (Local Power Range Monitor) detector housing tubes contain four copper wires and a TIP-tube in the middle. The TIP-tube is under normal operating conditions closed at its upper end and open to atmospheric pressure at its lower end. In a core melt accident the TIP-tube melts at its upper part thus opening a steam flow path through the lower end out of the pressure vessel. The amount of steam flow is small, because the inner diameter of a TIP-tube is only about 7 mm. The length of the tubes below the bottom of the pressure vessel is about 5.5 meters. Separate instrument casing tubes are not joined together at their lower ends, which means that a tube falls down, if it loses its strength below the weld.

The performed PASULA calculations are axisymmetric heat conduction and radiation analyses derived from the first principles. Heat conductivity and capacity dependencies on temperature are taken into account at all phases. Phase change from liquid to solid and vice versa is accounted for. The model uses explicit time integration.

For the thermal analyses of reactor pressure vessel wall and lower head penetrations it is necessary to define an effective heat conductivity coefficient in granular media. This heat transfer coefficient is lower than the thermal conductivity of solid homogeneous corium. The heat transfer from debris particle bed to lower head wall and to the penetration tubes is anticipated to be smaller than that from a melt pool.

The fundamental phenomena to be considered are radiation exchange between the adjacent debris particles and particles not adjacing each other and conductivity in the particle and in the steam surrounding particles. The particles may also be partly in direct contact. The voids between the particles are so small, that gas convection can be omitted.

The effect of steam in the interspace of the corium spheres enhances heat transfer. Even if the thermal conductivity of steam in the temperature range of 1500...2500 K (Fig. 16) is an order of magnitude lower than that of corium [representative value is around 15 W/(mK)], the small steam gap between the two spheres augments heat transfer between the spheres and thus increases the effective heat conductivity coefficient. For calculation purposes the thermal conductivity of steam is approximated with a fifth-order polynomial

$$\lambda(T) = -0.0206 + 3.09 \cdot 10^{-4} T - 7.72 \cdot 10^{-7} T^2 + 1.025 \cdot 10^{-9} T^3 - 5.46 \cdot 10^{-13} T^4 + 1.05 \cdot 10^{-16} T^5 \quad (4)$$

Equation (6) gives a good approximation for thermal conductivity of steam up to 3000 K. The dependency on pressure is negligible at high temperature (above ~ 900 K).

The contact area of two ideal spheres before material melting is very small. The size of the contact area depends on the force pressing the two spheres together. On the other hand the spheres may be partly in direct contact during refreezing and quenching and thus the contact area (radius r_c) is taken into account. The effective heat conductivity coefficient is written in the form

$$\lambda_{eff} = \frac{1}{\frac{1}{\lambda''_c} + \frac{1}{\lambda^*_c + \lambda^*_g + \lambda^*_r}} + \lambda''_r \quad (5)$$

where λ''_c is the conductivity of a corium sphere and λ''_r refers to radiation between corium sphere. Variables with * refer to the heat transfer contribution in the narrow gap including the conduction in the small contact area, steam conduction and radiation. The thermal resistances of the corium sphere and the steam gap are considered to be coupled in series. λ''_r represents the portion of radiation going over the narrow gap. With the help of a numerical analysis described in the report [33] the terms in equation (5) were determined to be:

$$\lambda_c'' = 0.792\ (1+ 0.785\ \frac{d_c}{d})\ \lambda_c$$

$$\lambda_c^* = 1.57\ \frac{d_c}{d}\ \lambda_c$$

$$\lambda_g^* = 11.3\ [1 - (\frac{d_c}{d})^{0.69}]\ \lambda_g$$

$$\lambda_r^* = 1.40\ [1 - (\frac{d_c}{d})^{0.92}]\ 4\ \varepsilon\ \sigma\ d\ T^3$$

$$\lambda_r'' = 0.259\ [1 - (\frac{d_c}{d})^{2.12}]\ \cdot\ 4\ \varepsilon\ \sigma\ d\ T^3\ , \qquad (6)$$

where d_c is the diameter of the small contact area and d is the diameter of the corium sphere. The thermal conductivity of steam was calculated from the equation (4). The parameters in equation (6) were determined searching minimum cumulative error.

The approximation (5) refers to the case, where the spheres reside inside a cylinder. In a cubic structure the spheres are located inside a square channel where part of the radiation escapes through the voids between the adjacent spheres. The ratio (area of square - area of circle)/area of square is $(1 - \pi/4)$ leading us to write the effective heat conductivity coefficient in the form

$$\lambda_{eff} = \frac{\pi}{4}\ (\frac{1}{\frac{1}{\lambda_c''} + \frac{1}{\lambda_c^* + \lambda_g^* + \frac{d_{eff}}{d}\lambda_r^*}} + \frac{d_{eff}}{d}\lambda_r'') + (1 - \frac{\pi}{4})\ 4\ \varepsilon\ \sigma\ d_{eff}\ T^3\ , \qquad (7)$$

where the last term represents the radiation escaping the two-sphere system. The effective diameter d_{eff} accounts for the different packings of the spheres. In the previous discussion the spheres were assumed to be at distance $d = 2r$ from each other. In reality the spheres are packed closer than in the corners of a cubic grid.

The real ratio of corium volume to total volume is typically 0.7 giving a porosity of $\alpha = 0.3$. Consider a cube with a side length of a and sphere with the diameter d_0. The number of spheres fitting into the cube is $(a/d_0)^3$. In case of the cubic packing of spheres with diameter d the porosity is

$$\alpha_0 = \frac{a^3 - (\frac{a}{d_0})^3\ V_0}{a^3} = 1 - \frac{V_0}{d_0^3} = 1 - \frac{\pi}{6} - 0.47\ , \qquad (8)$$

when the volume of a sphere is $V_0 = (4/3)\pi(d/2)^3$. If the uniform spheres are packed in a way that the porosity is $\alpha = 1 - V_0/d_{eff}^3$, then the effective distance of the particles is

$$d_{eff} = (\frac{1 - \alpha_0}{1 - \alpha})^{1/3}\ d\ . \qquad (9)$$

The simplest way of defining the effective thermal conductivity in a granular media can be done with the formula found in the open literature

$$\lambda_{eff} = \lambda_g + 4\ \varepsilon\ \sigma\ d\ T^3\ . \qquad (10)$$

In reactor applications the applicable temperature range starts from 500 K and ends at about 2500 K, when the core debris is molten and heat is transferred by conduction (and convection in the melt pool). For the calculation for the particle diameter d = 5 mm is chosen. The diameter d_c of the contact area is 20 % of the particle diameter, i.e. d_c = 1 mm.

The ultimate strength of examined materials are presented in Fig. 9. The strength of stainless steel is estimated to be lost at 1100 K, the strength of A533B at 1300 K and the strength of INCONEL at about 1500 K.

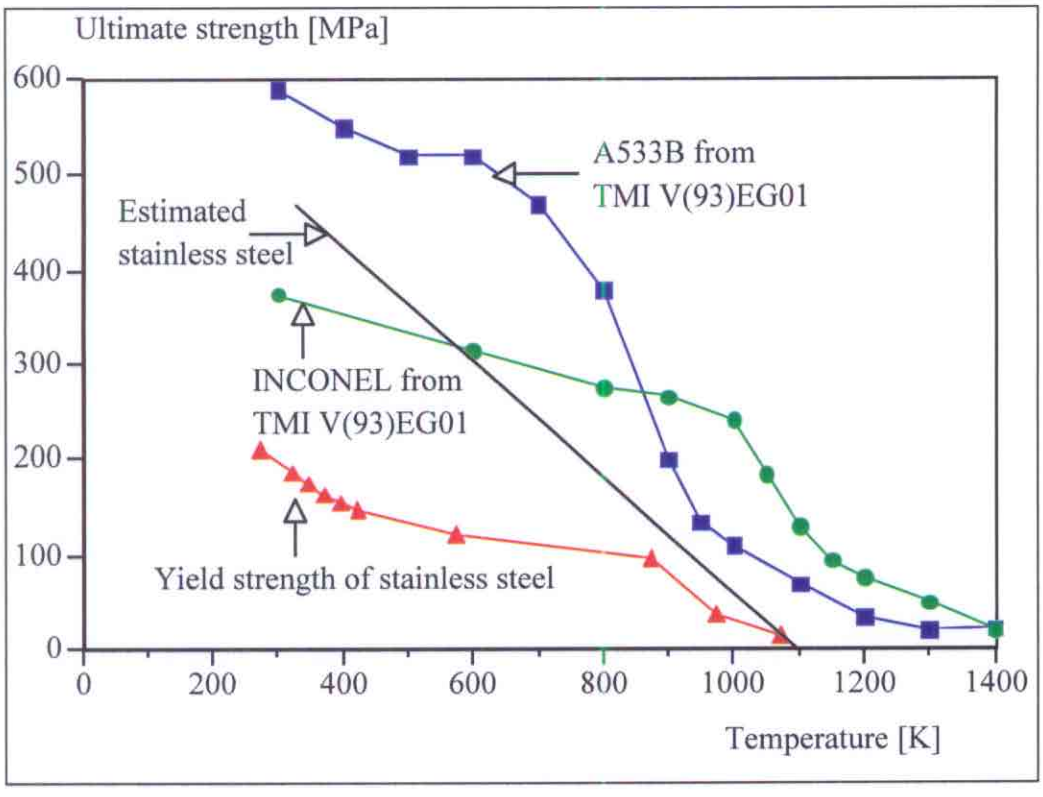

Figure 9. *Ultimate strength of materials as a function of temperature.*

5 SCOPE OF ANALYSIS

5.1 Olkiluoto Calculations

The studies of melt behaviour in the lower head with Olkiluoto 1 & 2 plant data were performed with the MELCOR 1.8.3 computer code. The initial core material masses in the applied MELCOR input for OL-1/OL-2 are listed in Figure 10.

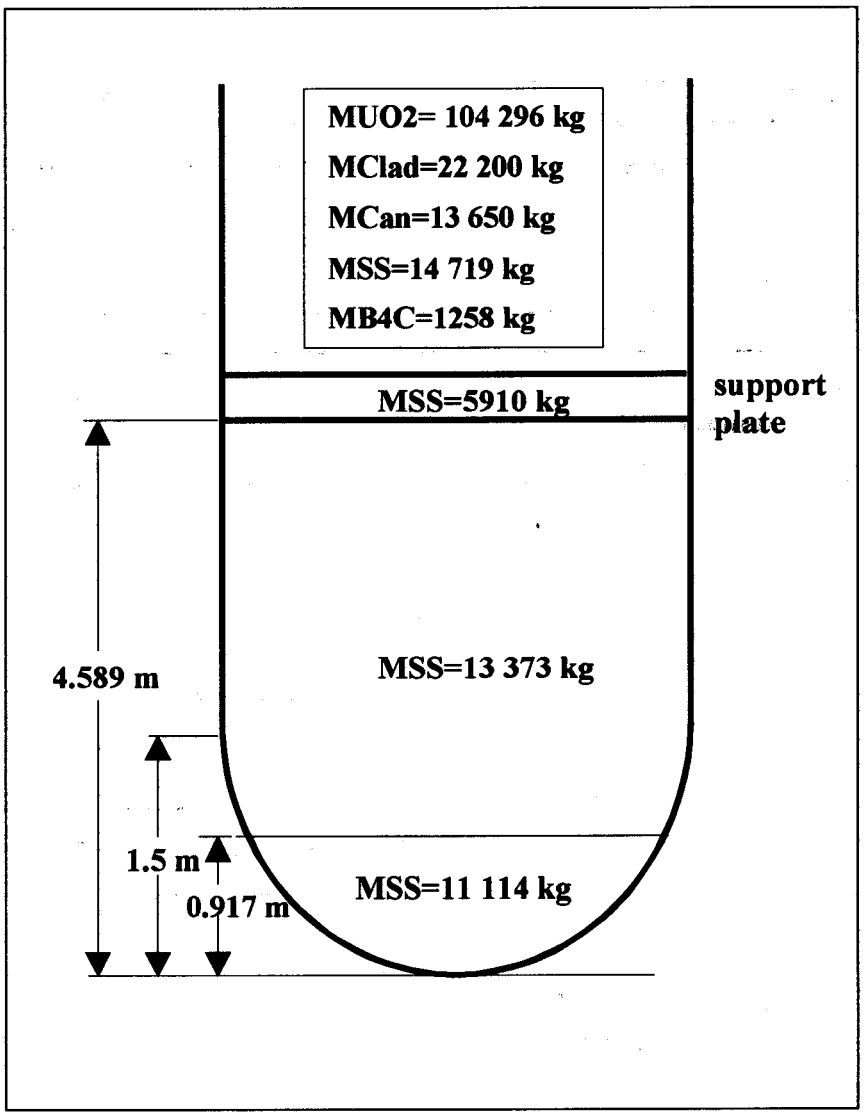

Figure 10. *Initial core material inventories in the OL-1/OL-2 MELCOR input.*

The investigated base accident scenarios were:

1. Station blackout with depressurization of the Reactor Coolant System at 1 hour into the accident

2. Station blackout with failure to depressurize RCS.

A number of sensitivity runs were performed varying the debris particle diameter and the initial debris porosity. Reflooding and coolability of a dry debris bed was investigated by varying the timing of reflood and the water injection rate. Lower head debris bed behaviour was studied both in case of instrument tube failure and in a case where instrument tube failure was excluded. The results from the cases without lower head penetrations also gave better boundary conditions and input data for the PASULA analyses for structural integrity of instrument tubes.

The parameter variations in the calculated sensitivity runs are presented in Table 1 of Appendix A. The motivation of the performed sensitivity runs is presented in the following:

Penetrations/no penetrations
The MELCOR/BH model seems to predict melt-through of instrument guide tubes relatively soon after initiation of the BH package. Sensitivity cases were run assuming no instrument guide tube failure to get longer stable debris bed temperature history to be used in the separate penetration failure studies with the PASULA code with a more representative model for Olkiluoto specific penetrations.

LH debris bed porosity
The BH package manual suggests that reasonable values for debris porosities lie between 0.259 and 0.476. Different porosities for oxides and metals can be given in the input. In these studies both oxides and metals had the same initial porosity of 0.3 or 0.45.

Debris particle diameter
The fuel pellet diameter in the SVEA-64 fuel used in Olkiluoto is 0.01044 m. Three different particle sizes were selected for these studies: diameter 0.01 m, 0.005 m and 0.002 m to study the effect of full pellet, medium size and finer fragmentation, respectively. Also the measured particle sizes of the fragmented corium in the FARO tests have been 0.0035 ... 0.0048 m, which supported the selection of the particle sizes.

Reflood rate
Since the structure temperatures close above the core were high (T=1100 K...1700 K) prior to lower head dryout, it was considered unrealistic to get reflood water through core spray. In the Olkiluoto plant only the high pressure injection system (327) can inject water to the downcomer (DC) with the capacity of 45 kg/s. Hypothetical DC injection cases with water mass rate of 340 kg/s (close to low pressure system 323 injection at 5 bar counter pressure) were performed for comparison with Forsmark 3/MAAP4 calculations.

Reflood timing
The starting time of water injection into the lower head was selected arbitrarily to cover cases with early and late start of coolant injection. However, the reflooding was started in all cases after initiation of the BH model and thus after lower head dryout. The cases with reflooding before total dryout of the lower head water pool were not investigated in this study.

Other important input parameters
The heat transfer coefficient from debris to water during debris relocation from the core plate to the lower head was in all cases 750 W/m^2K (default value 1000 W/m^2K). The debris fall velocity from support plate to the lower head was 0.1 m/s as recommended in the BH package manual (default value 5 m/s). Minimum Lipinski porosity for dryout heat flux calculation was 0.4 in all calculations (default value 0.15). Time constants for radial relocation (from ring to ring) of

material were redefined to be 360 s for solid material and 60 s for molten material - code defaults were 3 s and 1 s respectively.

5.2 Forsmark 3 Calculations

The current study with Forsmark 3 plant data was performed with the MAAP 4.0.2 BWR computer code. For information and comparison with the MELCOR Olkiluoto input the following masses were used in the MAAP4 F3 input.

Table 2. *Core material masses used in F3 input.*

CORE REGION	SUPPORT PLATE	LOWER PLENUM
M_{UO2} = 143 000 kg M_{Clad} = 33 400 kg M_{Can} = 21 100 kg M_{steel} = 21 919 kg M_{B4C} = 2 265 kg	M_{steel} = 6 000 kg	M_{steel} = 58 000 kg

Some other Forsmark 3 key input for comparison with the Olkiluoto plant:

	Forsmark	Olkiluoto
Thermal Power	3300 MW_{th}	2500 MW_{th}
Operating pressure	70bar	70 bar
Steam flow	1 780 kg/s	1350 kg/s
Number of fuel assemblies	700	500
RPV inner diameter	6.4 m	5.54 m
RPV inside height	20.8 m	20.8 m
Reactor Vessel Total weight	760 tons	630 tons

In the current study, only creep rupture of the RPV lower head was considered. Studies of the RPV failure with a modified penetration model relevant for ABB reactors has been performed earlier by Waaranperä [24]. The only failure modes encountered in that work were the creep rupture and the penetration ejection. In the preliminary calculations performed for the current studies penetration ejection occurred but these were later recalculated with the consideration of only the creep rupture. The other failure modes modelled in MAAP4 seem to be unlikely for ABB type of BWRs since they were never achieved either in the preliminary calculations of this study nor in the analysis in [24].

The Forsmark 3 calculations also address two different scenarios, a low pressure scenario and a high pressure scenario. All sequences were initiated by a total blackout with loss of the diesel power supply. The main effort is put into the low pressure cases with Automatic Depressurization System initiated at Level L4 - water level reaching the value 0,5 m above the active core. Some studies were also carried out in the case of failure to depressurize the reactor coolant system leading to a RPV failure at high pressure. In addition to the sensitivity studies, calculations of reflooding at different times and different conditions are performed.

In the sensitivity studies the influence of the following parameters was studied (cf. Appendix B):

- The lower head debris bed quenching by overlying water can be changed with a parameter for the flat plate critical heat flux. This parameter controls the ingress of water through the top of the debris bed, see cases L2 and H2.

- The entrainment coefficient of the debris jet from the core to the lower plenum. The increase of this parameter results in much less debris jet entrainment into particles during relocation, see cases L3 and H3.

- The porosity of the particulate debris bed formed by entrainment of the molten debris jet was decreased, see cases L4 and H4.

- The particle size from the entrained molten jet is reduced to half the size and ¼ the size given by the capillary size see case L5, L6, H5 and H6.

- For the low pressure base case a gap is created between the RPV wall and the lower debris crust for cooling by CHF boiling. For case L7 the gap CHF boiling model was disabled.

- As an alternative to the model with different debris material layers in the lower plenum there is a model with all materials in the lower plenum mixed into one pool see case H7.

6 RELOCATION OF DEBRIS INTO THE LOWER HEAD

In the calculated Olkiluoto low pressure scenarios (Appendix A) the total core uncovery took place at 1 h into the accident, when the blowdown of the reactor coolant system was initiated with the Automatic Depressurization System (ADS). The water level stabilized at the elevation of 3.2 m, which is 1.4 m below the active core region. This corresponds to 37 000 kg of water in the lower head. Slow evaporation took place in the lower head pool reducing the water mass to 32 000 kg prior to the start of debris slumping into the bottom head. The first core support plate radial ring failure showed sensitivity to the debris particle size. The earliest support plate failure occurred with largest particles (∅=1 cm) at 4 h 29 min and the latest support plate failure time was with intermediate particles (∅=5 mm) at 5 h 26 min. The other four radial rings followed the first ring in about 20 minutes except for the case with the small debris particles. In the case with 2 mm particles the lower head dried out after three radial rings had failed and the material from the last two rings poured into the lower head after dryout. The time delay in the failure of the last rings was caused by more effective evaporation due to larger particulate/coolant heat transfer area and subsequent steam cooling in the core region. Decreasing the debris bed porosity from 0.45 to 0.30 resulted also in earlier support plate failure by about one hour.

The first batches of corium were fully quenched. The following material batches were only cooled, because the metals fraction of core material was still high in the core region and oxidation induced by evaporation from the lower head pool increased the temperature of material in the core region. The later material pours relocated at higher temperature to the lower head and only partial quenching was achieved prior to lower head dryout. The boiloff of the lower head water pool took only 21-40 minutes with the loss of coolant through the reopened ADS valves. The evaporation during debris slumping (which may be unrealistically abrupt) caused a pressure spike in the RCS the height of which increased with decreasing particle size. However, the pressure spike in these calculations did not exceed 60 bar.

In the high pressure cases coolant boiled off slowly from the RPV through pressure relief valves that maintain the primary pressure at about 70 bar. The evaporation in the core enhances Zirconium oxidation which in turn speeds up the core degradation. The oxidation fraction of Zirconium prior to support plate failure was in low pressure cases ~ 30 % and in the respective high pressure case 57 %. The debris particle diameter in all calculated high pressure cases was 5 mm, but the porosity of debris was varied to be 0.3 or 0.45. The first support plate radial ring failed at about 2 h 40 min. If the debris bed porosity was higher, only three out of five support plate radial rings failed before lower head dryout, which took 47 min after the first corium batch arrived in the lower head. If the porosity of debris was 0.3 the debris from four out of five radial rings relocated into the lower head pool and the boiloff of water took a shorter time, 21 minutes. In both cases debris was quenched prior to debris bed dryout.

In the Forsmark 3 calculations (Appendix B) the depressurization of the reactor coolant system is initiated automatically, when the low water level (0.5 m above top of the active core) is reached and this occurred in the analysed MAAP cases at about 7 minutes into the accident, which is much earlier than in the respective Olkiluoto cases. The core was totally uncovered at about 32 minutes and the core heatup began. Core plate failure took place at 1 hour 24 minutes, which is hours earlier than in the respective MELCOR runs for Olkiluoto. The reason for this large difference might be that in the MELCOR runs the B_4C/steam reaction was activated and resulted in early melting and relocation of control rods into support plate node. The support plate nodes were 'filled' with steel at the time fuel relocations started. The heatup of the support plate structure occurred

only by axial conduction from the upper nodes. The B4C/steam reaction was not simulated in the corresponding MAAP calculations for Forsmark 3. The reason, why the support plate failure times were closer to each other in high pressure cases may be, that in the high pressure calculations the steam rich conditions (slow boiloff of water during heatup) guaranteed sufficiently steam for Zr-oxidation, causing more simultaneous relocation of steel and fuel materials. Thus in both calculations the support plate nodes contained an internal heat source and the initial debris temperatures were higher. Anyway the core support plate failure timing in the MELCOR calculations seem to be very sensitive to certain input parameters.

In the Forsmark calculations the core starts melting at about 1650 s after the total blackout and totally 228 tons of core material, out of which about 80 tons was molten, relocated into the lower plenum. The first relocation occured at the core plate failure at 5020 s (see Fig. 12). Four other core material relocations into the lower head followed during the next two hours, approximately. A relatively continuous debris jet of about 5 -10 kg/s into lower plenum was sustained between 1.7 hours and 2.3 hours. The boil-off of the lower head water pool after the support plate failure takes about 1 hour 15 minutes in the MAAP4 calculations (Fig. 11), whereas according to MELCOR the boiloff took at most 40 minutes.

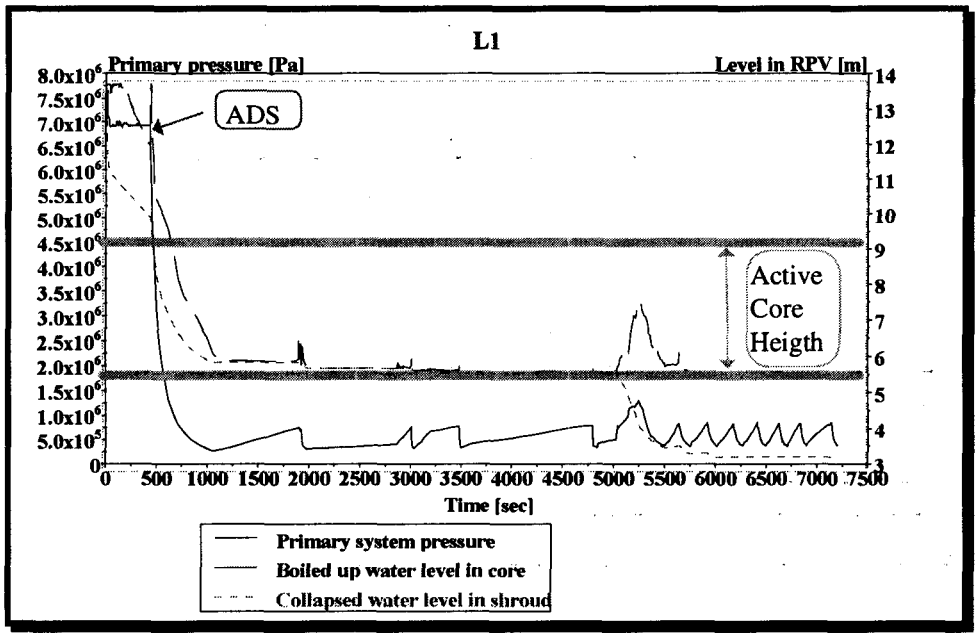

Figure 11. *Pressure and water levels in RPV, water level relative to bottom of RPV.*

In the MAAP4 calculations the first batch of core debris is fragmented and quenched. The following debris relocations occurring after the major boil-off, do not fragment but form a melt pool with a lower crust against the vessel lower head wall and lower head equipment. Finally a metal layer is formed on the upper crust, see Fig. 5.

When the last batch of some 33 tons of hot core material relocates from the core 29 min after the lower head dryout (i.e. at 11230 s, Fig. 12), a dramatic increase of steel masses in the lower plenum occurred caused by the melting of equipment (CRD tubes etc.). The 48 tons of steel structures in the lower plenum is melted away in a very short time. A large molten pool was formed and the particulated debris started melting as can be seen in the decrease of particulate debris mass in Fig. 12.

The shroud support and shroud structures were not assumed to melt in MAAP (contrary to MELCOR).

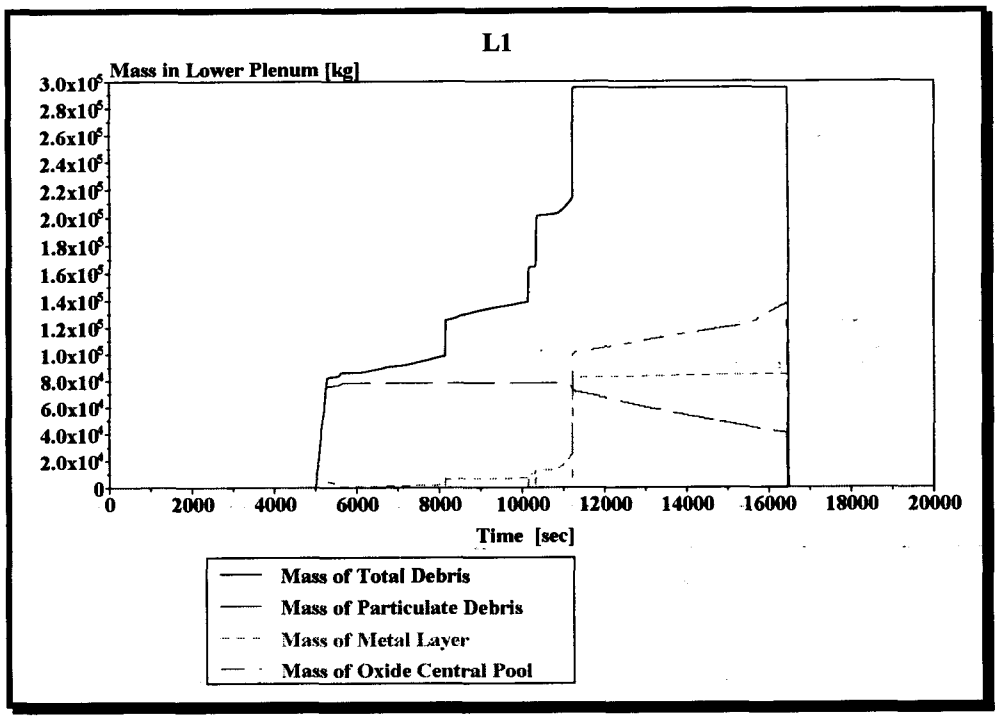

Figure 12. *Different forms of Debris in Lower Plenum for the Low Pressure base case L1.*

In the Forsmark high pressure cases larger masses of core material were relocated to the lower plenum during relatively short time intervals at two occasions, first at the core plate failure (50 tons) and the second time, when the remaining core mass (130 tons) relocated. Between these two major relocations there was an average melt stream of 10 kg/s for about 5 000 sec. The first corium batch was almost totally entrained (into particles). Particulate debris was only formed during the first 1000 seconds after core plate failure, when the water pool on top of the debris was more than 1 meter deep.

Small amounts of steel relocated in the beginning. It was not until the heat sinks in the lower plenum started to melt that any significant metal layer formation took place. At 2.8 h into the sequence the lower plenum dried out and the debris and the RPV wall started to heat up more rapidly. The particulate debris reached its melting point 20 minutes later.

7 LONG TERM DEBRIS BEHAVIOUR IN THE LOWER HEAD

7.1 Low Pressure Cases Without Lower Head Penetrations

7.1.1 Olkiluoto Calculations

The BH model is initiated after lower head dryout. The particulate debris bed is arranged into three debris layers. The height of the bottom layer is defined in the input and was in these studies 60 cm. The height of the second layer, determined by the model is typically about 90 cm in the Olkiluoto NPP case. The heap-like third layer is 1.5 m high in the middle and 0.5 m thick near the vessel wall. The heights of the debris layers vary with time. The initial temperatures, masses and porosities in the low pressure base case are shown in Figure 13 and the layer compositions are listed in Table 3. It is seen that the lowest layer has high metal contents (~2/3 of its mass), while the second and the third layer consist mostly of oxides.

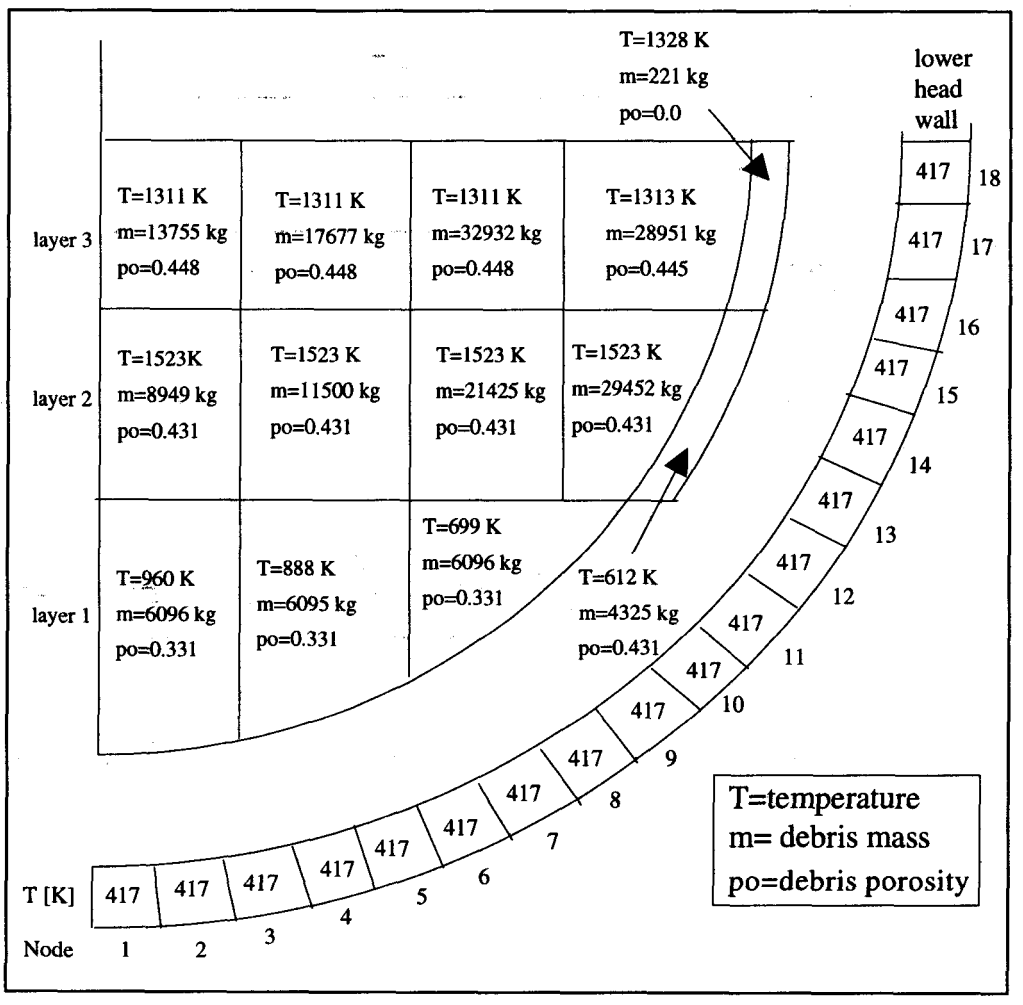

Figure 13. *Lower head debris temperatures (T), masses (m) and porosities (po) at the start of the BH model. Low pressure base case (case no 1).*

Table 3. *Composition of lower head debris bed at the start of the BH model in the low pressure base case (case no. 1).*

MATERIAL	LAYER NO 1.		LAYER NO. 2		LAYER NO. 3		ALL LAYERS	
State	solid [kg]	liquid [kg]	solid [kg]	liquid [kg]	solid [kg]	liquid [kg]	solid [kg]	liquid [kg]
Zr	2713	0	12624	0	14566	0	29903	0
Fe	6272	0	8050	0	16799	0	31121	0
Cr	1525	0	1958	0	4086	0	7570	0
Ni	678	0	870	0	1816	0	3364	0
B_4C	82	0	181	0	249	0	511	0
ZrO_2	367	0	3753	0	3913	0	8033	0
FeO	68	0	924	0	942	0	1934	0
Cr_2O_3	19	0	255	0	260	0	535	0
NiO	7	0	99	0	101	0	207	0
UO_2	6555	0	46937	0	50803	0	104296	0
Totals	18287	0	75651	0	93537	0	187476	0

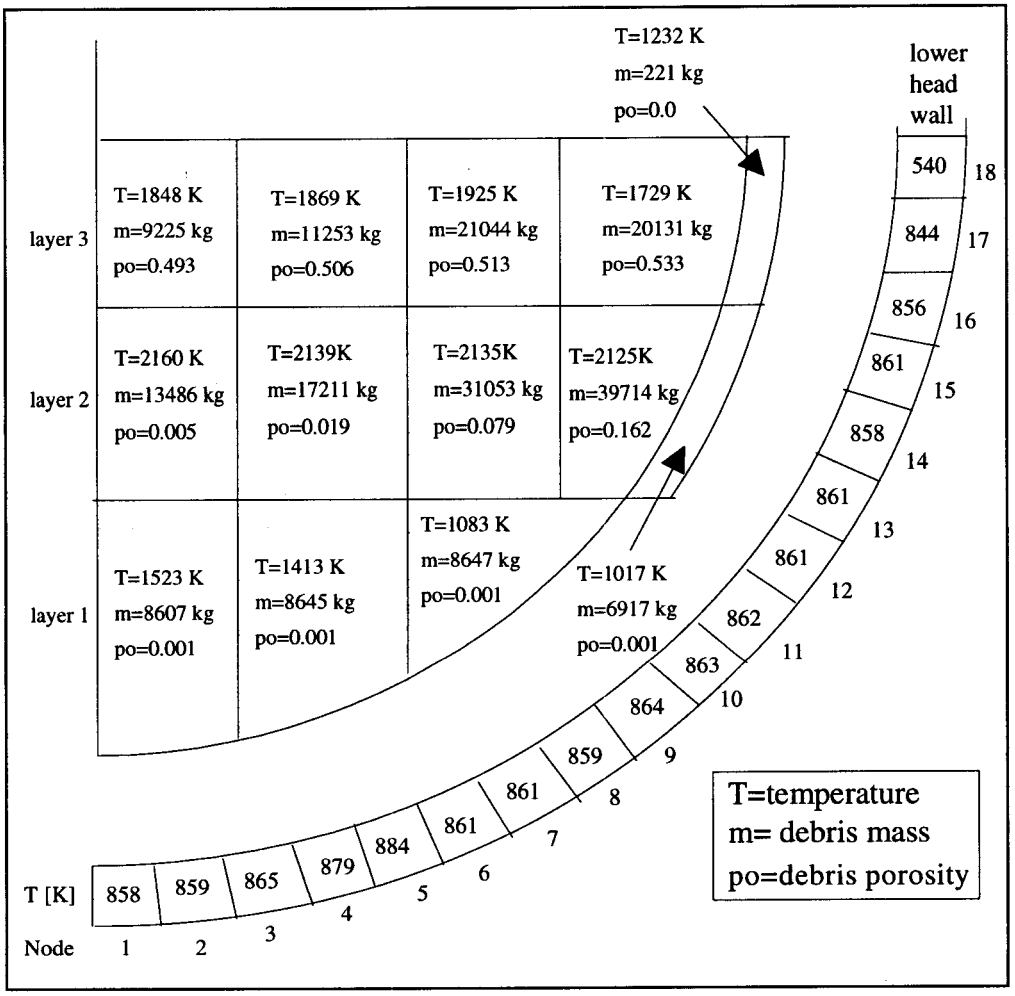

Figure 14. *Debris bed characteristics just after shroud failure (1 h 26 min after lower head dryout) in the low pressure base case (case no 1). Lower head wall temperature refers to the inner wall layer.*

In the base case #1 (Table 1, Appendix A.1) there were no penetrations in the lower head and the debris bed continued a long term heat up slowly after the dryout. Steel components in the debris bed reached their melting point and moved downwards. The porosity of the bottom layer became smaller. The temperatures of the lower head wall and the baffle plate structures increased. The debris bed characteristics are depicted in Figure 14 just after shroud melting and slumping. (1.5 hours after LH dryout).

At the time of shroud melting the lower head debris bed comprises both molten and solid materials. The melt fractions of material in layers 1, 2 and 3 are 3 % , 45 % and 1 %, respectively. In the base case 1 the reactor pressure vessel was predicted to fail 5.5 h after lower head dryout due to creep rupture in wall node 16 at the average nodal wall temperature of 1696 K. The inner wall temperature of 1811 K is near the melting point. This is ~ 160 K higher than the corresponding creep rupture temperature found by MAAP (cf. Fig. 17). The debris bed characteristics just before local creep rupture are shown in Figure 15. The respective debris bed composition is indicated in Table 4.

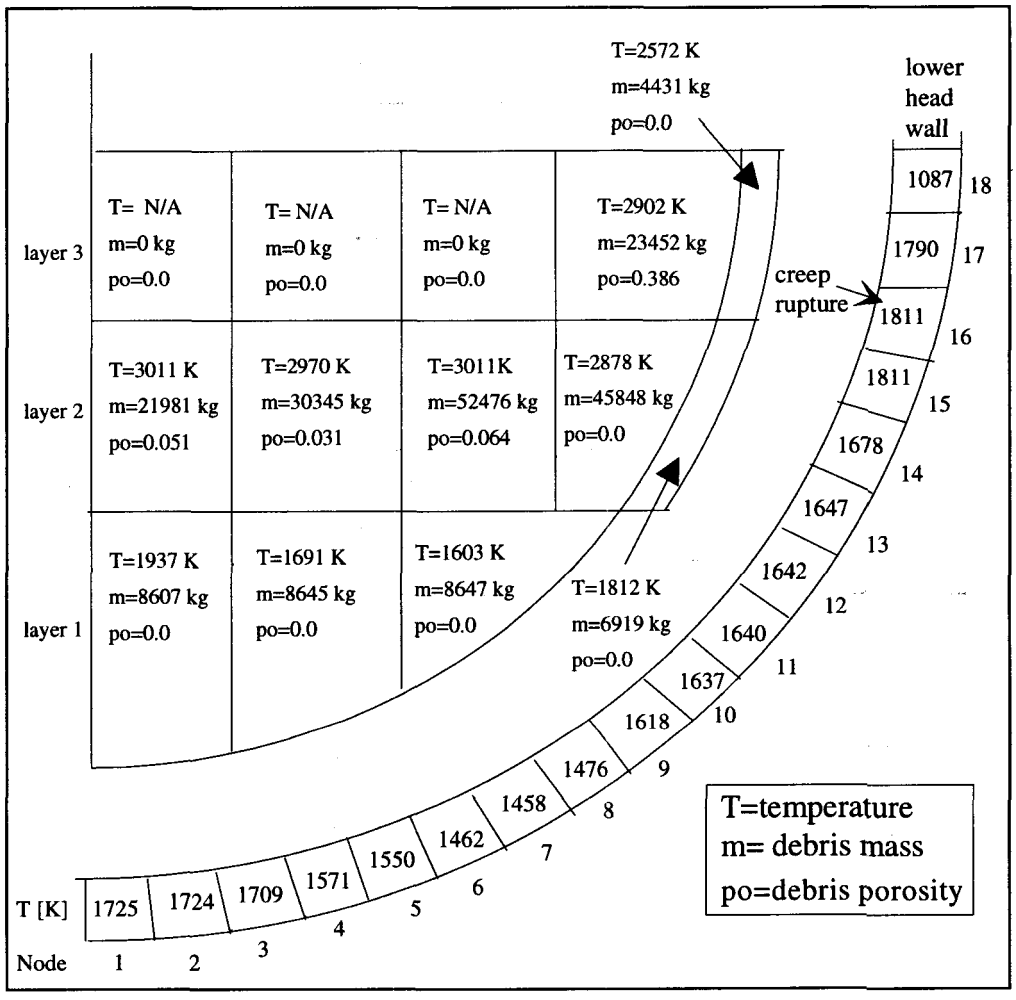

Figure 15. *Debris bed characteristics and lower head wall inner surface temperatures prior to local creep rupture in wall node 16 (case no 1).*

Table 4. *Material composition in the lower head just prior to lower head creep rupture.*

MATERIAL	LAYER NO 1.		LAYER NO. 2		LAYER NO. 3		ALL LAYERS	
State	solid [kg]	liquid[kg]	solid[kg]	liquid[kg]	solid [kg]	liquid[kg]	solid[kg]	liquid [kg]
Zr	1160	2700	608	25173	0	261	1768	28135
Fe	0	10908	0	36728	0	944	0	48580
Cr	0	2653	0	8934	0	223	0	11810
Ni	1	1176	0	3972	0	99	1	5247
B_4C	82	0	10	232	150	288	242	520
ZrO_2	367	0	215	4866	2121	464	2703	5330
FeO	23	246	0	1695	0	2	23	1943
Cr_2O_3	19	0	15	363	121	26	154	389
NiO	7	0	6	163	0	32	13	195
UO_2	6555	0	48161	26428	22997	155	77713	26583
Totals	8215	17685	49014	108554	25389	2494	82618	128733

Reflooding of the lower head did not prevent creep rupture. The maximum debris temperature increased in spite of coolant injection (Fig. 16). In the case of late reflooding (water injection was started 2 h 16 min after lower head dryout) the porosities of layers 1 and 2 were almost zero and water could not sufficiently penetrate the debris bed to cool the corium. Creep rupture occurred 5 h 19 min after dryout in wall nodes 1 and 2 at the average nodal wall temperature of 1696 K.

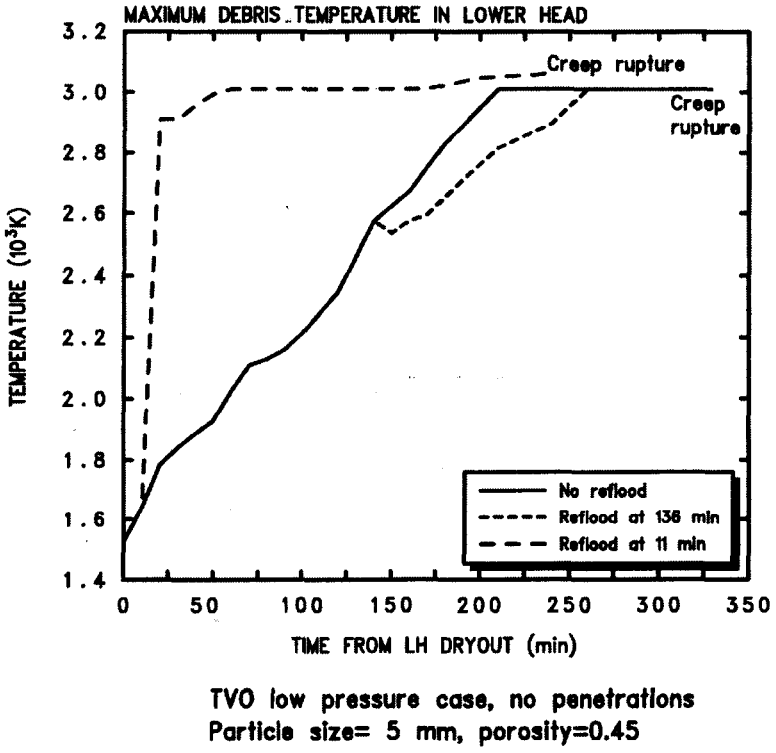

Figure 16. *Maximum debris temperature in the lower head in low pressure cases 1, 2 and 3 without lower head penetrations.*

In the case with early lower head reflooding (11 min after lower head dryout) the porosities of the debris bed were high enough for water to penetrate the porous bed, but the evaporation induced oxidation in the debris bed (800 kg of hydrogen was produced in 18 minutes) released more heat than was transferred to the coolant. Again material melted and porosities in layers 1 and 2 were reduced to zero and water ingress ceased. In this case the creep rupture occurred earlier, 4 h after initial lower head dryout in wall node 11 at the average nodal temperature of 1721 K.

7.1.2 Forsmark 3 Calculations

Parameter studies on the influence of different sensitivity coefficients and models in the lower plenum were performed (see Tables 3 and 4 in Appendix B). The base case L1 progressed as follows:

The first core relocation at core plate failure at 5020 seconds is almost totally entrained (into particles). The larger relocations that follows are not entrained at all and the melt instead forms a crusts on the equipment and RPV wall. It is not until about 8 000 sec that larger quantities of steel rstart relocating to the lower head (cf. Fig. 12) and form a metal layer on top of the debris crusts and the molten pool. At 9 500 seconds into the sequence the lower plenum is dry and the debris and RPV wall start to heat up more rapidly. The temperature distribution in the lower head at the time of dryout is illustrated in Fig. 17 (See Table 3 in Appendix B.1).

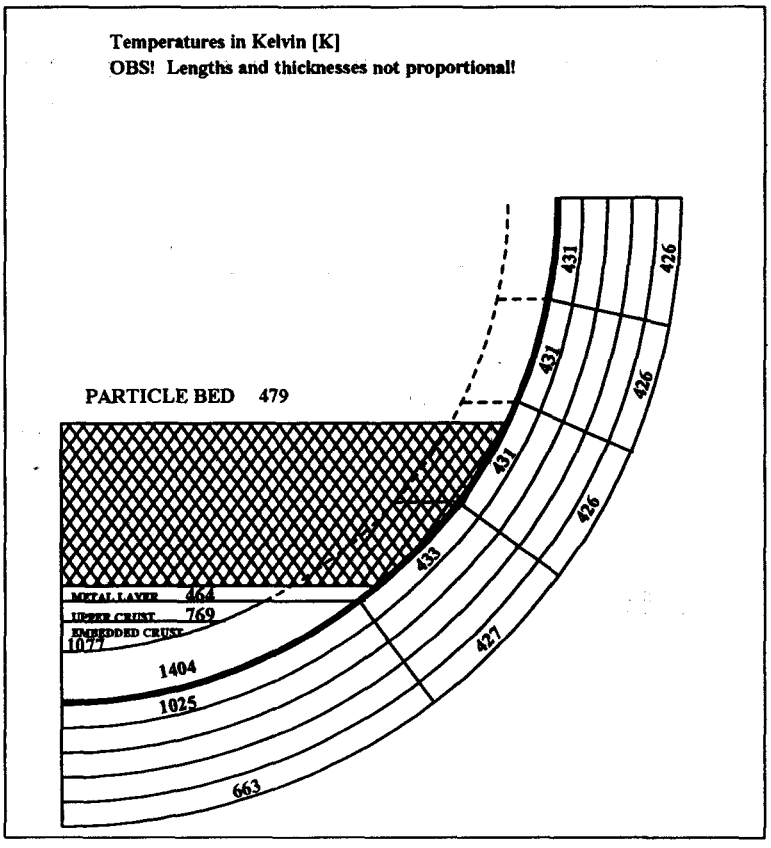

Figure 17. *Lower plenum temperature distribution at the time of lower head dryout. MAAP4 prediction for Forsmark 3.*

The process of particulate debris heat-up melting continued between 3.1 h and 4.3 h, when the upper crust started to melt. About 1 min after the start of upper crust melting the RPV wall failed by creep rupture in the lowermost node. The temperatures in the lower plenum at the time of vessel failure is shown in Figure 18.

When the creep rupture in the lowest node 1 occurred at 4.6 h the total debris mass of 295 tons in the lower head had the following mass composition:

Particulate Debris	14 %
Metal Layer	29 %
Oxide Central Pool	47 %
Debris Crusts	10 %

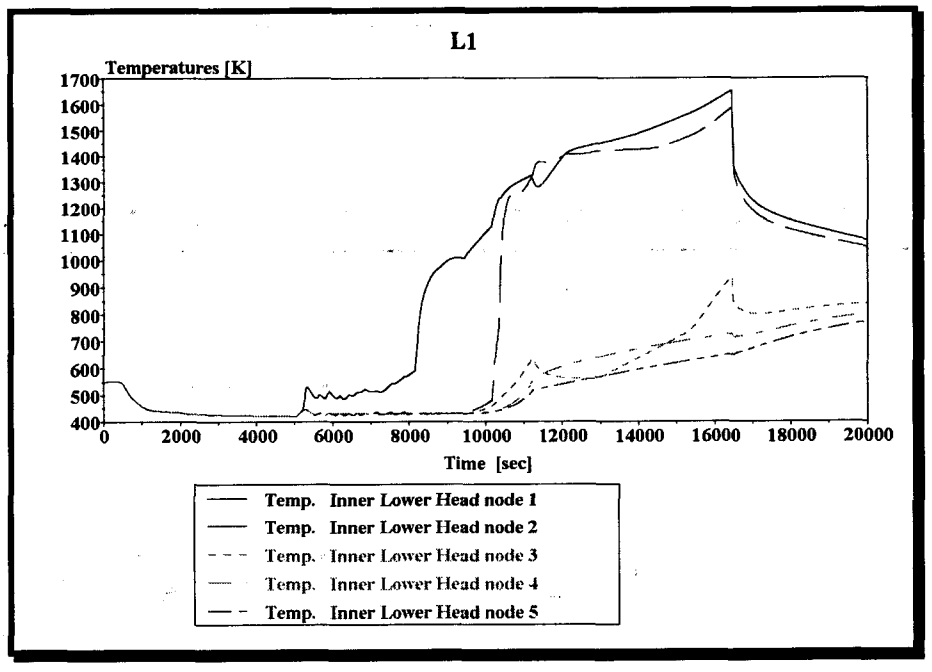

Figure 18. *Temperature history of the lower head structure in Forsmark 3 predicted by MAAP4 Node 1 is the lowermost and 5 the uppermost node.*

The temperature history of the lower head is shown in Figure 18. The temperatures increase in node 1 at 8000 seconds was due to the draining of hot melt from the core extending the lower crust to cover the whole node. The same phenomenon was recognized in node 2 at about 10 000 seconds. Node 3 was only partly covered by crust starting from 13 000 seconds. The dryout of the lower plenum at 9 500 seconds caused the temperature to increase for nodeS 2-5. Nodes covered only by particulate debris and the metal layer do not experience temperatures that would threaten the RPV integrity.

In case L2 the fraction of plate critical heat flux for lower head debris quenching was decreased. This means that less water can penetrate into the debris bed. The results were very similar to those of case L1, with the difference that the lower plenum dryout took a little longer time. The RPV wall and the lower crust had slightly higher temperatures than in case L1 and that resulted in creep rupture, 35 minutes earlier than in the base case L1.

In case L3 the entrainment coefficient of the debris jet from the core to the lower plenum was decreased. The effect of this parameter change was, that much less debris was entrained to particles during relocation to the lower head. That in turn decreased the steam generation in the lower plenum during and after relocation. Lower evaporation decreased the oxidation in the core region and slowed down the melting of the core. This changed the mode and timing of relocation from the core region to the lower plenum. The creep rupture occurred in node 2 at 4.4 h into the accident and since the location was not the bottom node only the debris above the failure was discharged to the containment. The bottommost node failed 41 minutes later and all remaining debris was discharged to the containment. This case was the only low pressure case where the creep rupture occurred in node 2.

In case L4 the default value (0.4) for the porosity of the particulate debris bed was changed to 0.3. As a result, the lower plenum dryout took more time, while the particulate debris started to melt somewhat earlier than in the base case.

For case L5 the entrained particle size was reduced to half. The average particle diameter was thus reduced from 3.6 mm to 1.8 mm. The lower plenum dryout as well as the creep rupture in the bottom most node occurred earlier than in the base case. The main difference compared to the other cases was the increased oxidation of the entrained particles in the lower plenum during relocation.

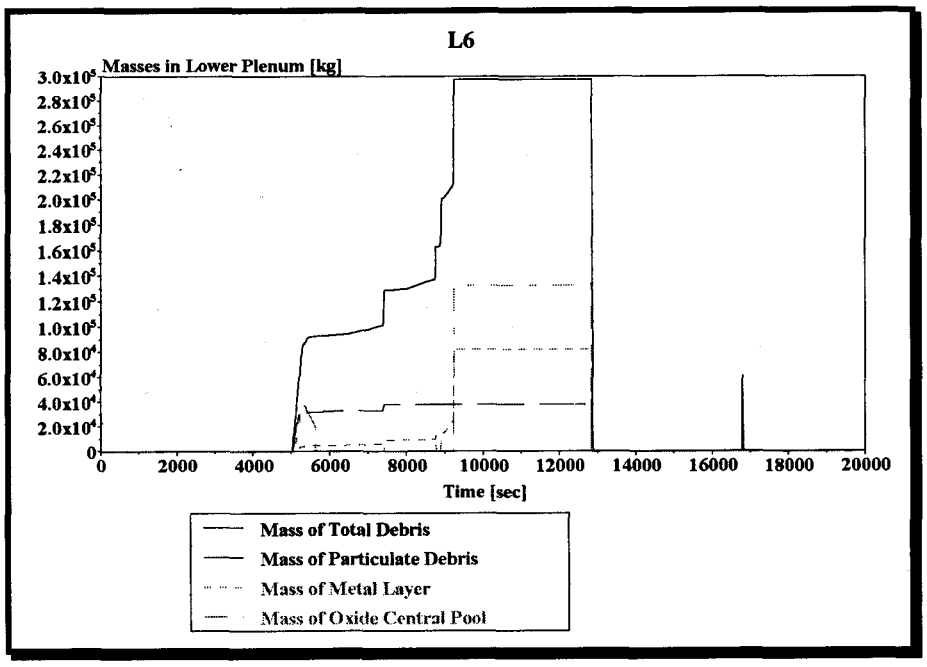

Figure 19. *Different forms of Debris in Lower Plenum Case L6.*

In case L6 the particle size was reduced further to ¼ of the default value, giving a mean particle size of 0.9 mm. This gave a violent oxidation of the entrained particles in the lower plenum, enough to melt half the entrained mass during the first 500 seconds of the relocation see Figure 19. The last batch of melt from the core region was relocated earlier than in the base case, which shows how sensitive the core relocation process is to the model parameters. The lower head experienced a short period of high temperature (1500 K) during the first debris relocation (at the time 5000- 6000

s), but was cooled down to about 1150 K before the lower plenum dried out (8000 sec). Thus, when the RPV wall started to heat up again after the dry out, it already was at an elevated temperature leading to an earlier creep rupture failure (by one hour) than in the base case L1.

In case L7 the default critical heat flux gap boiling model for in-vessel debris cooling was disabled. The case was almost identical to the base case L1. The total critical heat flux gap boiling is only about 25 kW between 8200 s and 9450 s accident time. Before 8200 s there is no gap and at 9 450 s the lower plenum became dry. It will be shown below that the gap CHF model does have a significant influence on the reflooding cases

A total of 7 low pressure scenarios with reflooding were calculated with MAAP4. The key input definitions and results are shown in Table 4 in B.2. It should be noted that cases 8-10 hadrefloding started prior to material relocations into the lower head and thus are not directly comparable with MELCOR studies.

In case L9 the system 323 core spray with 580 kg/s massflow was used for reflooding. This proved to be highly effective and cooled the core easily and fast. The similar SCDAP/RELAP calculation (case 7 in [25]) gave a similar result with a total H_2 generation of 118 kg in comparison to 80 kg according MAAP4 result.

In case L10 the system 323 downcomer injection mode with 580 kg/s massflow was used for reflooding. This cooled the core, but not as fast as the core spray. Oxidation for this case was also more effective than in the case with core spray reflooding, oxidation fractions 10.4 % and 3.3% , respectively. These observations are in line with the corresponding SCDAP/RELAP results (cases 7 and 8 in [25]), though the differences are stronger for MAAP.

Case L11 was calculated especially to compare with MELCOR calculation case 14. The particle size and the porosity of the particle debris bed were the same as in the MELCOR calculation. The reflooding mass flow was increased to 485 kg/s (compared to 340 kg/s used in the MELCOR calculation) to compensate for the different sizes of the Forsmark 3 and Olkiluoto plants. The debris configuration was easily coolable according to MAAP4, because the reflooding water could cool both the lower debris crusts and the RPV wall due to the CHF gap boiling model.

Case L12 was calculated to compare with MELCOR calculation case 7. The particle size and the porosity of the particle debris bed are the same as in the respective MELCOR calculation. The reflooding mass flow was adjusted to 485 kg/s like in case L11. The debris configuration was still coolable despite the late reflooding time. This shows the effectiveness of the gap CHF model in the reflooding scenarios.

Case L14 was identical with case L12, except for the disabling of the critical heat flux gap boiling model. The debris bed and lower head wall temperatures are shown in Figure 20. The temperatures of all parts of debris except for the metal layer started to decrease when the reflooding was initiated. The temperature on the lower head decreased during and after reflooding although not fast enough to avoid the creep rupture. The pressure increased in the vessel by the evaporation from the lower plenum pool, which increased the damage fraction.

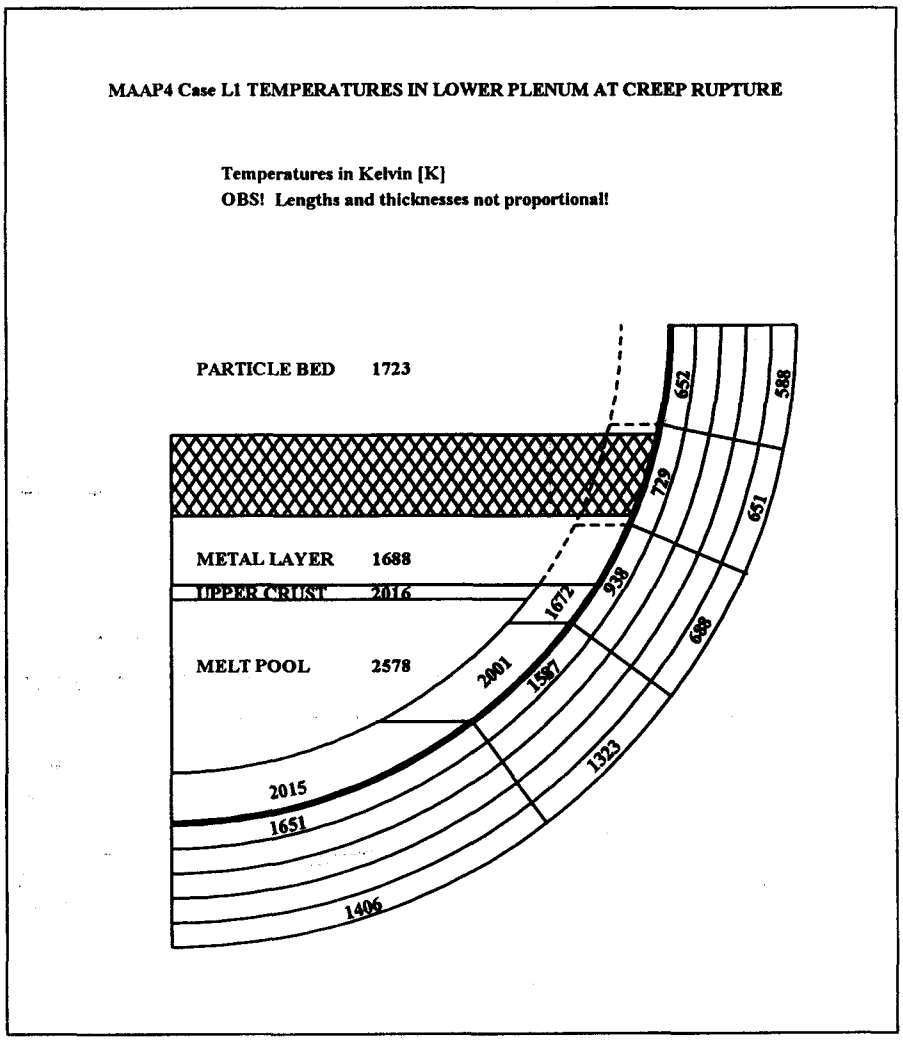

Figure 20. *Lower head debris and wall temperatures in F3 low pressure case (L1) at the time of creep rupture.*

7.2 Low Pressure Cases With Penetrations

If instrument tubes and lower head penetrations were modelled by the MELCOR code, the lower head failure occurred by instrument tube melt failure in multiple locations (radial rings 1,2, and 3) in the middle debris layer. In case 4 (Table 2)with debris porosity 0.45 and intermediate debris particle size (5 mm) the instrument tube melt failure occurred 13 minutes after lower head dryout. If the debris porosity was smaller (0.3) the instrument tube failure occurred about 57 min after lower head dryout. The main reason for the sensitivity to initial porosity is that in case of lower porosity the failure of only three radial core plate rings preceded the lower head dryout and thus the debris bed was better cooled at the initiation of the BH model.

The particle size affected also the instrument tube failure time. With the larger particles in case 12 (1 cm) the time gap from lower head dryout to instrument tube failure was doubled to 26 minutes compared to the case with 5 mm particles. In case 15 with 2 mm particles the time interval from lower head dryout to instrument tube failure was the longest, 1 h 10 min, but in this case, too, only three radial rings from the core region had slumped into the lower head prior to lower head dryout. However, all core support plate rings had failed before instrument tube failure (the time window

between the last 'debris batch' to arrive at the lower head and the failure of instrument tube in layer 2 was ~31 minutes).

Reflooding of the lower head debris bed after lower head dryout and initiation of the BH model could not prevent the failure of instrument tubes. On the contrary it made the instrument tubes fail earlier than in the dry base cases. The reason for faster temperature augmentation in the debris bed was oxidation. This conclusion is supported by the fact that the fastest instrument tube failure was reached in cases, where the debris porosity was high at the start of water injection (i.e. cases with early start of reflooding). Augmentation of reflooding capacity from 45 kg/s to 340 kg/s enhanced the oxidation and caused an even earlier instrument tube failure. The oxidation was efficient independent of the selected particle size. The Zirconium oxidation fraction in reflooding cases was 47 ... 75 % whereas in non-reflooding cases it was 16 %.

The MELCOR lower head nodes that were selected for detailed investigations with PASULA are illustrated in Fig 21. In the centre nodes the welds are embedded in the metallic bottom layer and the instrument tube is located in the hot upper layer, whereas the instrument tube welds locate in the hot centre layer in the periphery of the lower head hemisphere. The temperature and porosity histories of the melt in each node were extracted from the MELCOR/BH output. The time and composition dependent material properties (heat conductivity, specific heat capacity) were calculated for each node taking into account the changing node composition and temperature.

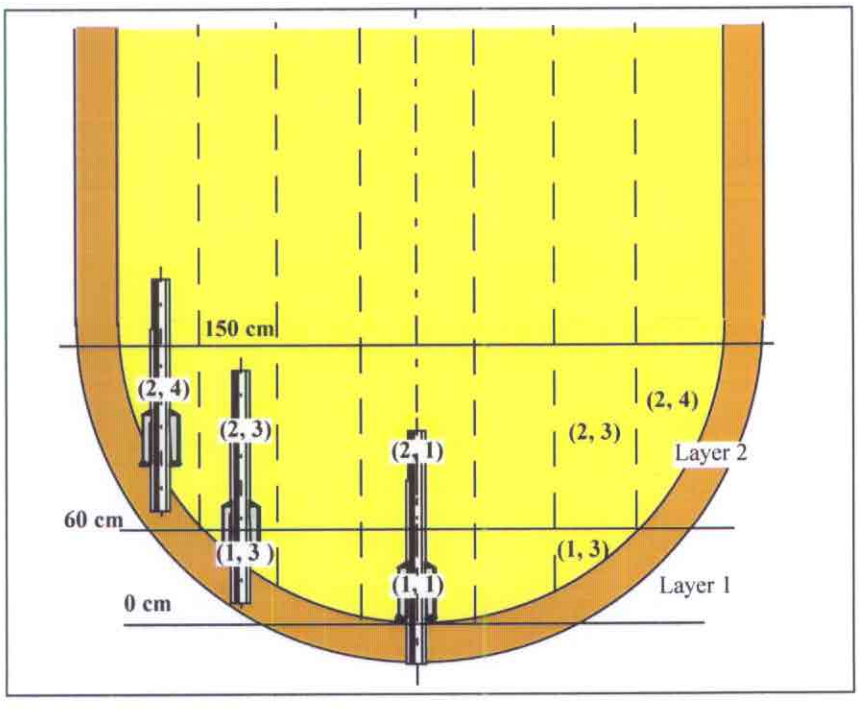

Figure 21. *Nodes in MELCOR analyses and three locations for analysed penetrations.*

The debris temperatures within in a node in the vertical direction between the two calculation nodes are linearly interpolated. For the penetration located in the nodes (1,1) and (2,1), the centre of the lower node (1,1) lies 0.3 m from the bottom of the vessel and the centre of the upper node (2,1) 1.05 m from the bottom. The penetration located in the nodes (1,3) and (2,3), the centre of the lower node (1,3) is assumed to lie 0.15 m from the vessel surface and the centre of the upper node (2,3) is then 0.75 m from the surface. For the penetration in the node (2,4) there is only one temperature value and no interpolation is applied.

Axisymmetric models are correct, when the penetration lies in the nodes (1,1) and (2,1). In other locations of the penetrations (nodes (1,3) and (2,3) or (2,4)) the penetrations are not perpendicular to vessel wall (Fig. 21), but obliquely attached. Axisymmetric models are only approximate in this case and a comprehensive analysis would need a 3-dimensional approach.

The calculations were performed using a finite difference/volume based computer code PASU2D developed at VTT Energy. The colour plottings were produced by a code VISU2D developed also at VTT Energy.

The strength of corium is assumed to be lost at 2000 K. This value, which is not based on any reference or validation, is only used for illustrating zones in colour plottings. Fig. 22 shows colour scales for different materials. Black colour means transition zone, where the strength of the material is lost (Fig. 10). For corium 2000–2500 K is not a zero strength zone, but it is chosen only for showing temperature 2000 K. Pink colour means transition zone from liquid phase to solid phase.

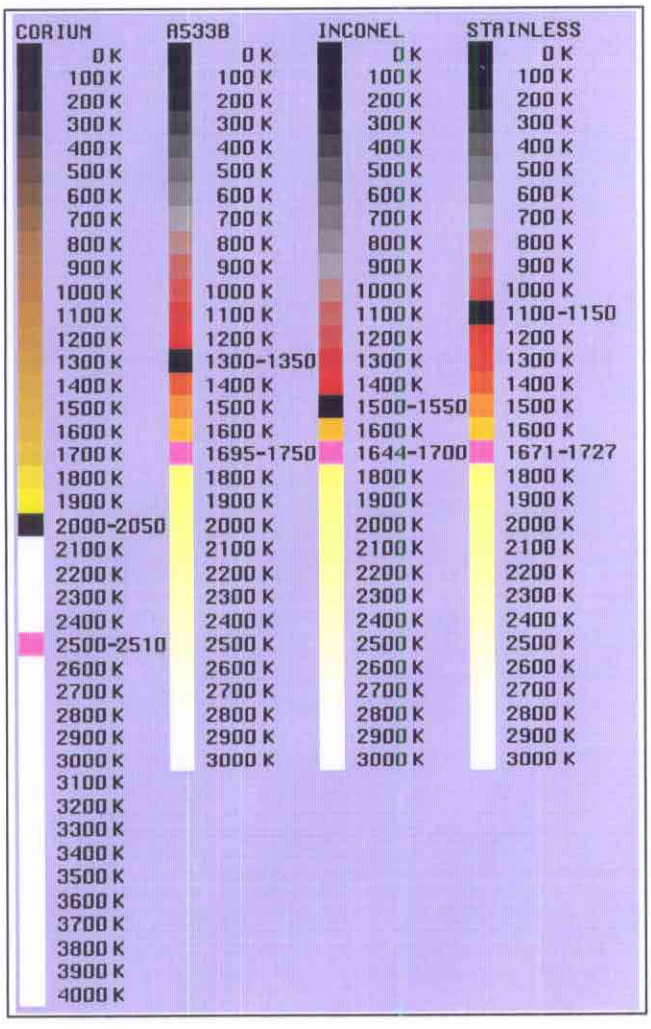

Figure 22. *Colour scales for different materials.*

7.2.1 Control Rod Nozzle

The most critical part of a control nozzle concerning the corium is the thermal sleeve tube above the carbon steel nozzle inside debris bed and the weld.

PASULA calculations for control rod nozzles showed that the strength of the control rod shaft of stainless steel is lost in 5000 s only in case, when the nozzle lies in the node (2,4). Figures 23-28 illustrate the material temperature histories in a control rod nozzle located at the periphery of the lower head hemisphere. The figures are scaled wider in the horizontal direction to get the temperature fields clearer.

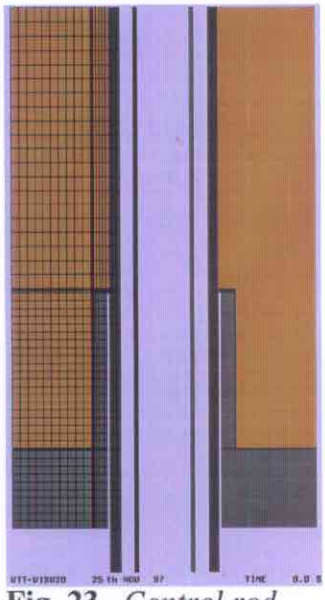

Fig. 23. *Control rod nozzle in the node (2,4) at 0 s.*

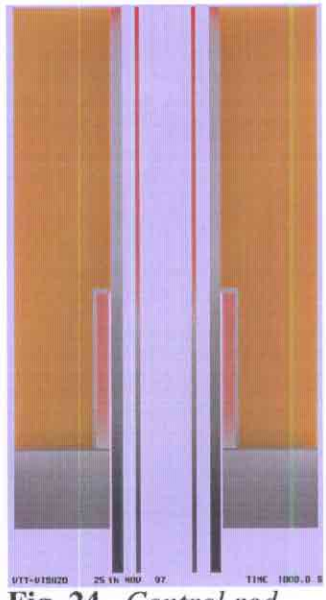

Fig. 24. *Control rod nozzle in the node (2,4) at 1000 s.*

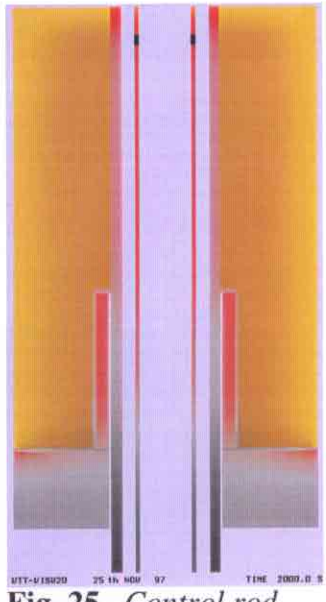

Fig. 25. *Control rod nozzle in the node (2,4) at 2000 s.*

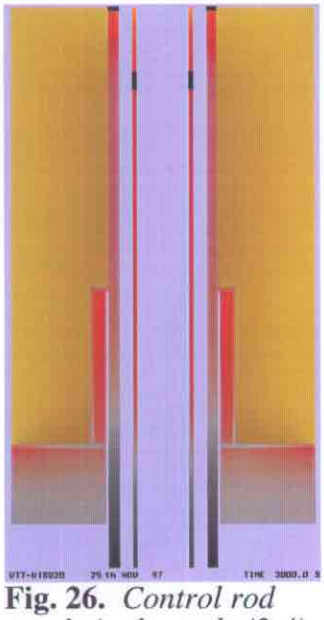

Fig. 26. *Control rod nozzle in the node (2,4) at 3000 s.*

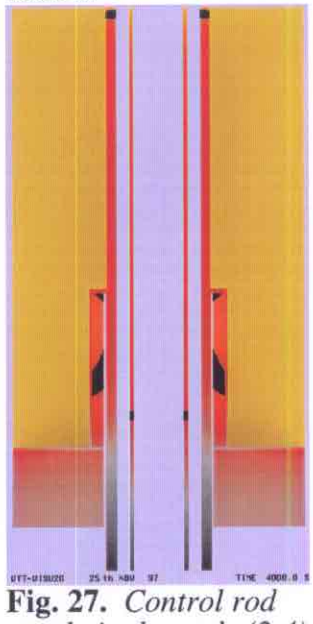

Fig. 27. *Control rod nozzle in the node (2,4) at 4000 s.*

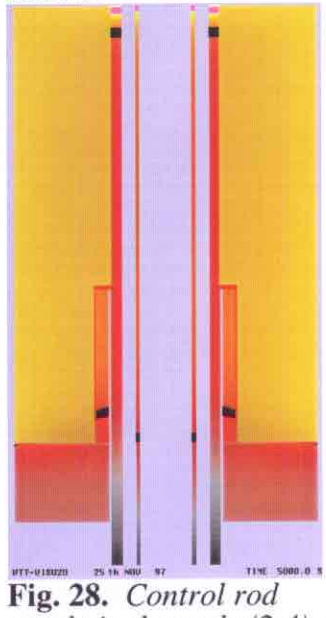

Fig. 28. *Control rod nozzle in the node (2,4) at 5000 s.*

Based on the PASULA results it can be concluded that the ejection of a control rod tube is not probable. Only the outer ring control rod support welds failed and since the control rods are connected to each other via a common tieplate, the intact control rods will be able to provide support to the failed ones. In a single control rod guide tube the corium flowing in the tube will

refreeze and block the tubes below the RPV. In absence of horizontal forces a large corium leakage through the control rod nozzle is not likely.

7.2.2 Instrument Tube Nozzles

The most critical part concerning corium leakage is the detector housing tube above the carbon steel nozzle and the weld inside debris bed. The plottings are scaled wider in the horizontal direction to get the temperature fields clearer.

Calculations with PASULA suggest that the instrument nozzle welds in the nodes (1,1) and (2,1) or (1,3) and (2,3) do not melt in 5000 seconds. Instrument tube in these nodes lose their strength in the part above the critical weld. Figures 29-34 show that for the instrument nozzle in the node (2,4), the zero strength zone of stainless steel passes through the weld at time between 3000 s and 4000 s.

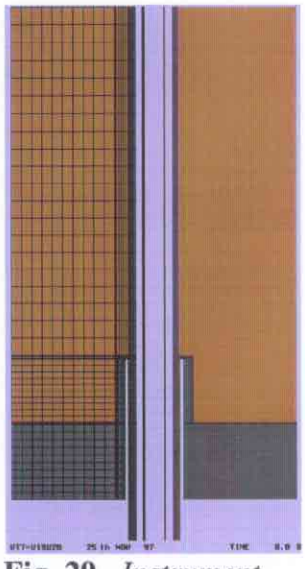

Fig. 29. *Instrument nozzle in node (2,4) at 0 s.*

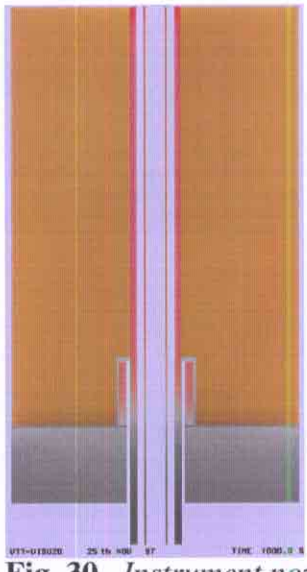

Fig. 30. *Instrument nozzle in node (2,4) at 1000 s.*

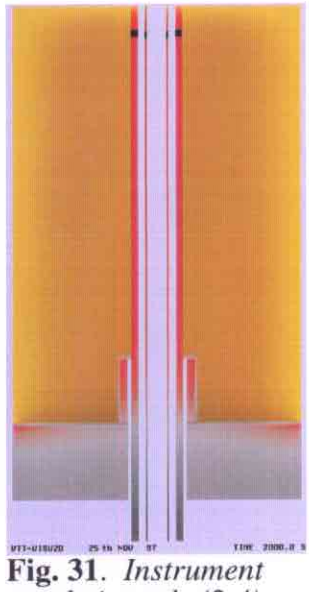

Fig. 31. *Instrument nozzle in node (2,4) at 2000 s.*

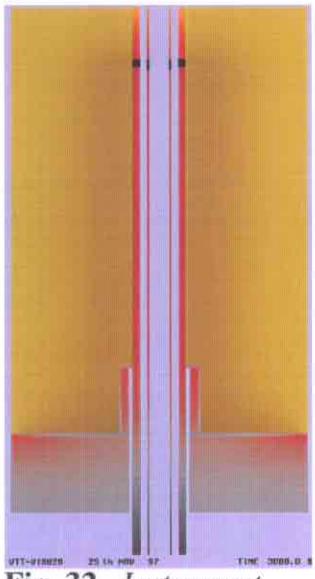

Fig. 32. *Instrument nozzle in node (2,4) at 3000 s.*

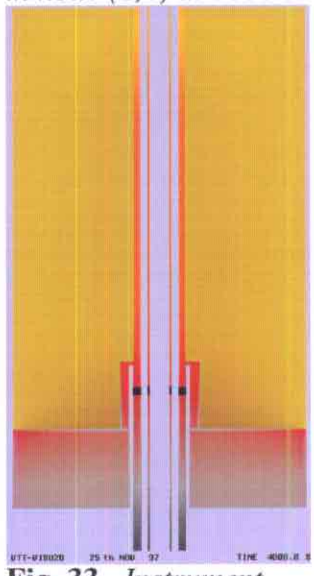

Fig. 33. *Instrument nozzle in node (2,4) at 4000 s.*

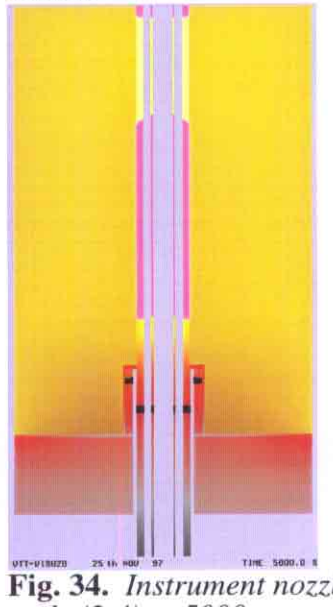

Fig. 34. *Instrument nozzle in node (2,4) at 5000 s.*

As a result the detector housing tube would drop downwards. However, the detector housing tube relocation may stop at the level of the flow limiter.

The detector housing tube is the most critical part of an instrument nozzle when considering corium leak through an instrument penetration. An internal pressure of 6 bar causes a vertical force of 2 400 N to the tube weld. The most critical point is the detector housing tube wall just below the weld. This is because the tube wall is made of stainless steel and the weld of INCONEL 82. The inner diameter of the tube is 45 mm and the pressure load 950 N. The weight of the detector housing and instrument casing tubes is about 2 000 N. Thus the total vertical force is about 2 950 N and the stress in the wall of the detector housing tube 0.94 MPa.

There is no pressure difference over the detector housing tube wall above the weld. However, the margin to liquid temperature of stainless steel is small throughout the wall. Thus it is justified to assume that liquid stainless steel flows downwards due to gravity and liquid corium fills the annular space between tubes.

The instrument tubes contain a flow limiter located 169 mm below the inner surface of the vessel bottom. The gap between the flow limiter and detector housing tube is about 0.25 mm. There is a possibility that downward flowing corium heats up the detector housing tube to such an extent that the tube expands against the flow limiter and friction prevents the tube ejection. In that case the tube will fail later below the vessel if the corium fills the tube annular space.

The analyses suggest that lower head is failed due to instrument tube weld failure at the outer boundary of the lower head hemisphere. The instrument nozzles located closer to the centre of the cylinder axis are more likely to maintain their integrity. The timing of the instrument tube failure is 3000–4000 s from the lower head dryout. This is a significantly longer time than predicted by MELCOR BH model (780 s).

The estimated failure time is much longer than in the cases previously calculated with the PASULA code [12] with a large melt mass and higher superheat. The assumptions used in the MELCOR modelling have a significant role in determining the delay: partial quenching of the debris during relocation was predicted, and debris heat-up was assumed to begin only after dry-out of the lower head debris.

The analyses refined the previous results concerning the initial pressure vessel failure location, i.e. the most probable place will be an instrument tube in vessel periphery. The subsequent failure propagation will be determined by the amount and composition of the molten debris and of the superheat the melt carries.

7.3 High Pressure Cases Without Penetrations

7.3.1 Olkiluoto Calculations

In the base 21 case the debris material from three out of five radial core rings resided in the lower plenum at the time of lower head dryout. The debris temperatures were low at the time of dryout due to quenching during the fall-down (Fig. 35). The last two support plate radial rings failed 28 min and 62 min after lower head dryout. Debris temperatures increased and material started to melt and flowed downwards. The porosities of layers 1 and 2 became small.

The debris bed composition at the time of lower head dryout is shown in Table 5. Due to efficient oxidation during core uncovery the debris arriving at the lower head contains more oxides than the respective low pressure case (cf. Table 3).

Table 5. *Lower head debris composition at dryout. High pressure case 21.*

MATERIAL	LAYER NO 1.		LAYER NO. 2		LAYER NO. 3		ALL LAYERS	
State	solid [kg]	liquid [kg]	solid [kg]	liquid [kg]	solid [kg]	liquid [kg]	solid [kg]	liquid [kg]
Zr	1584	0	7474	0	2095	0	11154	0
Fe	5702	0	8523	0	13478	0	27702	0
Cr	1387	0	2073	0	3278	0	6738	0
Ni	616	0	921	0	1457	0	2995	0
B_4C	68	0	68	0	31	0	167	0
ZrO_2	690	0	10927	0	2687	0	14304	0
FeO	77	0	1100	0	272	0	1449	0
Cr_2O_3	21	0	304	0	75	0	400	0
NiO	8	0	118	0	29	0	155	0
UO_2	3198	0	47624	0	11755	0	62578	0
Totals	13353	0	79131	0	35160	0	127644	0

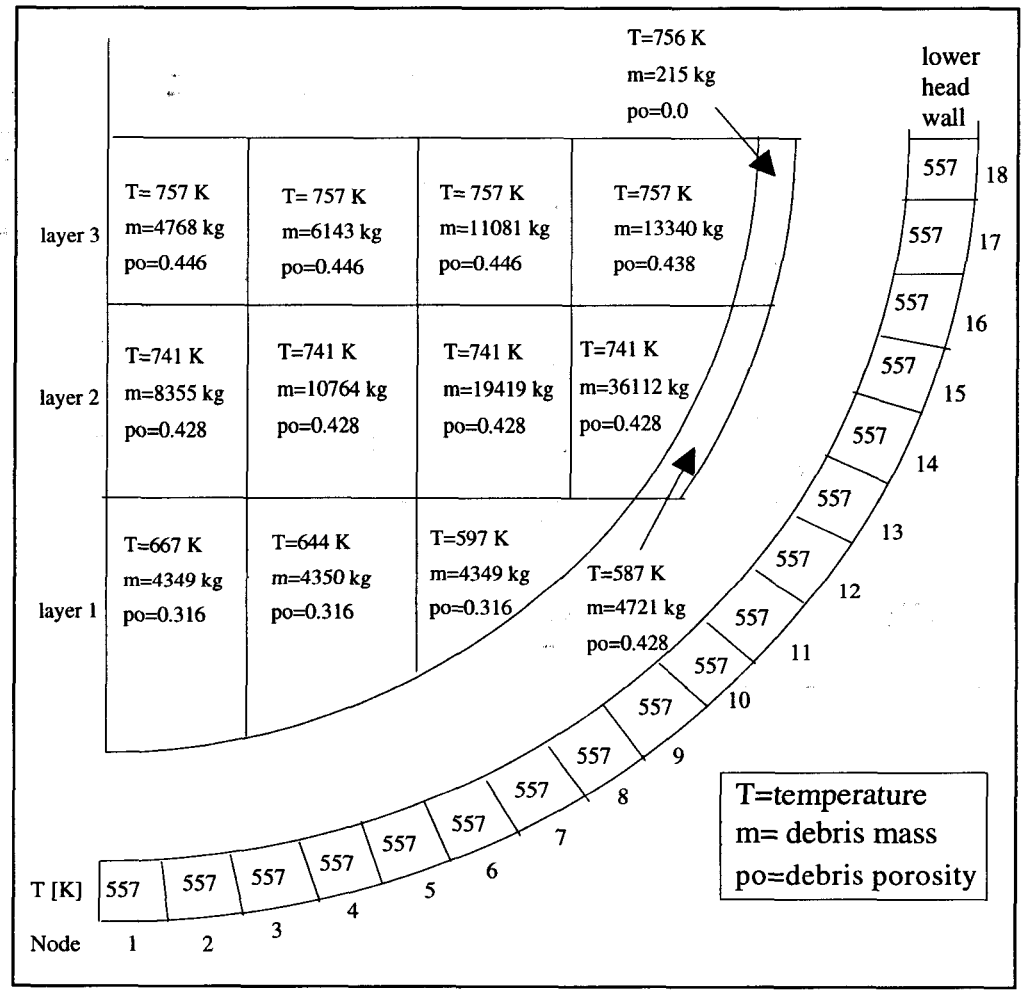

Figure 35. *Debris bed temperature, mass and porosity at lower head dryout. High pressure case 21, no lower head penetrations.*

The vessel wall temperatures increase slowly and the pressure in the vessel remains at about 70 bar. Creep rupture criteria is reached 3h 15 min after lower head dryout (at 6 h 33 min accident time) in the wall node 15 having an average temperature of 1061 K (Fig. 36). All remaining debris in the lower head is transferred to the drywell.

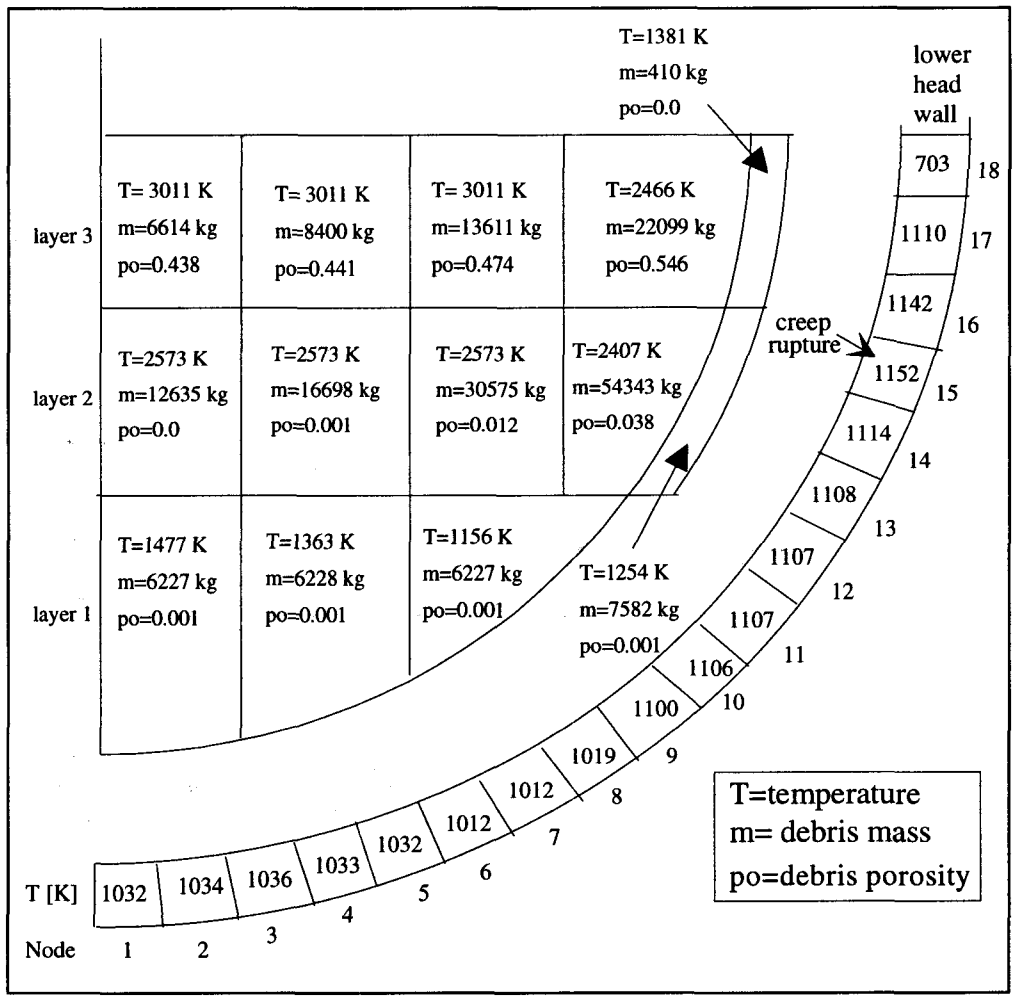

Figure 36. *Lower head debris characteristics and inner surface wall temperatures at time of local creep rupture. High pressure case 21, no reflooding.*

Two reflooding variations were run to investigate the debris bed coolability. In the first variation (case 22) reflooding was started just after lower head dryout. This was the only case in this study, where lower head failure was avoided. In this case the lower head was reflooded before the debris bed had reheated and all additional hot material from the core region slumped into the water pool and slowly quenched. Another case (23) was run where reflooding started 34 minutes after lower head dryout. In this case one additional core ring had failed prior to start of reflooding and debris temperatures became higher. Despite of a trend of slow cooling local creep rupture occurred 2 h 47 min after lower head dryout in wall node 7 with an average temperature of 1050 K. The state of lower head just before creep rupture in case 23 is shown in Fig. 37.

The maximum debris temperature in the lower head in cases 21, 22 and 23 is shown in Figure 38. The temperature 'flat period' at 2573 K in the base case and in case 23 is due to melting of ZrO_2-UO_2 eutectic mixture. Molten material moves down (to cooler regions).

The Zirconium oxidation fraction in reflooding cases was high 71-88 %.

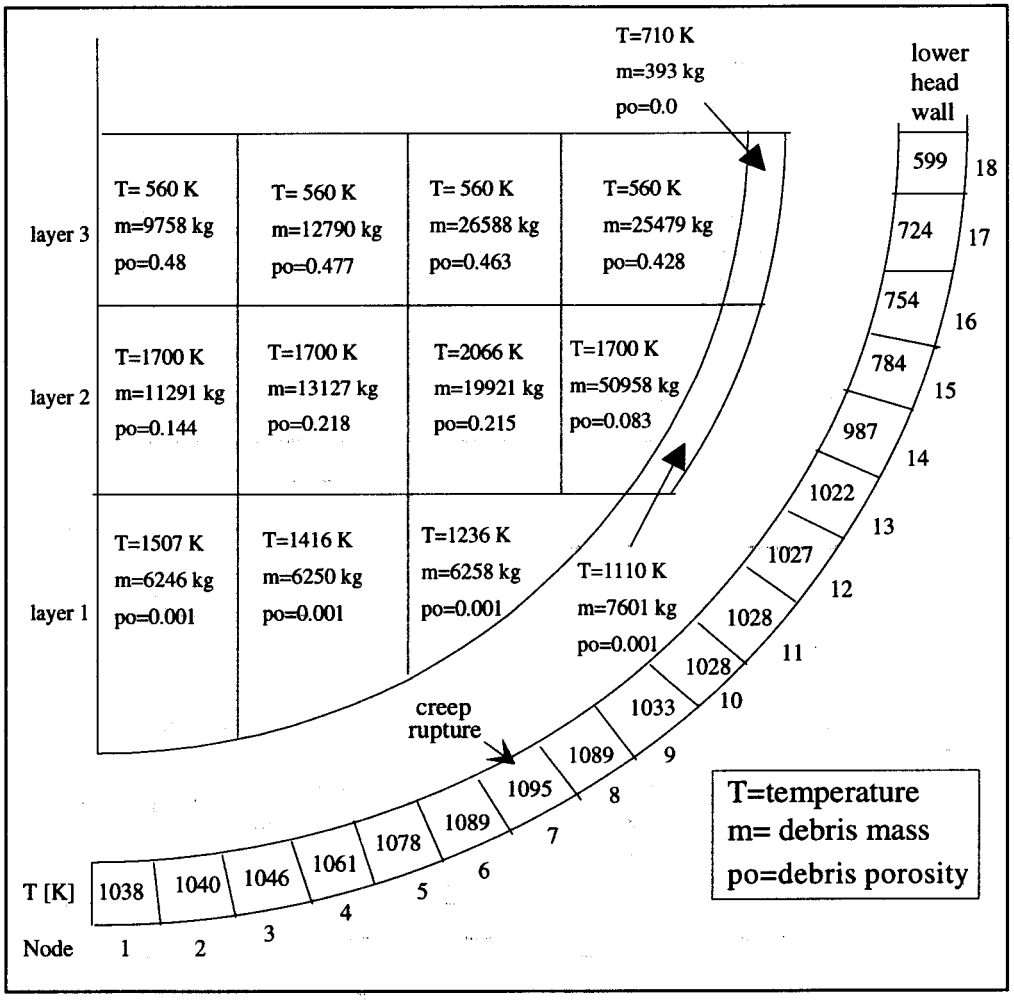

Figure 37. *Lower head debris temperatures, masses and porosities and inner surface wall temperatures prior to creep rupture. High pressure case 23, no penetrations, reflooding starts 34 minutes after lower head dryout.*

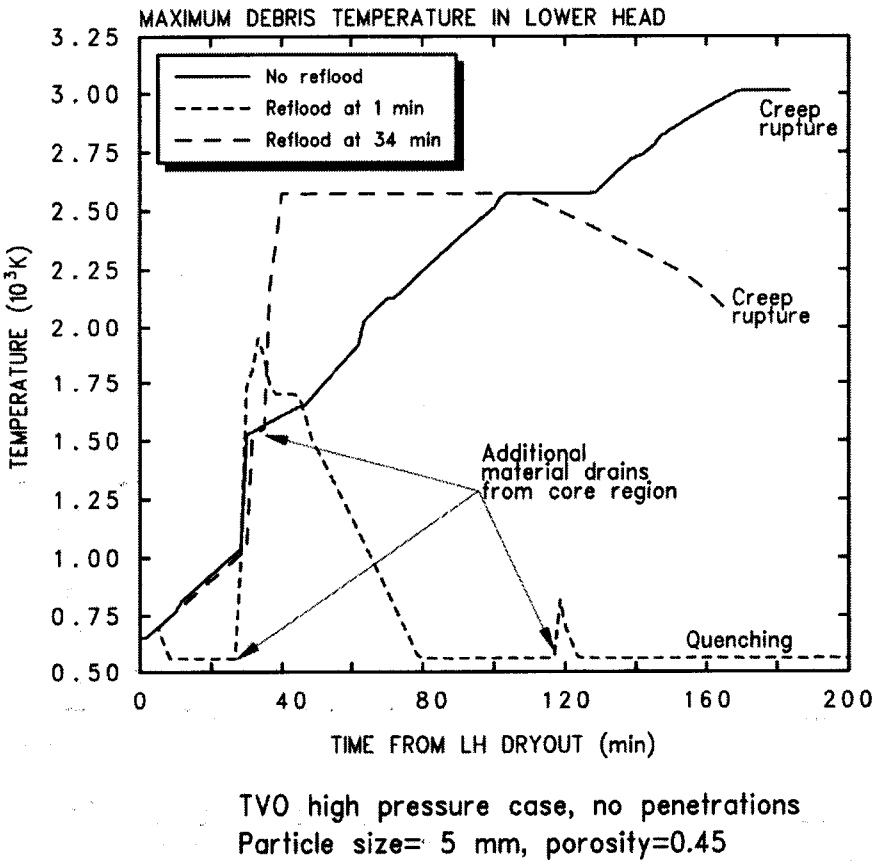

Figure 38. *Maximum debris temperature in the lower head. High pressure cases 21, 22, 23. No penetrations.*

7.3.2 Forsmark Calculations

The calculated high pressure cases of Forsmark 3 with timing of key events are shown in Tables 5 and 6 of Appendix B.3.

In the high pressure base case H1 all input parameters were set to their default values. The core uncovery started at 1240 s and was totally uncovered at 1 h 45 min (6 270 s, Fig. 39). The first material relocation to lower plenum was almost totally entrained (into particles). Particulate debris is formed only when the water pool on top of the debris is more than 1 meter high. The lower plenum debris bed dried out at 2 h 47 min (1 h 2 min after support plate failure). The debris bed and vessel wall temperatures at the lower head dryout are shown in Fig. 40. The heatup of the debris commenced after lower head dryout leading to melting of particulate debris ~ 20 minutes later. Major steel additions started 25 minutes after lower head dryout, when the lower head steel structures reached their melting point.

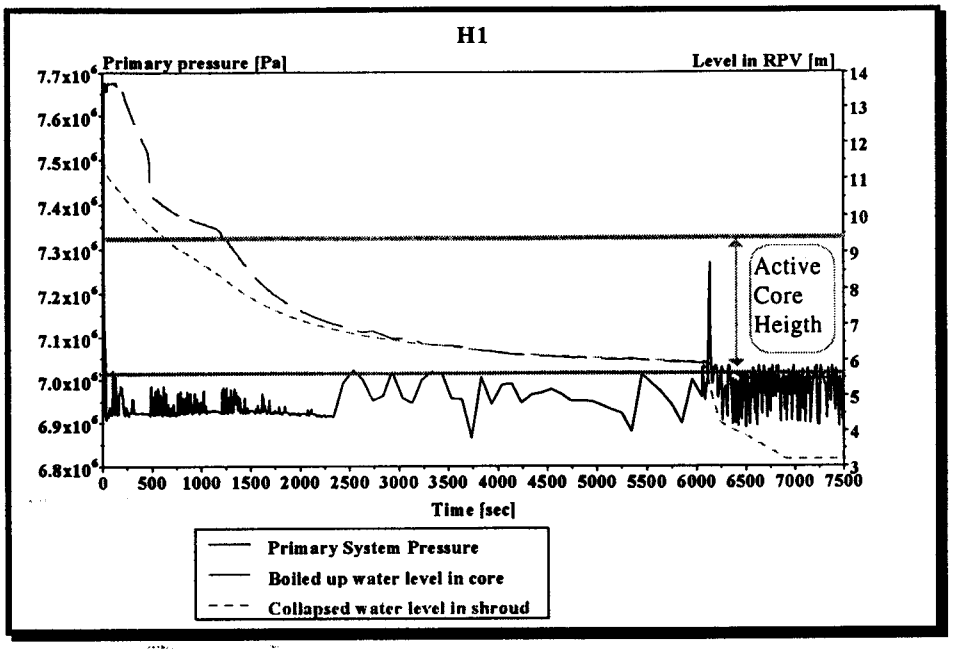

Figure 39. *Pressure and water levels in RPV, water level relative to bottom of RPV.*

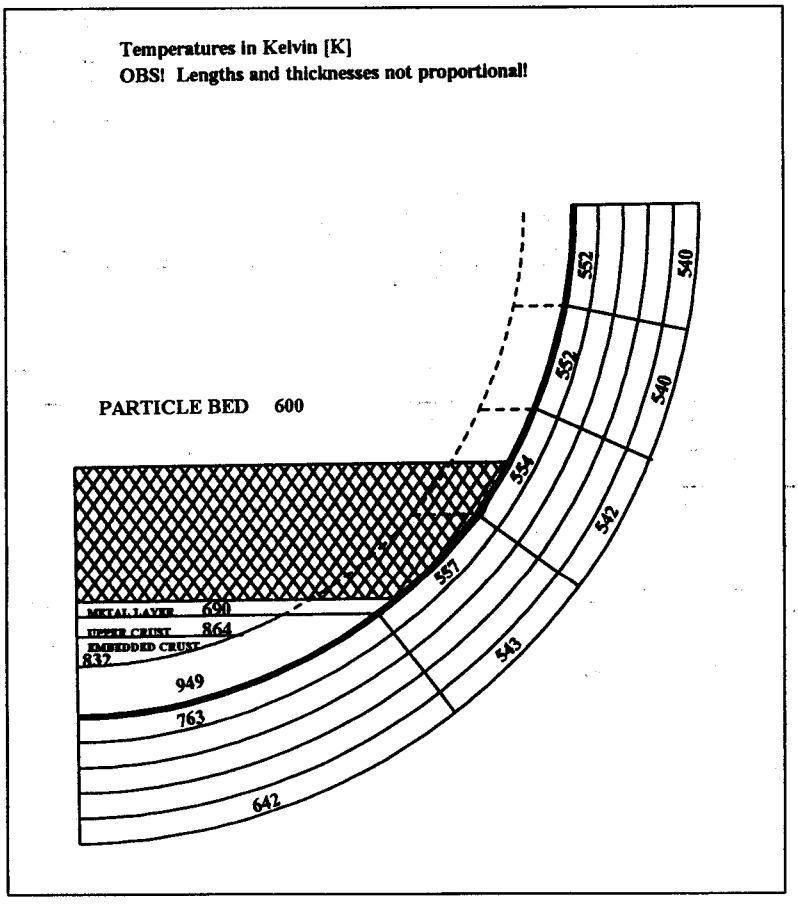

Figure 40. *Debris temperatures in the high pressure cases at the time of lower head dryout. MAAP4 prediction for Forsmark 3.*

Over the next 1000 sec 6 tons out of 152 tons of the molten pool solidifies on the upper and lower crusts. When the creep rupture in the lowest node 1 occurs at 3 h 41 min into the accident the total debris mass of 294 tons in the lower head has the following composition:

Particulate Debris	5 %
Metal Layer	29 %
Oxide Central Pool	50 %
Debris Crusts	16 %

The temperatures of the debris bed and the lower head wall are shown in Fig. 41.

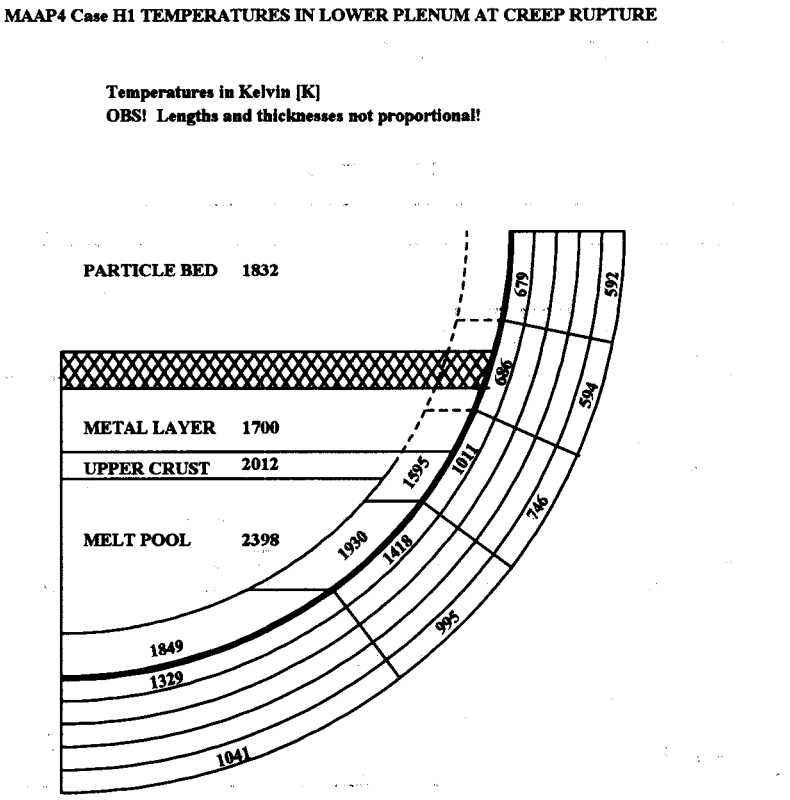

Figure 41. *Temperatures in the lower plenum at time of creep rupture in node 1 at the bottom. Forsmark high pressure case. RPV wall and upper and lower debris crusts thickness are exaggerated.*

In case H2 the fraction of plate critical heat flux for lower head debris quench was decreased. This meant that less water can ingress into the debris bed. In contrast to case H1 a gap is created between lower crust 1 and the lower head wall, but the lower plenum dried out only some seconds later. Hence, the heat removal from the crust and RPV wall due to the gap boiling had no significant influence.

In case H3 the entrainment coefficient of the debris jet from the core to the lower plenum was decreased. The resulted in much less debris jet entrainment to particles during relocation from the core. That in turn decreases the steam generation, and subsequently oxidation, in the lower plenum. A gap formed between lower crust and the lower head. This decreased the heat flux from the crust to the lower head. The creep rupture occurred shortly after that the remaining core material relocated at 4 h 5 min.

In case H4 the default value for the particulate debris bed porosity (0.4) was changed to 0.3 for sensitivity studies. The differences in comparison to the base case H1 were negligible.

In case H5 the entrained particle size was reduced to half the size. The first noticeable effect of the smaller particle size was that the oxidation and melting of the particles was enhanced. When the particle size was decreased further to ¼ (0.9 mm), a violent oxidation of the entrained particles in the lower plenum took place. The oxidation energy was high enough to melt almost half the entrained mass during the first 500 seconds. The particle bed mass was 31 tons compared to 55 in the base case H1. Nevertheless, the lower plenum dried out half an hour earlier than in the base case. A gap was created between lower crust 1 and the RPV wall, but since the lower plenum dried out so early, the gap boiling heat flux did not have much effect. The creep ruptureoccured in node 1 at 3 h 29 min. The damage fraction in node 2 indicated that a creep rupture also in node 2 was close.

As an alternative to the default assumption to material layering in the lower head, MAAP4 provides a user option to model all materials as a mixed pool. When compared with the base case calculation, the mixture pool model resulted in slightly faster water boil-off in the lower plenum. More important a gap was created between the lower crust 1 and the lower head node 1 almost immediately after core plate failure. Due to the gap critical heat flux lower head node 1 was cooled down. When the lower plenum dried out, the lower head node 2 had a significantly higher temperature than the node 1, and hence the creep rupture occurred in node 2.

The high pressure cases were calculated for comparison with earlier SCDAP/RELAP calculation (H8) and to study the time window for successfully saving the RPV from creep rupture by reflooding. The calculated cases and the key results are shown in Table 5 of Appendix B.3.

Case H8 was similar with the former SCDAP/RELAP calculation (case 6) in [25]. The criterion for starting the core spray (system 327) was the peak cladding temperature reaching the temperature of 1800 K. The reflooding in MAAP4 run started at 3560 s compared to 4370 s in the respective SCDAP/RELAP calculation, the boiled up water level in the core was the 0.7m (0.5m in SCDAP/RELAP run). Oxidation was enhanced at the start of reflooding, the temperatures increased and the melt fraction in the core increased. After reaching the peak values about 100 s after start of reflooding all these parameters started to decrease. The last part of melt present in the core seemed hard to cool down. The end time of the sequence was extended from 20 000 sec to 50 000 s but there was then still ~3 200 kg of melt present in the core. The corresponding SCDAP/RELAP results gave much less oxidation and cooled the core without any major fuel damage.

In the high pressure base case the creep rupture of the RPV occurred at 3 h 41 min. Case H9 was calculated to see, if the RPV can be saved by reflooding 10 minutes before the anticipated creep rupture. Although the temperatures on the RPV lower head slowly started to decrease at the start of reflooding, the increased stress on the RPV wall had a large effect and caused the creep rupture.

In case H10 the reflooding was started 20 minutes before the anticipated creep rupture. This was early enough to avoid creep rupture in the studied high pressure scenario. The main reason for the suggested possibility to save the RPV with reflooding so late in the accident is, the assumed formation of a gap between the lower crusts and the RPV wall. This gap gives very effective cooling of both the RPV wall and the lower crusts by the gap critical heat flux boiling.

7.4 High Pressure Cases with Penetrations

Penetration failures in high pressure case were calculated only with MELCOR. Due to resource limitations PASULA analyses were not extended to high pressure scenarios.

In high pressure cases relocation of only 3-4 radial core rings into the lower head preceded lower head dryout. The debris mass to coolant mass in the lower head was smaller and thus better quenching was achieved during fall down of material from the support plate. Due to slow coolant boil off during core heatup more Zirconium was oxidised in the original core boundary (57 % of Zr oxidised in core region) and thus the material entering the lower head was more oxidic than in the low pressure cases.

The heatup of initially well cooled debris layer 3 up to about 1670 K takes a longer time than in the low pressure cases. With the initial debris porosity of 0.45 the instrument tubes reach the failure temperature (~ 1670 K) in 1 h 17 min. If the porosity was lower, 0.3, the instrument tube failure occurred earlier in 55 minutes from the lower head dryout.

As in low pressure cases the reflooding of dry debris bed produced hydrogen which resulted in earlier instrument tube failure (6-9 minutes after start of reflooding). The Zirconium oxidation fraction in the lower head was high, about 80 %.

A detailed summary of the key results in the calculated MELCOR cases 1-23 are shown in Table 2 of Appendix A.2.

8 EVALUATION OF RESULTS

The evaluation of the results in this report focus on reviewing different publications on the experimental and analytical research performed in the field. In particular, it is important for this study to evaluate the appropriateness of the different key parameters affecting the results.

The late phase melt progression is affected by core melt progression in the core region, the performance of the core support plate and interaction of water and hot material falling through the lower head water pool and eventually the thermal response of lower head penetrations and reactor pressure vessel wall. Water injection into the partially damaged core or to the debris bed in the lower head will affect the accident progression as well.

Core melt progression in the core region will not be addressed in this report. This evaluation will concentrate on issues related to relocation of debris from the core region into the lower head and subsequent debris bed formation and evaluation of the pressure vessel failure mechanism. In the following a division of the lower head phenomena into three phases is made: first the period of melt slumping into the lower head water pool, second the formation of the lower head debris bed until the lower head dryout and third the period from dryout to vessel failure.

8.1 Relocation of Corium to the Lower Head

When comparing the results of MAAP and MELCOR the timing of the support plate failure differs significantly, particularly in the low pressure case. According to MAAP4 the time to support plate failure was 65 - 100 min for the low pressure cases and 100 - 150 min for the high pressure cases. The respective support plate failure times in the MELCOR calculations were 269 - 326 min in low pressure cases and 160 - 177 min in high pressure cases. The most likely reason for the large differences in the low pressure 'dry core' scenario results is the following: after activation of the MELCOR model for chemical reaction of steam and B_4C, the control rod melting occurs substantially earlier than the fuel relocations. The core support plate nodes are blocked with refrozen steel debris, when the oxidic debris reaches the bottom core nodes. Heat is tranferred downwards by axial conduction from relatively hot oxidic debris, and according to the current MELCOR model this heat transfer mechanism works slowly to heat up the steel mass to the specified failure temperature in the lowest core nodes. In the MAAP4 analyses the relocating melt is a mixture of oxides and metals and also usually at higher temperature than in the MELCOR predictions. These conditions enhance the heating up of support plate structures. The significantly smaller differences in support plate failure timing in the high pressure ('wet core') cases, could consequently be explained by the fact, that in wet core cases the in-core oxidation is the key heat source driving the core degradation. The fuel heatup occurs rapidly in the uncovered part of the core resulting in the very small time gap between the steel debris and the oxidic debris relocations. In the high pressure cases the support plate node is filled with debris containing a significant amount of internally heated oxidic debris. The support plate material reaches the defined failure temperature earlier. This also could explain the large time difference between the support plate failure times in the earlier low pressure MELCOR runs [25] and the calculations performed in this study: in the earlier studies the chemical reaction between B_4C and steam was precluded by input option. In those calculations the time window between the control rod and fuel relocations was very small, and the debris in the support plate node contained large fraction of UO_2. Both MAAP4 and MELCOR have simple, parametric models for estimation of the onset of material transport to the lower head, which is justified considering the complexity of the phenomenon and the primary purpose of the two codes. Although the MELCOR prediction for the support plate failure time seems unrealistically long for the reason proposed above, the results after the material relocation to

the lower head could be evaluated and could be deemed to give some insight to the thermal and structural behaviour of the debris bed and the lower head.

The models of debris transfer from the support plate into the lower head in MELCOR and MAAP4 are very different. MELCOR assumes that all debris is entrained to particles with a specified size . MAAP has a simple model for how much of the relocated mass is entrained into particles depending e.g. on the water depth and a model to calculate the size of the entrained particles. Another observation from the MAAP calculations is the relatively strong coupling between the phenomena in the lower plenum and the relocation pattern. This applies also to the MELCOR model. Differences in particle size and debris porosity in the lower head affects the core relocation sequence.

Considering the disparate late phase melt progression results obtained with different codes when trying to simulate the TMI-2 accident, the disparities for the present BWR simulations might be expected. They are partly the result of deviations in the early phase core degradation propagated to the late phase. This includes differences in blockage formation and debris migration in the lower core region prior to the core plate failure.

None of the codes followed the TMI-2 like 'wet core' path in the high pressure cases as was hypothesized in connection with the XR experiments (cf. Chapter 3, Fig. 2). It is interesting to note that core pool formation and side crust failure as in TMI-2 could be achieved with MAAP4 in some of the early reflooding cases considered previously [25]. If the TMI accident had progressed further without reflooding, the question is whether total dryout of the core would have led to remelting and downward migration of the lower crust, eventually leading to core plate failure (before side crust failure). This would be analogous to the progression in the present high pressure cases. The MP experiments are insufficient to answer that question.

Core plate failure is based on a simple temperature criterion (1500 K) in both codes. Due to the coarse radial partitioning the relocation occurs in a stepwise fashion with large mass relocations at each 'support plate failure' in the five regions. At the time of core plate failure the debris was partially molten. However, the debris is allowed to accumulate in each individual region and relocate at the respective core plate ring failure. Cross-flow of molten material between the regions was simulated on the basis of input specified time constants (uncertain due to lack of experimental basis). The relocating debris with temperatures of ~ 2200 - 2900 K, was constituted by molten metals and particulate or molten ceramics.

Obviously, the stepwise relocation is a discretization effect that does not have any physical connection with the temporary blockages followed by abrupt drainages of molten metal as observed in the XR-2.1 experiment. With many parallel flow channels through the core plate such blockages seem unlikely to occur simultaneously, so the continuous flow path (Fig. 2) seems a realistic low pressure scenario. In that case, the designation 'core plate failure' looses its original meaning (in a double sense, since ABB reactors have no continuous core plate). A description of a mechanistic core plate failure model [30] shows that originally this concept was literally understood as temperature-dependent tensile stress failure of the GE core plate, whose flow pathways via the fuel support pieces were assumed plugged by previously frozen Zircaloy and steel. For the ABB reactors the individual control rod guide tubes with their respective core support pieces may collapse earlier, when they are weakened by draining molten metal. The remaining rubblized ceramics are envisaged to relocate more or less continuously as the guide tubes collapse.

8.2 Quenching in Lower Head Water Pool

Both MAAP4 and MELCOR calculations gave a quenched or partially quenched state of debris for the first material relocations from the core. In the MAAP4 predictions all the debris was quenched in the lower head as long as there was water left in the lower plenum. In the MELCOR results the later debris relocations were only cooled, not quenched.

The key assumption in the MELCOR model is, that the falling core material becomes fully fragmented by quenching in the lower head. The debris particle size and initial porosity are important input parameters that were selected based on fuel fragment sizes and experience from the CCM and FARO experiments as previously described. The quenching/cooling of the particles is calculated by the code on the basis of a specified average heat transfer coefficient over a time range that extends beyond normal settling times to include cooling in the bed corresponding to the cooling period in the experiments. This is achieved by using the recommended fall velocity of 0.1 m/s (irrespective of particle diameter), i.e. smaller than the terminal velocities in the CCM tests (~0.33 to 0.4 m/s). However, the selection of appropriate input values is a difficult problem. The minimum porosity for Lipinski's dryout heat flux correlation can be redefined as model sensitivity coefficient.

Another important issue in debris relocation into lower head is the heat transfer and quenching in the lower head water pool. In MELCOR calculations the fuel-to-coolant mass ratio was ~ 6 for the first material batch to slump into lower head water, which is significantly higher than in any of the experiments discussed in Chapter 3. With water depths of the order of 3 m at the time of the first support plate ring failure the full fragmentation assumption is in fair agreement with the CCM and FARO experience. The five support plate ring failures occurred within a relatively short time period, in many cases rulting in total relocation before complete dryout. However, the jet break-up fraction should decrease in shallow water. Only the first debris batches are released in deep water. After the third batch, almost all the water has evaporated, so that at least the molten debris fraction of the last two batches ought to remain unfragmented. The melt fraction of the debris would then further increase due to conglomeration of unfragmented debris and particulate debris in the lower head.

The MAAP4 model applies a simple jet fragmentation model (see Chapter 4). All the debris is assumed to remain quenched as long as there is water in the lower plenum. The debris that is not entrained into particles is assumed to form a solid crust on the RPV wall and on the CRD tubes and other equipment in the lower plenum. Without detailed modelling of the two-phase mixing zone around the jet, however, such a model cannot be expected to give accurate predictions of fragmentation and quenching. The core plate failure for the five regions occurs over a much larger time span than MELCOR. Hence, the fragmentation ceases already before the second ring failure, when the water level has dropped below the 1-m limit (a rather high level seen in the light of the experiments). Subsequently, the relocated material is assumed to form a continuous debris bed beneath the particulate bed in a predetermined, rather schematic way involving separation into a metallic and an oxidic layer. No such layering was observed in TMI-2, but it is fair to add that the conditions were quite different.

When assessing the calculated results in the light of the CCM and FARO experiments one should keep in mind that the experimental conditions in CCM and FARO deviate from those, which are relevant for the simulated systems, in the following respects:

- Generally, the molten corium in FARO was purely oxidic, whereas the relocating materials in the plant calculations had high metallic fractions. A small metallic Zr fraction added in one FARO experiment was completely oxidized and had a considerable effect on the fragmentation during the fall stage. Oxidation was also observed with purely oxidic melts.

- In the CCM tests the steel fraction became oxidized by up to 35 % in saturated water, whereas the simulated steel oxidation fractions (over the whole accident) were negligible.

- The melt was always superheated in the experiments. Jets of heterogeneous, multiphase mixtures of partially molten materials may show less or no fragmentation.

- Multiple jets, so closely spaced that the void fraction increases between the jets, showed reduced fragmentation in a CCM test.

- In the experiments, the jets were released vertically, with circular cross section, and far from structures. In the reactor case, the melt released sidewards from the support piece flow ports into the lower plenum 'tube forest' may stream in rivulets down the tubes without significant fragmentation. Relocation inside the guide tubes may be unlikely due to blockage formation on the velocity limiter (cf. XR experiments).

8.3 Long Term Lower Head Response

Owing to the different initial lower head debris configurations emerging from the respective relocation calculations the focus is different in evaluating the heatup and reflooding responses calculated by the codes. Without a full scale test for comparison, it is hard to tell, how close or far the configurations are from reality and hence, which of the codes is better than the other.

8.3.1 Particle Bed Coolability

The lower head particulate debris bed established in the MELCOR cases is probably in a more favourable state for cooling than can be expected in a real accident, where complete fragmentation is unlikely. Nevertheless, the simulations show that even if water injection is re-established soon after the completion of relocation to the lower head, the bed cannot be cooled in time to confine the debris within the RPV. This is not in immediate accordance with the statement in the DCC-3 report [22] that "... a homogeneous bed of the large particulate (4.67 mm) would be coolable (~1.0 W/g) under most accident scenarios". However, it should be noted that the DCC experiments did not progress to very high temperatures. The heatup and cooling by reflooding is a dynamic process in which the water penetration is delayed due to countercurrent flow limitation by escaping steam. At high temperatures the delay is increased not only by increasing capacitive heat but also by oxidation heat. The time factor is important because the porosity, and hence the permeability of the bed decreases as the particles reagglomerate and melt. Thus the quenching front may be arrested leaving the interior in an uncoolable state. Of course, the similar phenomena in MAAP4 are of minor importance due to less fragmentation.

Several sources of uncertainty in the quenching calculations have been identified as follows:

- The applied Lipinski model correlates reasonably well with the DCC dryout heat flux results. However, the experiments concern incipient dryout during heatup of an initially flooded cold

particle bed. Quench heat fluxes at the flooding of a hot, dry particle bed are significantly lower than dryout heat fluxes [22].

- Three differently defined average particle sizes are used to characterize the DCC debris beds, whose particle diameters have a log-normal mass distribution, approximately [21]. It should be noted, that the "mass-median diameter" (e.g. 0.75 mm in DCC-1) is consistent with the CCM and FARO definitions. However, the above-mentioned correlation between the Lipinski model and DCC results used the considerably smaller "effective diameter (with shape factor)", e.g. 0.31 mm in DCC-1. It should be added, though, that the size dependence is less severe in the turbulent flow regime applying to larger particles (transition range ~1 to 5 mm).

- Local dryout effects and fingering were observed in the DCC-2 experiment in which a small amount of "fines" had created an inhomogeneity. In DCC-3 the bed was stratified to simulate the effect of a layer of fine fragments (e.g. from a steam explosion) overlying a coarser layer. The special dryout effect for this configuration may be of minor interest here. However, the enhanced cooling effect obtained by bottom water injection in the same experiment seems of interest in relation to injection via the control rod cooling system.

- The simulated lower head debris had a large metallic fraction, while the DCC experiments used UO_2 particles. Oxidation heat generation was simulated by the codes. However, there are no experimental data showing the effect of hydrogen generation on the dryout/quench heat flux. It is important to note that this heat flux is flow limited (not a boundary layer problem), so perhaps the effect is insignificant as there is no volume change associated with the transformation of steam to hydrogen.

- The dryout heat fluxes apply to unconsolidated particle beds. Morphological changes of pores (especially the pore throats) during conglomeration and settling of the bed seem to be neglected in the model. It is well known from geophysical studies of sedimentary rocks from oil and gas reservoirs that there is not a unique correlation between porosity (used in the model) and the permeability (which is the real controlling parameter).

8.3.2 Gap Formation and Boiling Heat Transfer

The gap model applied in MAAP4 is a hypothetical model that was developed in an attempt to solve the TMI-2 lower head coolability problem. The TMI-VIP scoping calculations showed that there had to be an explanation in terms of channels and gaps but did not lead to formulation of an adequate mechanistic model [3]. The mechanism assumed in MAAP is that initially a microscopic gap is created between the vessel wall and the debris crust during formation and that growth of this gap (within the order of a millimetre) due to creep expansion of the wall at about 1100 °C is sufficient to cool the vessel by water ingress and boiling [29]. However, a crucial assumption that still lacks adequate explanation is that water could somehow penetrate to the hot spot, which was the only place in TMI-2, where the temperatures were high enough to expand the gap. Furthermore, it is tacitly assumed in the model that the continuous debris mass is self-supporting and completely stiff so that the gap can remain open. Thermal deformations of the vessel wall and the crust are not properly taken into account. In TMI-2 a high pressure was available to enhance the creep deformation. In the present low pressure calculations, the model becomes questionable, because the driving stresses for creeping are smaller.

Even if the gap formation hypothesis is accepted, the water penetration potential remains to be experimentally proved. The critical heat flux model is a steady-state, natural convective boiling correlation originally developed for boiling in vertical rectangular channels submerged in water. Here, the deviating geometry is an inferior problem. The crucial assumption in MAAP4 is that sufficient water immediately penetrates to the bottom of the gap. The water is assumed to perlocate into the gap. Without modelling this flow, however, the code disregards the flow restriction at the cooler edge, where the gap is narrower. Thus, the model does not consider the time delay and the less favourable cooling conditions caused by countercurrent flow limitation. In TMI-2 it took about half an hour for the water to reach the hot spot. A related problem is that dryout of the gap is not considered in MAAP4. If the calculated heat transfer from crust and wall to gap water exceeds the maximum critical heat flux based on the above-mentioned steady-state correlation, this maximum flux is distributed between the two surfaces. In that case, it would be more appropriate to assume dryout.

In conclusion, the gap model needs further development and experimental proof before it can be applied with confidence to predict under which conditions a potentially coolable configuration occurs.

8.3.3 Failure of Lower Head

The failure times of the lower head for the MAAP4 and MELCOR calculations are very different. There are several reasons for this: different plant input, different models and assumptions as well as different settings of phenomenological parameters. In the MAAP4 studies only the creep rupture was considered and hence only the results from the creep rupture cases can be compared with MELCOR. As mentioned in section 7.1.1, the creep rupture temperature predicted by MELCOR is considerably higher than that of MAAP. In addition to the difference in assumptions of the debris composition and state in the lower plenum, an important model approach taken in MAAP4 is the formation of a gap, in the presence of water. The most significant difference caused by this model is in the suggested possibility of saving the RPV wall from creep rupture by late reflooding.

According to MELCOR, reflooding had to be initiated immediately after dryout of the lower head to save the RPV. Another important model difference is that MAAP does not assume any oxidation in the lower head debris bed (only occurs during relocation), while MELCOR calculates oxidation of particulate debris during reflooding. Oxidation of metallic particles was the main reason for the result that the BWR lower head failure was not prevented by late reflooding of the lower head.

The BH model generally predicted that the failure of the Olkiluoto RPV occurred by melting of instrument tubes relatively shortly after lower head dryout (after 13-57 min in low pressure cases and 55-78 min in high pressure cases). PASULA analyses using MELCOR temperature histories and material compositions as boundary conditions suggest that the Olkiluoto pressure vessel would fail due to instrument tube weld failure at the periphery of the lower head hemisphere after about 1 h from the dryout. If the instrument tube failure was precluded by user option, the RPV failed due to creep rupture in low pressure case at about 5.5 h (T_{wall} =1696 K) and in high pressure case at 3.2 h (T_{wall}=1061 K) after lower head dryout.

Rempe et al. have published a comprehensive study on lower head failure in LWRs [26]. The study addresses the occurrence and conditions for similar lower head failure modes as modelled in the BH package and thus constitutes an interesting reference for comparison with the calculated plant results. Rempe et al. estimate the lower head pool boiloff time to be ~1-6 hours. The MELCOR

calculations for Olkiluoto resulted in boiloff times of 21-47 minutes. In the MAAP4 results for Forsmark 3 the respective times were 36 min - 1.7 h.

Rempe et al. consider three types of debris beds: a) a uniform debris bed that is primarily metallic. b) a uniform debris bed that is primarily ceramic and c) a layered debris bed with metallic debris near the vessel and ceramic debris on top. The debris bed in the MELCOR/BH calculations for Olkiluoto was closest to the type c) and in the MAAP4 calculations for Forsmark 3 the debris pool, having an oxidic bottom layer at high temperature, could be considered closest to type b).

Rempe et al. conclude that peak vessel temperatures in case of debris bed types a) and b) occur at the bottom of the vessel near the debris/wall interface, whereas in debris bed type c) the locations of peak vessel temperatures vary during the transient and tend to occur higher at the debris/wall interface, near the point, where the skirt attaches to the vessel. These results agree with the calculated MAAP4 and MELCOR results. The finite-element analysis for debris bed types a) and b) indicate that in-vessel tube melting will occur in any of the BWR and PWR vessel designs with lower head penetrations. If the flow path through the tubes becomes blocked due to crust formation, the ceramic melt pool case will result in creep rupture in less than 4 hours. In case of metallic debris bed, vessel creep rupture did not occur (before at least 100 hours). Rempe et al. conclude about the lower head failure mode in GE type BWR as shown in Table 6.

Table 6. *Dominant failure modes for GE BWRs [26].*

Debris composition	Debris arrival state	Lower head failure mode
Metallic	Coherent jet (<5%)	None
Ceramic slurry	Coherent jet (<7%)	Localized or global failures for P> 20 bar and T_{wall}>1100 K; tube failure for P< 20 bar and T_{wall} >1600 K
Ceramic pool	Coherent jet (<10 %)	Tube failure for all pressure ranges and vessel inner surface temperatures > ~1200 K

In the analysed BWR high pressure scenario in [26] the creep rupture occurred after 3.7 hours, when the inside wall temperature was 1210 K. The result of MELCOR/BH calculation of the Olkiluoto high pressure scenario (without tube failure) is in rather good agreement with that (creep rupture at 3.3 h, inside wall temperature 1060 K). In the respective MAAP4 calculation the creep rupture occurred significantly earlier, in 54 minutes at the wall temperature ~ 1300 K.

Suh and Henry have studied the lower head debris pool behaviour with internal and external cooling [28]. The study deals with a homogeneous oxidic melt pool with a metallic melt layer on top and addresses perhaps more a PWR than a BWR case. With no external lower head cooling they have calculated that the lower head would fail due to creep rupture in about 4000 s if the whole core is dumped into the lower head coherently.

The MELCOR/BH prediction of Olkiluoto lower head instrument tube failure, however, differs from the specifications in Table 6. For example, in low pressure case 4 the instrument tubes are predicted to fail with all vessel wall nodes below 616 K. The melt pool temperature in debris layer 2, where the instrument tubes failed, was about 1700 K. The melt fraction of layer 2 at the time of instrument tube failure was 6.6 % and thus the layer could be considered at most a slurry.

In the respective high pressure case 17, the hot spot of the vessel wall (936 K) was near the debris bed surface/ reactor vessel wall contact point. The temperature of the layer 2 was above 1621 K with a melt fraction of 32 %.

It seems that typically the BH model gives in the Olkiluoto plant case slightly lower vessel wall temperatures than was obtained in analyses in [26]. However, Rempe et al. emphasize that the temperatures and pressures (in Table 6) should only be considered as approximate values because there is considerable uncertainty associated with those values. Also, the studies of Rempe et al. do not address the effects of water injection into the lower head debris bed.

Lower head thermal behaviour in BWR case was investigated also at the RIT [1,2]. The model developed at RIT treats the case of a uniform composition, initially quenched, debris bed of zero porosity, which is slowly converted into a melt pool. The hemispherical lower head wall is included in the modelling and its melt-through due to thermal attack of the melt pool is calculated. However, no structural calculations are performed.

The model was applied to the BWR scenario of lower head melt pool formation, and vessel melt-through. The heat sinks of the control rod guide tubes and instrumentation tubes were ignored. Also ignored was the presence of any Zircaloy in the BWR debris, which may lead to chemical energy addition.

Two cases were calculated, 1) with the assumption of constant internal heat generation equal to 1.0 MW/m^3 (= 16 MW) and 2) with internal pool heat generation of 2.0 MW/m^3 (=32 MW). These thermal powers are within the range of Olkiluoto and Forsmark whole core decay heats after two hours from scram. The initial debris bed mass was 135 metric tons and the initial debris temperature was 1000 K. The model predicted the failure of vessel wall due to thermal ablation to occur at 3 hours 46 minutes and 1 hour 54 minutes in cases 1) and 2) respectively. This analysis for the BWR, however, ignored the possibility of vessel failure through structural and/or creep loading prior to melt-through.

9. CONCLUSIONS

The core debris bed behaviour and thermal response of structures in the reactor vessel lower head was studied in case of the Olkiluoto and Forsmark BWRs. The plant analyses were performed with MELCOR/BH and MAAP4 computer codes, respectively. Both low and high pressure scenarios were analysed with sensitivity studies addressing the effects of various parameters like debris bed porosity, debris particle size and reflooding after debris bed dryout. Lower head failure mechanisms and timing was examined with MELCOR by allowing instrument tube failure (normal case) or by deactivating the penetration failure model by an input option. A detailed thermal/structural analysis was performed for the control rod and instrument tube penetrations with the separate PASULA code. A literature study on late phase melt progression issues was carried out and the obtained results were evaluated in the light of current experimental observations.

In the low pressure cases the falling debris was partially quenched during the initial release from the core region. The timing of the core support plate failure was found to be 4.5 - 5.4 h with MELCOR, but 1.4 h with MAAP4. The lower head water pool boiled off in 21-40 minutes in the Olkiluoto MELCOR calculations and in 51 min - 1 h 41 min in the Forsmark MAAP4 calculations. If the lower head penetration model was active, the lower head failed by instrument tube melting in multiple radial locations above 60 cm (debris layer 2) from the bottom of the vessel 13 - 57 minutes after lower head dryout. According to PASULA calculations for Olkiluoto low pressure case, the lower head failure would occur most likely due to instrument tube weld failure at the periphery of the lower head hemisphere about 1 h after lower head dryout. The instrument tubes in the centre of the lower head would fail due melting in about 5000 s at an elevation of about 1 m from the bottom wall. However, it is unlikely, that the debris pouring into the flow channel would not freeze and block the channel before discharging out of the vessel. According to PASULA calculations the control rod nozzles would also loose strength at about 4000 s after lower head dryout near the periphery of the lower head, but since the control rod guide tubes are supported by a common tieplate, this failure is deemed not to lead into debris discharge out of the vessel.
In case the instrument tube failure was precluded, the lower head failed due to creep rupture. MAAP4 and MELCOR predictions of the time of lower head creep rupture differed substantially. Without reflooding MELCOR predicted that lower head creep rupture occurs 5.5 hours after lower head dryout and the respective prediction with MAAP4 was 1.9 h. MELCOR predicted that reflooding of the dry debris bed could not prevent lower head failure, on the contrary the failure occurred earlier due to heat release from Zirconium oxidation. The MAAP4 calculations lead to quite the opposite result, with successful prevention of lower head failure with late reflooding in most analysed cases. The reason for the efficient coolability predicted by MAAP4, was the assumption of gap cooling at the wall/debris bed interface.

In the high pressure cases the debris was initially quenched in the lower head water pool. The timing of the core support plate failure was found to be 2.7 - 3.0 h with MELCOR and 1.7 h with MAAP4. The boiloff of the pool took 21-47 minutes according to MELCOR and 35 min- 1h 25 min according to MAAP4. The lower head failed due to instrument tube melting also in multiple radial rings above 60 cm from the vessel bottom from 55 minutes to 1 h 17 minutes from the lower head dryout. If penetration failure was precluded the lower head failed due to creep rupture, according to MELCOR about 3.3 hours from the lower head dryout and according to MAAP4 about 1 h after the lower head dryout. Reflooding of the dry lower head debris bed prevented the (creep rupture) failure of the lower head in the MELCOR calculations only if reflooding was started immediately (1 min) after lower head dryout. MAAP4 predicted a larger time margin for the start of reflooding. A coolable state was reached if reflooding was initiated at least 20 min before the calculated creep rupture time.

The experimental data and also the performed code calculations suggests that the debris is to significant extent fragmented and cooled during the fall down from the support plate to the lower head. Large differences in the codes exist in the models for the formation of the debris bed, especially with respect to the degree of fragmentation. The order in which the different materials relocate from the support plate determines the composition of the debris bed. In the BH model the metal-rich layer resides at the bottom of the debris bed, leading to a hot, oxidic centre of the debris bed. The MAAP4 model is based on the assumption that heavy oxides flow to the bottom of the debris bed. This approach also gives arguments for the gap formation, which in turn gives favourable results in debris coolability. However, the hypothetical gap formation and critical heat flux models are debatable. These issues need further experimental demonstration.

The performed studies suggest that the instrument tube welds fail first in the Nordic BWRs. Even if the failure of an instrument tube occurs, large uncertainties exist in the debris discharge rate to the containment, which is dependent on the debris composition and melt fraction. If only creep rupture failure is considered, the calculated lower head creep rupture times in the high pressure cases are in agreement with the work performed earlier by Rempe et al. However, large uncertainties exist in the creep rupture times under low pressure conditions.

The key uncertainties in the presented analyses are:

1. The melt progression and blockage formation in the core region and the simple core support plate failure criterion cause large uncertainty in the time to core plate failure and material relocation to the lower head.

2. Initial quenching fraction of debris, when slumping into the lower head water pool. The performed studies suggested that the debris is fragmented to a significant extent. Quenching is predicted with fully parametric models, which, however, could be sufficient if input parameters could be reliably defined.

3. The debris configuration and the coolability of the particulate debris bed in the lower head by reflooding. Large differences exist in the code predictions. The validation of the models is, however, difficult since there is little information about the oxidation in a rubble bed and its effects on thermal response of lower head. And, also the gap formation in the debris bed near the lower head wall and its cooling capability still lack experimental proof.

4. The structural behaviour of ABB reactor specific instrument tubes.

5. Corium flow out of the reactor pressure vessel through failed instrument tubes. The blocking crust formation is highly dependent on turbulence of the flow and the diameter of the initial hole.

10. SYMBOLS

Acronyms

ABB	Asea Brown Bovery
ACRR	Annular Core Research Reactor (Sandia)
ADS	Automatic Depressurization System
BH	Bottom Head
BWR	Boiling Water Reactor
CHF	Critical Heat Flux
CRD	Control Rod Drive
GE	General Electric
HPI	High Pressure Injection
LH	Lower Head
LOCA	Loss of Coolant Accident
MP	Melt Progression
PWR	Pressurized Water Reactor
RCS	Reactor Coolant System
RIT	Royal Institute of Technology, Stockholm, Sweden
RPV	Reactor Pressure Vessel
SNL	Sandia National Laboratory
SSt	Stainless steel
TMI-2	Three Mile Island PWR, Unit 2
VIP	Vessel Investigation Project

Mathematical

a	lenght of a side of a cube
A	cross-sectional area
d	diameter of a spherical corium particle
d_c	diameter of small contact area of two sperical particles
d_0	diameter of a sphere
d_{eff}	equivalent diameter of debris particles (accounting for the shape factor)
M	mass
Δp	pressure difference
R	radius of the reactor pressure vessel
r	radius of coriumparticle = $d/2$
$S_{tensile}$	tensile stress
T	temperature
t	time
V_0	volume of a sphere = $(4/3)\pi(d/2)^3$
We	Weber number

Greek

α	effective porosity of granular corium
α_0	porosity of debris bed (particle diameter d) with cubic packing
ε	emissivity of material

λ	thermal conductivity
$\lambda_c^{"}$	thermal conductivity of a corium material
λ_c^{*}	heat transfer coefficient of a contact area between two particles
λ_g^{*}	thermal conductivity of interstitial steam between corium particles
λ_r^{*}	radiation heat transfer coefficient in the interstitial gas between particles
$\lambda_r^{"}$	radiation leakage in s asystem of radiation exhange between two spherical particles
λ_{eff}	effective heta transfer coefficient of granular corium
π	3.141593...
σ	Stefan-Boltzmann constant

11. REFERENCES

1. B.R. Sehgal, T.N. Dinh, T.J. Okkonen, V.A. Bui, R.R. Nourgaliev, J. Andersson, Studies on Melt-Water-Structure Interaction During Severe Accidents, Technical Report NKS/RAK-2(96)TR-A2. October 1996.

2. V.A. Bui, T.N. Dinh, B.R. Sehgal, In-Vessel Melt Pool Formation During Severe Accidents, Proceedings of the 1996 National Heat Transfer Conference, August 3-6, 1996, Houston, Texas, USA.

3. J.R. Wolf et al., TMI-2 Vessel Investigation Project Integration Report. NUREG/CR-6197, TMI V(93)EG10, EGG-2734, March 1994.

4. K.L. Thomsen, Literature Study on the TMI-2 Accident Evaluation And Vessel Investigation Projects, Riso-R-1004, December 1997.

5. T.J. Tautges, MELCOR 1.8.2 Assessment: The MP-1 and MP-2 Late Phase Melt Progression Experiments, Sandia report SAND-0133, Sandia National Laboratories, May 1994.

6. R.D. Gasser, R.O. Gauntt, S.C. Bourcier, R.C. Schmidt, L.C. Humphries, and K.O. Reil, Late Phase Melt Progression Experiment - MP-2: Results and Analysis. NUREG/CR-6167, SAND93-3931. January 1994.

7. J. M. Broughton, P. Kuan, D.A. Petti, E.L. Tolman, A Scenario of the Three Mile Island Unit 2 Accident. Nuclear Technology 87 (1989) 34-53.

8. R.O. Gauntt and P.H. Helmick, Preliminary Results of the XR2-1 Experiment, Presented at the Water Reactor Safety Meeting (WRSM), October 1995.

9. R.O. Gauntt, L.H. Humphries, P.H. Helmick, R.C. Schmidt, K.O. Reil, Results of the XR2-1 Metallic Melt Relocation Experiment, Presentation at the USNRC Cooperative Severe Accident Research Program (CSARP) Meeting, Bethesda, MD, USA, May 6-10, 1996.

10. M. Epstein and H.K. Fauske, Steam Film Instability and the Mixing of Core-Melts of Jets and Water, ANS Proc., 1985 National Heat Transfer Conference, ANS #700101, Denver, CO, USA, August 1985.

11. B.W. Spencer, K. Wang, C.A. Blomquist, L.M. McUmber, J.P. Schneider, Fragmentation and Quench Behaviour of Corium Melt Streams in Water. Argonne National Laboratories. NUREG/CR-6133, ANL-93/32. February 1994.

12. A. Annunziato, C. Addabbo, H. Hohmann and D. Magallon, COMETA Code Calculation of FARO Melt Quenching Tests, Proceedings of Int. Conf. On 'New Trends in Nuclear System Thermohydraulics', Vol. II, Pisa, Italy, May 30-June 2, 1994.

13. D. Magallon and H. Hohmann, High Pressure Corium Melt Quenching Tests in FARO, Presented at the CSNI-FCI Specialist Meeting, Santa Barbara, CA, USA, January 5-8, 1993.

14. H.U. Wider, A. Annunziato, H. Hohmann, D. Magallon and A. Yerkess, Corium Debris Cooling in the FARO Experiments, Proceedings SMIRT '93.

15. H.U. Wider, Transient Cooling of Shallow Debris Beds in the First Two FARP LWR Experiments, Nucl. Eng. Des. 157 (1995) 395-408.

16. H. Hohmann, D. Magallon, P.F. Stella, Report on the FARO Programme, Presentation at the CSARP Semi-annual Review Meeting, Bethesda, MD, USA, May 2-6, 1994.

17. H. Hohmann, D. Magallon, I. Huhtiniemi, A. Annunziato, A. Yerkess, Advance in the FARO/KROTOS Melt Quenching Test Series, Proceedings of 22nd Water Reactor Safety Meeting, Bethesda, MD, USA, October 24-26,1994.

18. D. Magallon and H. Hohmann, Experimental Investigation of 150-kg-scale Corium Melt Jet Quenching in Water, Proc. NURETH-7, Saratoga Springs, NY, USA, September 10-15, 1995.

19. D. Magallon, I. Huhtiniemi, A. Annunziato, A. Yerkess, H. Hohmann, Status of the FARO/KROTOS Melt-Coolant Interactions Tests, Presented at the 23rd Water Reactor Safety Information Meeting, October 1995.

20. A. Annunziato, D. Magallon, I. Huhtiniemi, A. Yerkess, C. Addabbo, H. Hohmann, Progress of the FARO/KROTOS test Programme. Presentation at the USNRC Cooperative Severe Accident Research Program (CSARP) Meeting, Bethesda, MD, USA, May 6-10, 1996.

21. A.W. Reed, K.R. Boldt, E.D. Gorham-Bergeron, R.J. Lipinski, T.R. Schmidt, DCC-1/DCC-2 Degraded Core Coolability Analysis. Sandia National Laboratories. NUREG/CR-4390-R3. October 1985.

22. K.R. Boldt, A.W. Reed, T.R. Schmidt, DCC-3 Degraded Core Coolability: Experiment and Analysis. Sandia National Laboratories. NUREG/CR-4606. September 1986.

23. Summers, R.K. Cole Jr., R.C. Smith, D.S. Stuart, S.L. Thomson, S.A.Hodge, C.R. Hyman, R.L. Sanders, MELCOR Computer Code Manuals, Sandia National Laboratories. NUREG/CR-6119, SAND93-2185, March 1995.

24. Y. Waaränperä, APRI-MAAP4 Simulation of Reflooding at Forsmark3/Oskarshamn 3, ABB Atom Report NT95-042.

25. I. Lindholm, L. Nilsson, E. Pekkarinen, H. Sjövall, Coolability of Degraded Core under Reflooding Conditions in Nordic Boiling Water Reactors, Technical Report NKS/RAK-2(95)TR-A1. September 1995.

26. J.L. Rempe, S.A. Chavez, G.L. Thinnes, C.M. Allison, G.E. Korth, R.J. Witt, J.J Sienicki, S.K. Wang, L.A. Stickler, C.H. Heath, S.D. Snow, Light Water Reactor Lower Head Failure Analysis. Idaho National Engineering Laboratory. NUREG/CR-5642,EGG-2618. October 1993.

27. D.W. Akers, J.M. jensen, B.K. Schuetz, Examination of Relocated Fuel Debris Adjacent to the Lower Head of the TMI-2 Reactor Vessel. Idaho National Engineering Laboratory. NUREG/CR-6195, TMI V(92)EG10, EGG-2732. March 1992.

28. K.Y. Suh, R.E. Henry, Integral Analysis of Debris Material and Heat Transport in Reactor Vessel Lower Plenum. Nuclear Engineering and Design 151 (1994) pp. 203-321.

29. R.E. Henry, D.A. Dube, Water in the RPV: A Mechanism for Cooling Debris in the RPV Lower Head, Proceedings of the Specialist Meeting on "Selected Severe Accident Management Strategies", SKI Report 95:34, NEA/CSNI/R(95)3, Stockholm, Sweden, 1994.

30. Ministry of Industry, Steam Explosions in Light Water Reactors, Report of the Swedish Government Committee on Steam Explosions, Ds I 1981:3.

31. S.H. Kim et al., The Development of APRIL.MOD2 - A Computer Code for Core Meltdown Accident Analysis of Boiling Water Nuclear Reactors, NUREG/CR-5157, ORNL/Sub/81-9098/3, July 1988.

32. R.M. Summers, R.K. Cole Jr., R.C. Smith, D.S. Stuart, S.L. Thomson, S.A. Hodge, C.R. Hyman, R.L. Sanders, MELCOR Computer Code Manuals Vol. 1 & 2, NUREG/CR-6119, SAND93-2185, Sandia National Laboratories. March 1995.

33. K. Ikonen, Heating and Melting Calculations of Control and Instrument Vessel Penetrations for BWR Reactor Pressure Vessel. Proceedings of CORVIS Task Force Meeting, 9-10 February 1995, Villigen, Switzerland. Paul Scherrer Institute. 14 p.

APPENDIX A.1

Table 1. *MELCOR calculation matrix for Olkiluoto. Core melt behaviour in the lower head.*

Case no	RCS pressure L= with ADS H= no ADS	LH penetrations modelled y=yes, n=no	Debris porosity	Debris particle diameter (m)	Reflood rate (kg/s)	Reflood time (s)
1	L	N	0.45	0.005	-	-
2	L	N	0.45	0.005	45	29000 s (136 min after LH dryout)
3	L	N	0.45	0.005	45	21500s (11 min after LH dryout)
4	L	Y	0.45	0.005	-	-
5	L	Y	0.45	0.005	45	21000 s (11 min after LH dryout)
6	L	Y	0.30	0.005	-	-
7	L	Y	0.30	0.005	340	21000 s (33 min after LH dryout)
8	L	Y	0.30	0.005	-	-
9	L	Y	0.30	0.005	45	21600 S (54 min after LH dryout)
10	L	Y	0.30	0.005	45	20367 s (30 min after LH dryout)
11	L	Y	0.30	0.005	45	19900 s (26 min after LH dryout)
12	L	Y	0.45	0.01	-	-
13	L	Y	0.45	0.01	45	18000s (6 min after LH dryout)
14	L	Y	0.45	0.01	340	18000 s (6 min after LH dryout)
15	L	Y	0.45	0.002	-	-
16	L	Y	0.45	0.002	45	20000 s (7 min after LH dryout)
17	H	Y	0.45	0.005	-	-
18	H	Y	0.45	0.005	45	13100 s (10 min after LH dryout)
19	H	Y	0.3	0.005	-	-
20	H	Y	0.3	0.005	45	12000 s (13 min after LH dryout)
21	H	N	0.45	0.005	-	-
22	H	N	0.45	0.005	45	12000 s (1 min after LH dryout)
23	H	N	0.45	0.005	45	14000 s (34 min after LH dryout)

APPENDIX A.2

Table 2. *Summary of Olkiluoto key results from the lower head debris behaviour study with MELCOR/BH model.*

Case	RCS pressure L= with ADS H=no ADS	Key event time (s)	Total H_2 generated (kg) COR:before dryout BH:after dryout	Additional comments
1	L	beginning of FP gap release: 5228 s support plate 1 failure: 19571 s support plate 3 failure: 19699 s support plate 2 failure: 19871 s support plate 4 failure: 20450 s support plate 5 failure: 20750 s BH activation/LH dryout: 20850 s melting and slumping of shroud structures to LH pool: 26041 s LH penetration failure: - LH ablation failure: - LH creep rupture failure: 40572 s	COR: 475 kg BH: - total: 475 kg (Zr-ox:16.6%)	Calculation end time: 42000 s ex-vessel debris mass at end of calculation: 211 351 kg
2	L	beginning of FP gap release: as in #1 support plate failure: as in # 1 BH activation/LH dryout: 20850 s melting and slumping of shroud structures to LH pool: 26041 s reflooding: 29000 s LH instrument tube failure: - LH penetration failure: - LH ablation failure: - LH creep rupture failure: 40017 s	COR: 475 kg BH: 95 kg total: 570 kg (Zr-ox: 22.6%)	Calculation end time: 41493 s (CPU limit termination) ex-vessel debris mass at end of calculation: 196 955 kg
3	L	beginning of FP gap release: as in #1 support plate failure: as in #1 BH activation/LH dryout: 20850 s reflooding: 21500 s LH instrument tube failure: - LH penetration failure: - LH ablation failure: - LH creep rupture failure: 35114 s	COR: 475 kg BH: 807 kg total: 1282 kg (Zr-ox: 67.5%)	Calculation end time: 43120 s (excessive DT reductions - MEXDTH) ex-vessel debris mass at end of calculation: 194 083 kg
4	L	beginning of FP gap release: 5228 s support plate 1 failure: 19571 s support plate 3 failure: 19699 s support plate 2 failure: 19870 s support plate 4 failure: 20450 s support plate 5 failure: 20750 s BH activation/LH dryout: 20850 s LH instrument tube failure: 21644 s melting and slumping of shroud structures to LH pool: 25890 s LH penetration weld failure: 28498 s LH ablation failure: - LH creep rupture failure: -	COR: 475 kg BH: - total: 475 kg (Zr-ox:16.6%)	Calculation end time: 30000 s ex-vessel debris mass at end of calculation: 84235 kg

Case	RCS pressure L=with ADS H=No ADS	Key event time (s)	Total hydrogen generated (kg)	Additional comments
5	L	beginning of FP gap release: as in #4 support plate failure: as in #4 BH activation/LH dryout: 20850 s reflooding: 21000 s LH instrument tube failure:21024 s LH penetration weld failure: - LH ablation failure: - LH creep rupture failure: -	COR: 475 BH: 925 total:1400 (Zr-ox: 75%)	calculation end time: 30000 s ex-vessel debris mass at end of calculation: 59701 kg (LH pool quenched)
6	L	beginning of FP gap release: 5151 s support plate 1 failure: 16103 s support plate 3 failure: 16268 s support plate 2 failure 16535 s BH activation/LH dryout: 18978 s support plate 4 failure: 20072 s support plate 5 failre:21058 s melting and slumping of shroud structures to LH pool: 21684 s LH instrument tube failure: 22388 s LH penetration weld failure: - LH ablation failure: - LH creep rupture failure: -	COR: 490 BH: 8 total: 498 kg (Zr-ox: 18.4%)	calculation end time: 25000 s ex-vessel debris mass at end of calculation: 48652 kg
7	L	beginning of FP gap release: as in #6 support plate 1-3 failure: as in #6 BH activation/LH dryout: 18978 s support plate 4 failure: 20072 s reflooding: 21000 s LH instrument tube failure: 21251 s support plate 5 failure: 21473 s LH penetration weld failure: - LH ablation failure: - LH creep rupture failure: 36040 s	COR: 490 BH: 557 total: 1047 (Zr-ox: 53%)	calculation end time: 40000 s ex-vessel debris mass at end of calculation: 186 385 kg (before creep rupture: 55 000 kg)
8	L	beginning of FP gap release: 5150 s support plate 1 failure: 15638 s support plate 3 failure: 15808 s support plate 2 failure: 15992 s BH activation/LH dryout: 18367 s support plate 4 failure: 19805 s support plate 5 failure: 21051 s melting and slumping of shroud structures to LH pool: 21441 s LH instrument tube failure: 21691 s LH penetration weld failure: - LH ablation failure: 32063 s LH creep rupture failure: -	COR: 380 BH: 10 total: 390 (Zr-ox: 16.5%)	calculation end time: 32061 s (BHRUN2 - gross head fail fp error) ex-vessel debris mass at end of calculation: 194 552 kg

case	RCS pressure L=with ADS H=No ADS	Key event time (s)	Total hydrogen generated (kg)	Additional comments
9	L	beginning of FP gap release: as in #8 support plate 1-3 failure: as in #8 BH activation/LH dryout: 18367 s support plate 4 failure: 19805 s support plate 5 failure: 21011 s reflooding: 21600 s melting and slumping of shroud structures to LH pool: 21432 s LH instrument tube failure: 21806 s LH penetration weld failure: - LH ablation failure: - LH creep rupture failure: -	COR: 380 BH: 600 total: 980 (Zr-ox:53.7%)	Calculation end time 27000 s ex-vessel debris mass at end of calculation: 67232 kg (LH pool quenched)
10	L	beginning of FP gap release: as in #8 support plate 1-3 failure: as in #8 BH activation/LH dryout: 18367 s support plate 4 failure: 19805 s reflooding: 20367 s LH instrument tube failure: 20673 s LH penetration weld failure: - LH ablation failure: - LH creep rupture failure: -	COR: 380 BH: 424 total: 804 (Zr-ox: 47.5)	Calculation end time: 36122 s (CPU limit) ex-vessel debris mass at end of calculation: 67232 kg (LH pool quenched)
11	L	beginning of FP gap release: as in #8 support plate 1-3 failure: as in #8 BH activation/LH dryout: 18367 s support plate 4 failure: 19804 s reflooding: 19900 s LH instrument tube failure: 20294 s LH penetration weld failure: - LH ablation failure: - LH creep rupture failure: -	COR: 380 BH: 456 total:836 (Zr-ox: 50%)	calculation end time: 26067 s (CPU time limit) ex-vessel debris mass at end of calculation: 38281 kg (LH pool quenched, except for bottom layer of the pool)
12	L	beginning of FP gap release: 5150 s support plate 3 failure: 16146 s support plate 1 failure: 16322 s support plate 2 failure: 16386 s support plate 4 failure: 16900 s support plate 5 failure: 17599 s BH activation/LH dryout: 17668 s LH instrument tube failure: 19250 s melting and slumping of shroud structures to LH pool: 23225 s LH penetration weld failure: - LH ablation failure: - LH creep rupture failure: -	COR: 495 kg BH: 0 total: 495 (Zr-ox: 16.1%)	Calculation end time: 25000 s ex-vessel debris mass at end of calculation: 60102 kg

Case	RCS pressure: L=with ADS H=No ADS	Key event time (s)	Total hydrogen generated (kg)	Additional comments
13	L	beginning of FP gap release: as in #12 support plate 1-5 failure: as in #12 BH activation/LH dryout: 17668 s reflooding: 18000 s LH instrument tube failure: 18244 s LH penetration weld failure: - LH ablation failure: - LH creep rupture failure: -	COR: 495 BH: 919 total: 1414 (Zr-ox: 74.1%)	Calculation end time: 22000 s ex-vessel debris mass at end of calculation: 58422 kg (LH pool quenched)
14	L	beginning of FP gap release: as in #12 support plate 1-5 failure: as in #12 BH activation/LH dryout: 17668 s reflooding: 18000 s LH instrument tube failure: 18123 s LH penetration weld failure: - LH ablation failure: - LH creep rupture failure: -	COR: 495 BH: 896 total:1391 (Zr-ox: 72.6%)	calculation end time: 22000 s ex-vessel debris mass at end of calculation: 47311 kg (LH pool quenched)
15	L	beginning of FP gap release: 5152 s support plate 3 failure: 17216 s support plate 1 failure: 17306 s support plate 2 failure: 17409 s BH activation/LH dryout: 19597 s support plate 4 failure: 20894 s support plate 5 failure: 21953 s LH instrument tube failure: 23792 s LH penetration weld failure: - LH ablation failure: - LH creep rupture failure: -	COR: 465 BH: - total: 465 (Zr-ox: 16%)	Calculation end time:23792 (cavity surface error) ex-vessel debris mass at end of calculation: N/A
16	L	beginning of FP gap release: as in #15 support plate 1-3 failure: as in #15 BH activation/LH dryout: 19598 s reflooding: 20000 s LH instrument tube failure: 20442 s support plate 4 failure: 20855 s LH penetration weld failure: - LH ablation failure: - LH creep rupture failure: -	COR: 465 BH: 765 total: 1230 (Zr-ox: 75.8%)	Calculation end time: 22000 s ex-vessel debris mass at end of calculation: 28877 kg (LH pool quenched, except for bottom layer of the pool)

Case	RCS pressure: L=with ADS H=No ADS	Key event time (s)	Total hydrogen generated (kg)	Additional comments
17	H	beginning of FP gap release: 4750 s support plate 3 failure: 9634 s support plate 4 failure: 9697 s support plate 2 failure: 9944 s BH activation/LH dryout: 12478 s support plate 1 failure: 12535 s support plate 5 failure: 15694 s LH instrument tube failure: 17103 s melting and slumping of shroud structures to LH pool: 18396 s LH penetration weld failure: - LH ablation failure: - LH creep rupture failure: -	COR: 905 BH: 516 total: 1421 (Zr-ox: 75%)	Calculation end time: 20000 s Zr oxidation in BH-package occurs rapidly after instrument tube failure ex-vessel debris mass at end of calculation: 90622 kg
18	H	beginning of FP gap release: as in #17 support plate 2-4 failure: as in #17 BH activation/LH dryout: 12478 s reflooding: 13100 s LH instrument tube failure: 13636 s LH penetration weld failure: - LH ablation failure: - LH creep rupture failure: -	COR: 905 BH: 510 total:1415 (Zr-ox: 81.2%)	Calculation end time: 20000 s. ex-vessel debris mass at end of calculation: 4208 kg (LH pool quenched except for upper layer of the pool)
19	H	beginning of FP gap release: 4748 s support plate 3 failure: 9851 s support plate 1 failure: 9956 s support plate 2 failure: 9964 s support plate 4 failure: 10506 s BH activation/LH dryout: 11219 s LH instrument tube failure: 14537 s melting and slumping of shroud structures to LH pool: 16364 s LH penetration weld failure: - LH ablation failure: 22438 s LH creep rupture failure: -	COR: 885 BH: 455 total: 1340 (Zr-ox: 69.2%)	Calculation end time: 23000 s ex-vessel debris mass at end of calculation: 213 644 kg (before ablation failure: 111 670 kg)
20	H	beginning of FP gap release: as in #19 support plate 1-4 failure: as in #17 BH activation/LH dryout: 11219 s reflooding: 12000 s LH instrument tube failure: 12335 s LH penetration weld failure: - LH ablation failure: - LH creep rupture failure: -	COR: 885 BH: 330 total: 1215 (Zr-ox: 65.4%)	Calculation end time: 14000 s ex-vessel debris mass at end of calculation: 2992 kg (LH pool quenched)

Case	RCS pressure: L=with ADS H=No ADS	Key event time (s)	Total hydrogen generated (kg)	Additional comments
21	H	beginning of gap release:4751 s support plate 3 failure:10603 s support plate 2 failure: 10838 s support plate 4 failure: 11000 s BH activation/LH dryout: 11940 s support plate 1 failure: 13641 s support plate 5 failure: 15642 s LH instrument tube failure: - LH penetration weld failure: - LH ablation failure: - LH creep rupture failure: 23611 s	COR: 1040 kg BH: - total: 1040 kg (Zr ox: 56 %)	Calculation end time: 30000 s ex-vessel debris mass at end of calculation: 191 650 kg
22	H	beginning of gap release as in # 21 support plate 2-4 failure as in #21 BH activation/LH dryout: 11940 s reflooding: 12000 s support plate 1 failure: 13632 s support plate 5 failure: 19906 s LH instrument tube failure: - LH penetration weld failure: - LH ablation failure: - LH creep rupture failure: -	COR: 1040 kg BH: 354 kg total: 1394 kg (Zr-ox: 71 %)	Calculation time: 30000 s No RPV failure
23	H	beginning of gap release as in # 21 support plate 2-4 failure as in #21 BH activation/LH dryout: 11940 s reflooding: 14000 s support plate 1 failure: 13642 s support plate 5 failure: 17833 s LH instrument tube failure: - LH penetration weld failure: - LH ablation failure: - LH creep rupture failure: 21953 s	COR: 1040 kg BH: 627 kg total: 1667 kg (Zr-ox: 88 %)	Calculation time: 25000 s

APPENDIX B.1

Table 3. *Summary of Key events for Forsmark 3 low pressure cases without reflooding, calculated with MAAP4.*

Case	**L 1**	**L 2**	**L 3**	**L 4**	**L 5**	**L 6**	**L 7**
Variation	-	**Quenching =0.2 (1.0)**	**Entrainment =0.01 (0.09)**	**Porosity =0.3 (0.4)**	**Particle size=1/2**	**Particle size=1/4**	**No CHF gap boiling**
Scram	8.35	8.35	8.35	8.35	8.35	8.35	8.35
ADS	430	430	430	430	430	430	430
Core Uncovered	620	620	620	620	620	620	620
Total core uncovery	1950	1950	1950	1950	1950	1950	1950
Core plate Failure	5 020	5 020	5 020	5 020	5 020	5 020	5 020
Average debris particle size	3,6 mm	3,6 mm	3,6 mm	3,6 mm	1,8 mm	0,9 mm	3,6 mm
Crust-RPV gap (time for gap creations)	**Node 1 (8 160 sec)**	**Node 1 (8 190 sec)**	**Node 1 (5 170 sec) Node 2 (9 250 sec)**	**Node 1 (9 770 sec)**	**Node 1 (8 680 sec)**	**Node 1 (5 210 sec)**	-
Lower plenum dry	**9 500**	**9 940**	**11 070**	**9 920**	**8 980**	**8 090**	**9 520**
Vessel failure	**16 450**	**14 370**	**15 880**	**15 990**	**15 810**	**12 820**	**16 510**
Vessel failure mode (Only creep allowed)	Creep rupture in Node 1	Creep rupture in Node 1	Creep rupture in Node 2	Creep rupture in Node 1	Creep rupture in Node 1	Creep rupture in Node 1	Creep rupture in Node 1
Time between LP dry out and vessel failure	6 950	4 430	4 810	6 070	6 830	4 730	6 990
Zr Oxidation	16,4 %	16,4 %	15,9 %	16,2 %	16,2 %	15,3 %	16,4 %

APPENDIX B.2

Table 4. *Summary of key events for Forsmark 3 low pressure reflooding cases, calculated with MAAP4.*

Case	L 8	L 9	L 10	L 11	L 12	L 13	L 14
Variation	Refloodin g with 327 Core spray	Reflooding with 323 Core spray	Reflooding with 323 DC inject	Reflooding with 323 DC inject	Reflooding with 323 DC inject	as case11 but no CHF gap boiling	as case12 but no CHF gap boiling
Total core uncovery		-	-	1 950	1 950		1 950
Core plate Failure		-	-	5 020	5 020		5 020
Average debris particle		-	-	1 mm	0,5 mm		0,5 mm
Start of reflood		**1 920**	**1 920**	**8 360**	**9 280**		**9 070**
Reflooding rate		580 kg/s Core spray	580 kg/s DC inject	485 kg/s DC inject	485 kg/s DC inject		485 kg/s DC inject
Time to cover core with reflooding water		70 sec	140 sec	270 sec	350 sec		
Lower plenum dry		**-**	**-**	**8 000**	**7 300**		**7 090**
Vessel failure		-	-	-	-		14 363
Vessel failure mode		-	-	-	-		Creep rupture in Node 1
Coolable		Yes	Yes	Yes	Yes		No
Time between LP dry out and vessel failure		-	-	-	-		7 270
ZR Oxidation fraction		3,3 %	10,4 %	15,6 %	15,2 %		
Comments	***Instabiblity***	**Comparable with SCDAP/ RELAP case 7 ***	**Comparable with SCDAP/ RELAP case 8 ***	**Compare with MELCOR Case 14**	**Compare with MELCOR Case 7]**	*Instability*	

** Cases L8, L9 and L10 are not relevant for this report. Water injection started before lower head dryout.*

APPENDIX B.3

Table 5. *Summary of key events for Forsmark 3 high pressure cases without reflooding, calculated with MAAP4.*

Case	**H 1**	**H 2**	**H 3**	**H 4**	**H 5**	**H 6**	**H 7**
Variation	-	Quenching =0.2 (1.0)	Entrainment =0.01 (0.09)	Porosity =0.3 (0.4)	Particle size= 1/2	Particle size= 1/4	One Mixed Pool
Scram	8.35	8.35	8.35	8.35	8.35	8.35	8.35
Core Uncovered	1240	1240	1240	1240	1240	1240	1240
Total core uncovery	6270	6270	6410	6170	6170	6 110	6 100
Core plate Failure	6 060	6 060	6 060	6 060	6 060	6 060	6 060
Lower plenum dry	10 030	11 010	11 130	10 010	9 190	8 240	9 500
Crust-RPV gap (time for gap creation)	-	Node 1 (10 790 sec)	Node 1 (6 200 sec)	-	-	Node 1 (6 920 sec)	Node 1 (6 150 sec)
Vessel failure mode	Creep rupture in node 1	Creep rupture in node 1	Creep rupture in node 2	Creep rupture in node 1	Creep rupture in node 1	Creep rupture in node 1	Creep rupture in node 2
Vessel failure	13 260	13 870	14 780	13 200	12 200	12 510	13 720

Table 6. *Summary of key events for Forsmark 3 high pressure reflooding calculations*

Case	H 8	H 9	H 10
Variation	Reflooding with 327 Core spray	Reflooding with 327 Core spray	Reflooding with 327 Core spray
Total core uncovery [s]	-	6 270	6 270
Core plate Failure [s]	-	6 060	6 060
Average debris particle size [mm]	-	3,6	3,6
Start of reflood [s]	3 560	12 660	12 060
Reflooding rate	45 kg/s Core spray	45 kg/s Core spray	45 kg/s Core spray
Time to cover core with reflooding water [sec]	3 090	-	-
Lower plenum dry [s]	-	10 030	10 030
Vessel failure [s]	-	13 400	-
Vessel failure mode	-	Creep rupture in node 1	
Coolable	yes*	no	yes
Time between LP dry out and vessel failure [s]	-	3 010	-
Zr Oxidation fraction	11,4 %	22,9 %	23 %
Comments	**Comparable with SCDAP/ RELAP case 6**		

*The amount of melt is still decreasing at the end of the run.

DISTRIBUTION:

Beredskabsstyrelsen
Attn: Björn Thorlaksen
Louise Dahlerup
P.O.Box 189
DK-3460 Birkeröd

Risö National Laboratory
Attn: Povl Ölgaard
Frank Höjerup
Knud Ladekarl Thomsen (4)
P.O.Box 49
DK-4000 Roskilde

Finnish Center of Radiation
and Nuclear Safety
Attn: Lasse Reiman (3)
Kalevi Haule
Timo Karjunen
Juhani Hyvärinen
P.O.Box 14
FIN-00881 Helsinki

Teollisuuden Voima Oy
Attn: Markku Friberg
Heikki Sjövall
Seppo Koski
Risto Himanen
FIN-27160 Olkiluoto

IVO International Ltd
Attn: Harri Tuomisto
Petra Lundström
Olli Kymäläinen
FIN-01019 IVO

Jussi Vaurio
Loviisan Voimalaitos
P.O.Box 23
FIN-07901 Loviisa

Björn Wahlström
VTT Automation
P.O.Box 13002
FIN-02044 VTT

VTT Energy
Attn: Lasse Mattila
Ilona Lindholm (8)
Risto Sairanen (5)
Kari Ikonen
Esko Pekkarinen
Ari Silde
P.O.Box 1604
FIN-02044 VTT

Tord Walderhaug
Geislavarnir Rikisins
Laugavegur 118 D
IS-150 Reykjavik

Institutt för Energiteknikk
Attn: Egil Stokke
Oivind Berg (3)
P.O.Box 175
N-1750 Halden

Sverre Hornkjöl
Statens Strålevern
P.O.Box 55
N-1345 Österås

Swedish Nuclear Power Inspectorate
Attn: Wiktor Frid (5)
Oddbjörn Sandervåg
Gert Hedner
Ninos Garis
S-10658 Stockholm

Vattenfall Energisystem AB
Attn: Klas Hedberg (5)
Veine Gustavsson
P.O.Box 528
S-16216 Stockholm

Forsmarks Kraftgrupp AB
Attn: Gustaf Löwenhielm (2)
Henning Danielsson
S-74203 Östhammar

Kenneth Persson (3)
Vattenfall AB
Ringhalsverket
S-43022 Väröbacka

Emil Bachofner (3)
OKG AB
S-57093 Figeholm

Jan-Anders Svensson (3)
Barsebäck Kraft AB
P.O.Box 524
S-24625 Löddeköpinge

Studsvik Eco & Safety AB
Attn: Lars Nilsson (4)
Lise-Lotte Johansson
S-61128 Nyköping

ABB Atom AB
Attn: Yngve Waaranperä
Timo Okkonen
S-72163 Västerås

ES-Konsult AB
Attn: Erik Söderman
Ferenc Muller
P.O.Box 3096
S-16103 Bromma

Lennart Hammar
ES-Konsult AB
c/o Dalvägen 63A
S-18733 Täby

Kjell Andersson
Karinta Konsult HB
P.O.Box 6048
S-18306 Täby

Antti Vuorinen
Otakallio 2 B 22
FIN- 02150 Espoo

Torkel Bennerstedt
NKS
PL 2336
S-76010 Bergshamra

Royal Institute of Technology
Attn: Bal Raj Sehgal
T. N. Dinh
R. R. Nourgaliev
Nuclear Power Safety
S-10044 Stockholm

Oak Ridge National Laboratory
Attn: Stephen Hodge
Robert Sanders
P.O.Box 2009
Oak Ridge
Tennessee 37831-8057
U.S.A

U.S. Nuclear Regulatory Commission
Attn: Charles Ader
Sudhamay Basu
Washington, DC 20555
U.S.A

Brian Turland
233/A32
AEA Technology
Winfrith
Dorchester
Dorset DT2 8DH
UK